

# COMPUTER-AIDED DESIGN AND ANALYSIS OF A THREE-POLE RADIAL MAGNETIC BEARING

by

DÁNIEL MARCSA  
B.Sc. in Electrical Engineering

supervisor

DR. MIKLÓS KUCZMANN, PH.D.  
Associate Professor

A thesis submitted to the  
Széchenyi István University  
for the degree of  
MASTER OF SCIENCE  
IN MECHATRONICS ENGINEERING

Department of Materials- and Vehicle Manufacturing  
Laboratory of Electromagnetic Fields  
Széchenyi István University  
Győr  
2010

# Contents

<b>1</b>	<b>Introduction</b>	<b>1</b>
1.1	The Magnetic Bearing . . . . .	2
1.1.1	The Magnetic Bearing as a Controlled Suspension . . . . .	3
1.2	Y-Shaped Radial Magnetic Bearing . . . . .	4
1.2.1	The Problem Definition . . . . .	4
<b>2</b>	<b>Equations of the Static Magnetic Field</b>	<b>7</b>
2.1	Maxwell's Equation . . . . .	7
2.2	The Regions and Boundaries . . . . .	8
<b>3</b>	<b>Potential Formulation</b>	<b>10</b>
3.1	Formulation with Magnetic Vector Potential, the $\vec{A}$ - Formulation . . . . .	10
3.2	Weak Formulation of the $\vec{A}$ - Formulation . . . . .	13
3.2.1	The Weak Formulation with Galerkin's Method . . . . .	13
<b>4</b>	<b>Nonlinear Equation Solvers</b>	<b>16</b>
4.1	Newton-Raphson Method . . . . .	17
4.2	The Polarization Method . . . . .	20
4.3	Fixed Point Method . . . . .	22
<b>5</b>	<b>The Finite Element Method</b>	<b>25</b>
5.1	Fundamentals of FEM . . . . .	25
5.1.1	Preprocessing . . . . .	25
	A. Model Specification . . . . .	25
	B. 2D Finite Element Mesh . . . . .	27
	C. 3D Finite Element Mesh . . . . .	29
5.1.2	Shape Functions . . . . .	31
5.1.3	Finite Element Simulation . . . . .	31
	A. Solvers . . . . .	32
5.1.4	Postprocessing . . . . .	33
	A. Flux Linkage . . . . .	33
	B. Electromagnetic Force . . . . .	35
<b>6</b>	<b>Numerical Optimization</b>	<b>37</b>
6.1	Nelder-Mead Simplex Search Algorithm . . . . .	38
6.2	The FEM-Based Numerical Optimization . . . . .	40
6.3	Optimization Results . . . . .	41

<b>7</b>	<b>Analytic Analysis of the Force</b>	<b>44</b>
7.1	Lumped Model of Force . . . . .	45
<b>8</b>	<b>Solution of the Problem</b>	<b>50</b>
8.1	Results of the Linear Simulations . . . . .	50
8.2	Results of the Nonlinear Simulations . . . . .	58
<b>9</b>	<b>Conclusions and future works</b>	<b>66</b>
<b>10</b>	<b>Acknowledgement</b>	<b>68</b>
<b>11</b>	<b>Bibliography</b>	<b>69</b>

# List of Notations and Abbreviations

$\vec{A}$	Magnetic vector potential [Vs/m]
$A$	Unknown magnetic vector potential [Vs/m]
$\mathbf{A}$	Unknown magnetic vector potential vector
$\Delta\mathbf{A}$	Residual term in a Newton-Raphson method
$\vec{B}$	Magnetic flux density vector [T]
$B$	Length of magnetic flux density vector [T]
$\vec{e}_x, \vec{e}_y, \vec{e}_z$	Cartesian based normal vectors
$\vec{F}$	Electromagnetic force [N]
$\vec{H}$	Magnetic field intensity vector [A/m]
$H$	Length of magnetic field intensity vector [A/m]
$\vec{I}$	Nonlinear residual term in a fixed point method [A/m]
$\vec{J}_0$	Source current density [A/m <sup>2</sup> ]
$\mathbf{J}, J_{ij}$	Jacobian matrix
$L$	Axial length of the magnetic bearing [mm]
$\vec{n}_B, \vec{n}_H$	Outer normal unit vectors
$N$	Scalar weighting function
$N_w$	Number of turns of winding
$\mathbf{r}$	Vector of the residuum in a Newton-Raphson method
$S$	Surface [m <sup>2</sup> ]
$S_c$	Cross section area of coil [m <sup>2</sup> ]
$\mathbf{S}, S_{ij}$	System matrix
$\vec{T}_0$	Impressed current vector potential [A/m]
$\vec{\mathbf{T}}_m$	Maxwell's stress tensor
$\mathbf{u}, u_i$	Column vector with entries of excitations
$\vec{W}$	Vector weighting function
$\Gamma$	Line along the air gap [m]
$\Gamma_B, \Gamma_H$	Boundaries of the problem
$\mu_0$	Permeability of vacuum [Vs/Am=H/m]
$\mu$	Permeability [Vs/Am=H/m]
$\nu_0$	Reluctivity of vacuum [Am/Vs]
$\nu$	Reluctivity [Am/Vs]
$\nu_o$	Optimal value of reluctivity [Am/Vs]
$\vec{\sigma}$	Force on the arbitrary oriented surface
$\Phi$	Magnetic flux or flux [Tm <sup>2</sup> =Vs=weber=Wb]
$\Psi$	Flux linkage [Tm <sup>2</sup> =Vs=weber=Wb]

---

$\Omega$	Whole problem region
$\Omega_0$	Nonmagnetic region
$\Omega_m$	Magnetic material region
$\mathcal{B}^{-1}\{.\}$	Inverse nonlinear function
AMB	Active Magnetic Bearing
BF	Brute-Force search
CAD	Computer-Aided Design
DSP	Digital Signal Processing
FEM	Finite Element Method
FEMM	Finite Element Method Magnetics software
FP	Fixed Point method
MAGLEV	Magnetic Levitation
NM	Nelder-Mead simplex search algorithm
NR	Newton-Raphson method
PMB	Passive Magnetic Bearing

# List of Figures

1.1	The basic magnetic bearing control loop and its elements. . . . .	3
1.2	The arrangement of Y-shaped magnetic bearing fed by two amplifiers. . .	5
1.3	The three-dimensional geometry of radial magnetic bearing. . . . .	5
2.1	The structure of the two-dimensional static magnetic field problem. . . .	8
2.2	The regions and boundaries of the simulated magnetic bearing. . . . .	9
4.1	The magnetization curve of the laminated parts. . . . .	16
4.2	The geometrical construction of Newton-Raphson method. . . . .	17
4.3	Flowchart of the Newton-Raphson method. . . . .	20
4.4	The $\nu_r$ relative reluctivity as a function of the $B^2$ square magnetic flux density. . . . .	21
4.5	The graphical form of the polarization method. . . . .	21
4.6	The geometrical construction of fixed point method. . . . .	23
4.7	Flowchart of the fixed point technique. . . . .	24
5.1	Steps of simulation by finite element method. . . . .	26
5.2	The model specification in COMSOL Multiphysics. . . . .	27
5.3	Linear (first order) finite elements in the two-dimensional $x - y$ plane. . .	27
5.4	Quadratic (second-order) finite elements in the two-dimensional $x - y$ plane.	28
5.5	The triangular discretization of the 2D magnetic bearing geometry. . . .	28
5.6	Enlargement of the discretization. . . . .	29
5.7	Linear (first-order) finite elements in three dimensions. . . . .	29
5.8	The three-dimensional discretization of the bearing geometry. . . . .	30
5.9	The generated two-layer mesh in the air gap. . . . .	30
5.10	One part of the script of the fixed point technique. . . . .	32
5.11	Representation of the impressed current vector potential $\vec{T}_0$ . . . . .	33
5.12	The computation of flux linkage of magnetic bearing. . . . .	34
5.13	The rotor under magnetic field surrounded by the surface $\Gamma$ and the vector diagram of $\vec{\sigma}$ stress tensor. . . . .	35
6.1	Main operations of Nelder-Mead algorithm for a two-dimensional problem.	39
6.2	The optimized parameter of the magnetic bearing. . . . .	40
6.3	Field plot of the result of the optimization methods in linear case. . . .	42
6.4	Field plot of the result of the optimization methods in nonlinear case. . .	43
7.1	Independent loops and nodes of Y-shaped magnetic bearing. . . . .	45
7.2	The force vectors and its components of magnetic bearing. . . . .	47

8.1	The magnetic flux density inside the magnetic bearing. . . . .	51
8.2	The surface plot and vectors of magnetic flux density inside the magnetic bearing with linear material. . . . .	51
8.3	The surface plot of magnetic flux density inside the magnetic bearing at same maximum value of the scale. . . . .	52
8.4	The flux linkage - current characteristic at nominal air gap. . . . .	53
8.5	The flux linkage the function of the $y$ -directed displacement of the rotor and of the variation of the current in two-dimensional case. . . . .	53
8.6	The flux linkage the function of the $y$ -directed displacement of the rotor and of the variation of the current in three-dimensional case. . . . .	54
8.7	The flux linkage the function of the $y$ -directed displacement of the rotor and of the variation of the current by the FEMM. . . . .	54
8.8	The electromagnetic force - current characteristic at nominal air gap. . .	55
8.9	The electromagnetic force the function of the $y$ -directed displacement of the rotor and of the variation of the current in two-dimensional case. . .	56
8.10	The electromagnetic force the function of the $y$ -directed displacement of the rotor and of the variation of current in three-dimensional case. . . . .	56
8.11	The electromagnetic force the function of the $y$ -directed displacement of the rotor and of the variation of the current by the FEMM. . . . .	57
8.12	The electromagnetic force the function of the $y$ -directed displacement of the rotor and of the variation of the current by the analytic computation. . . . .	57
8.13	The relative tolerance the function of the number of iterations at $I_2=5A$ current. . . . .	59
8.14	The magnetic flux density inside the magnetic bearing. . . . .	60
8.15	The surface plot and vectors of magnetic flux density inside the magnetic bearing with nonlinear material. . . . .	60
8.16	The flux linkage - current characteristic at nominal air gap. . . . .	61
8.17	The flux linkage the function of the $y$ -directed displacement of the rotor and of the variation of the current in two-dimensional case. . . . .	61
8.18	The flux linkage the function of the $y$ -directed displacement of the rotor and of the variation of the current in three-dimensional case. . . . .	62
8.19	The flux linkage the function of the $y$ -directed displacement of the rotor and of the variation of the current by the FEMM. . . . .	62
8.20	The electromagnetic force - current characteristic at nominal air gap. . .	63
8.21	The electromagnetic force the function of the $y$ -directed displacement of the rotor and of the variation of the current in two-dimensional case. . .	63
8.22	The electromagnetic force the function of the $y$ -directed displacement of the rotor and of the variation of the current in three-dimensional case. . .	64
8.23	The electromagnetic force the function of the $y$ -directed displacement of the rotor and of the variation of the current by the FEMM. . . . .	64

# List of Tables

6.1	Required Performances and Design Contrains. . . . .	41
6.2	Data of the Optimized Design Parameters. . . . .	42
8.1	The computation time and the number of iterations of the nonlinear equation solvers. . . . .	58

# Chapter 1

## Introduction

The ideas of levitating a body hover without any contact by using magnetic forces is an old dream of mankind. As early as 1842, the British minister and nature philosopher, Samuel Earnshaw (1805 - 1888), examined this question and stated a fundamental proposition known as Earnshaw's theorem. The essence of this theorem is that it is impossible for an object to be suspended in a stable equilibrium purely by means magnetic or electrostatic forces [1–3].

First technical applications of a levitation by magnetic field were proposed in 1937, when Kemper applied for a patent for a hovering suspension, while Beams and Holmes were working on electromagnetic suspension. This experiment was the predecessor of the later magnetically levitated vehicles. The most familiar levitation vehicle nowadays is the MAGLEV (derived from *magnetic levitation*), which uses the electromagnetic principle, is suspended without any contact by several magnets from the iron track [1, 2, 4].

Later, in the sixties a principle of magnetic bearings was used in space technology for the magnetic suspension of momentum-wheels to control the attitude of satellites. First industrial applications appeared in the late seventies mainly for turbines and for high-speed machine tools. Because of the magnetic bearing offer a novel way to solve classical problems of rotor dynamics by suspending a spinning rotor with no contact, wear and lubrication, and controlling its dynamic behaviour [1].

There are several types of total and partial magnetic levitation systems [2]:

- Permanent magnets (only partial stability);
- Diamagnetic materials (e.g. bismuth) in a magnetic field;
- Electromagnets with feedback control;
- Electromagnets with dynamic currents;
- Eddy currents - alternating current (AC) devices;
- Eddy currents - moving conductors;
- Superconductors and permanent magnets;
- Superconductors and superconducting magnets;
- Hybrid - for example, permanent magnets with feedback controlled electromagnets of controlled magnets with superconductors.

Magnetic levitation requires two necessary subsystems [2]:

- a primary system for generating the magnetic field and;
- a system for shaping or trapping the magnetic flux.

In the case of electromagnetic levitation, electric currents in a wire wound produce the primary magnetic field while the ferromagnetic coil holder and the ferromagnetic based core produce a magnetic circuit. In the case of eddy current levitation with moving magnet over a conductor, the source of the field can be permanent magnet or a normal or superconducting wire wound. The relative motion of the magnet and conductor provides the field-shaping system due to the induced eddy currents in the conductor. Finally, in the case of a passive superconducting levitator, a permanent magnet serves as the primary magnetic field source while the bulk or thin film superconductor provides the magnetic field shaping due to the induced currents [1, 2].

## 1.1 The Magnetic Bearing

Mechatronics is an interdisciplinary area of engineering sciences based on the classical fields of mechanical and electrical engineering and on computer science. With its interconnection of mechanical and electronic components and with a large amount of software being part of the system, the electromagnetic bearing represents a typical product of mechatronics. The magnetic bearing system picks up signals from its environment, process them on an intelligent way and react, for example, with force or motion. Methods for connecting the various area of knowledge, mechanical, electrical engineering and computer science are provided by the basic engineering sciences, system theory, control techniques and information processing [1].

After more than thirty years of industrial utilization of magnetic bearing it has become evident that the active magnetic bearings (AMB) are clearly favored over passive magnetic bearings (PMB). The term active implies that the bearing forces are actively controlled by means of electromagnets, a suitable feedback control loop and other element such as sensors and power amplifier. Here, only the active magnetic bearing is introduced.

Some advantages of the magnetic bearings are the follows: The AMBs will not suffer from any mechanical wear or give rise to any related contamination. The absence of aerodynamic drag losses and the low energy consumption of the bearing is a welcome feature for flywheels for energy storage. The high precision that can be attained and the high rotating speed with relative high load capacity. Furthermore, it is possible to simplify the machine construction, as there are no bearing fluids by seals. Other important features that have been corroborated by practical experience are the inherent means for self control and diagnosis, the very low maintenance costs, and the low energy consumption [1, 2].

The various advantages of the magnetic bearing have led to applications mainly in the five follows area [1]:

- Vacuum and cleanroom systems;
- Machine tools;

- Medical devices;
- Turbo-machinery;
- Superconducting bearings.

### 1.1.1 The Magnetic Bearing as a Controlled Suspension

Fig. 1.1 shows the simplest example of a magnetic bearing control loop through comprising all the necessary components of a standard active magnetic bearing system. In the following, these elements and functionalities are briefly described [1, 2].

The rotor is to be levitated freely at a prescribed distance  $x_0$  from the bearing electromagnets. A contact-less position sensor (most often an eddy current or inductive type sensor) steadily measures the deviation between desired position  $x_0$  and actual rotor position  $x$  and feeds this information into a controller (nowadays digital controllers are widely used). The primary goal of the controller is to maintain the rotor position at its desired value. For this not only an equilibrium of the envolved force, here just the magnetic force  $f_m$  and the rotor weight  $mg$  must be established, but also as a most important quality of the control, a stabilization of the control loop must be achieved. Finally, the controller sends out a positioning command signal to a power amplifier which transforms this signal into an electric current in the coil of the bearing electromagnet

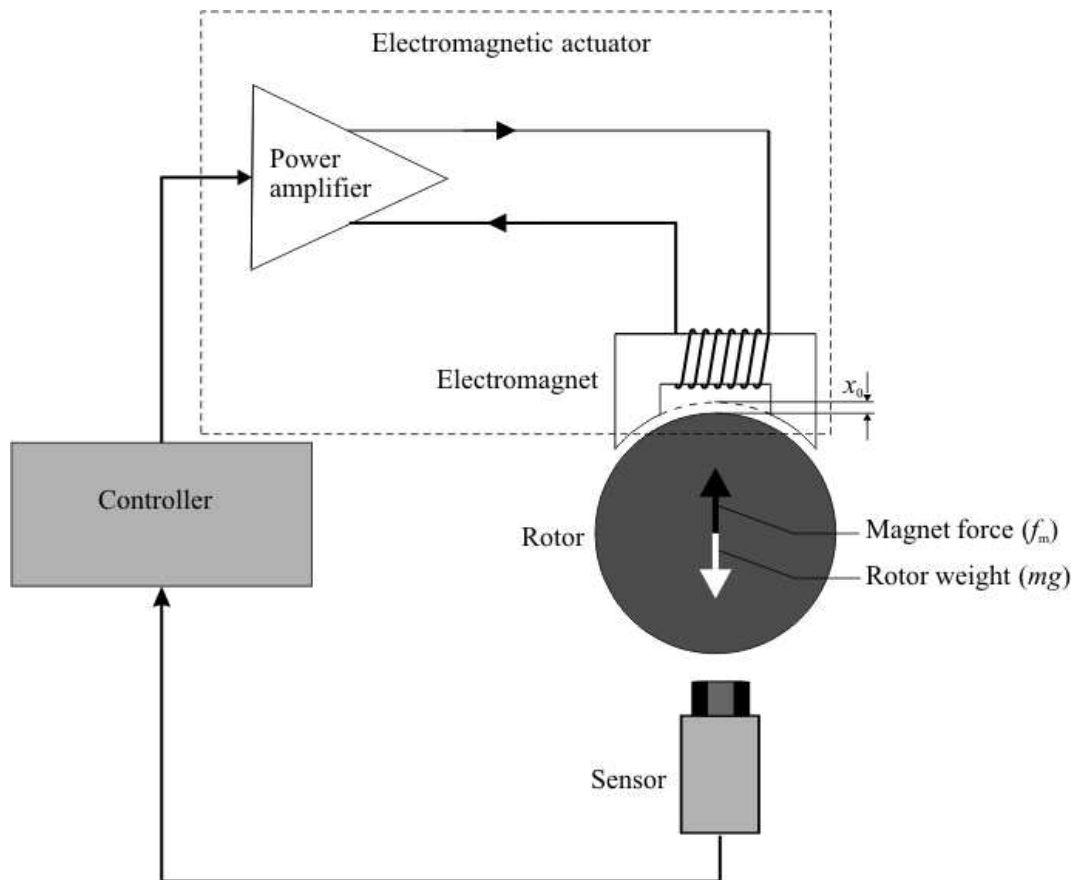


Fig. 1.1: The basic magnetic bearing control loop and its elements.

and a magnetic field in the iron core of the magnet, thus generating the desired magnetic force  $f_m$  [1, 2].

The setup of Fig. 1.1 describes a one degree of freedom single-channel rigid body system, which corresponds to a strong simplification of a real magnetic bearing. Rotations and tranverse motions of the rotor cannot be controlled by a single electromagnet and require a more complex arrangement of several electromagnets and a multi-channel control. Nevertheless, the basic properties of a magnetic bearing control loop can be easily investigated using this simple bearing example.

## 1.2 Y-Shaped Radial Magnetic Bearing

High speed and high accuracy are the main tasks for rotating machines in our days. In this regard, active magnetic bearing (AMB) is an important element since it can provide noncontact suspension. However, the opportunity of its industrial application has not been completely explored yet. One of the main reasons is its high cost. The sensors and power amplifiers account for a major portion of the cost. The number of required power amplifier is closely related to the number of magnetic poles in the AMB.

A more feasible way to lower the costs is to reduce the number of magnetic poles. The minimum pole number for an AMB is three. The three-pole AMB has several advantages, for example the use of only two amplifiers is possible and reducing the pole number can leave more space for heat dissipation, coil winding and sensor installation. All of these advantages can lead to lower the costs for the three-pole AMB.

However, the major disadvantages of the three-pole magnetic bearing is its strong nonlinearity due to magnatic flux coupling. It was very difficult to design and implement controllers for such a strong nonlinear system before. With the progress of nonlinear control theory and the increase on computing and sampling speed in PC/DSP-based (Personal Computer / Digital Signal Processing) control technologies, nonlinear controllers have become feasible today.

### 1.2.1 The Problem Definition

This work will be present the design and numerical simulation of a radial magnetic bearing. This bearing is a Y-shaped three-pole magnetic bearing fed by two amplifiers. This type of magnetic bearing can be seen in Fig. 1.2. The future task is to built up the prototype of this magnetic bearing.

This work consists of two main parts. One of these parts is the numerical geometry optimization. The other part is the numerical simulation of the magnetic bearing.

The magnetic bearing is optimized supposing a two-dimensional problem. The assumption of the two-dimensionality is usually valid if the axial length of the analyzed body is far greater than the dimensions in the cross-section plane. In the radial magnetic bearing, this is usually not the case. However, when the rotor is rotating, the eddy currents push the magnetic flux out of the solid shaft and the magnetic flux flows only through the laminated structure of the rotor. This results in a static magnetic field problem. Furthermore, the effect of the end-region fields has been neglected in the two-dimensional case [5].

In the simulation part, the optimized bearing geometry is simulated in 2D and 3D. The main goal of these simulations are the effect of end-region field to the bearing force.

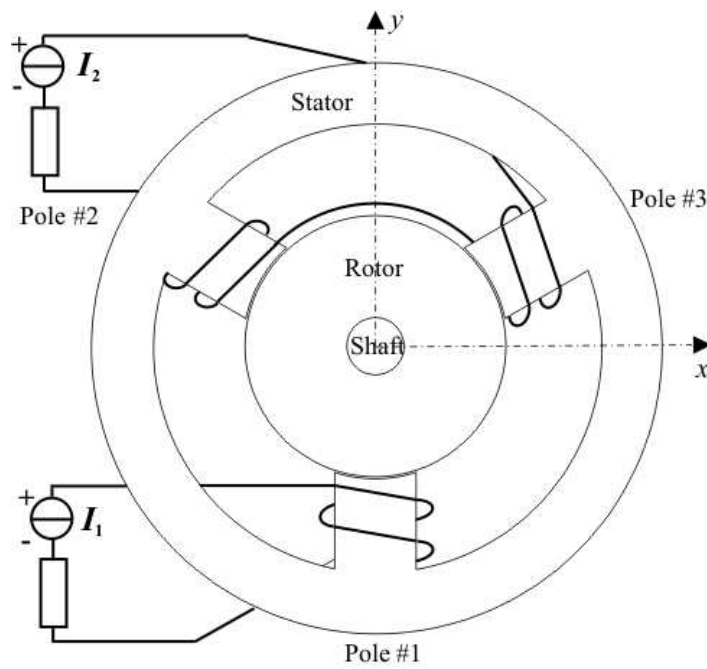


Fig. 1.2: The arrangement of Y-shaped magnetic bearing fed by two amplifiers.

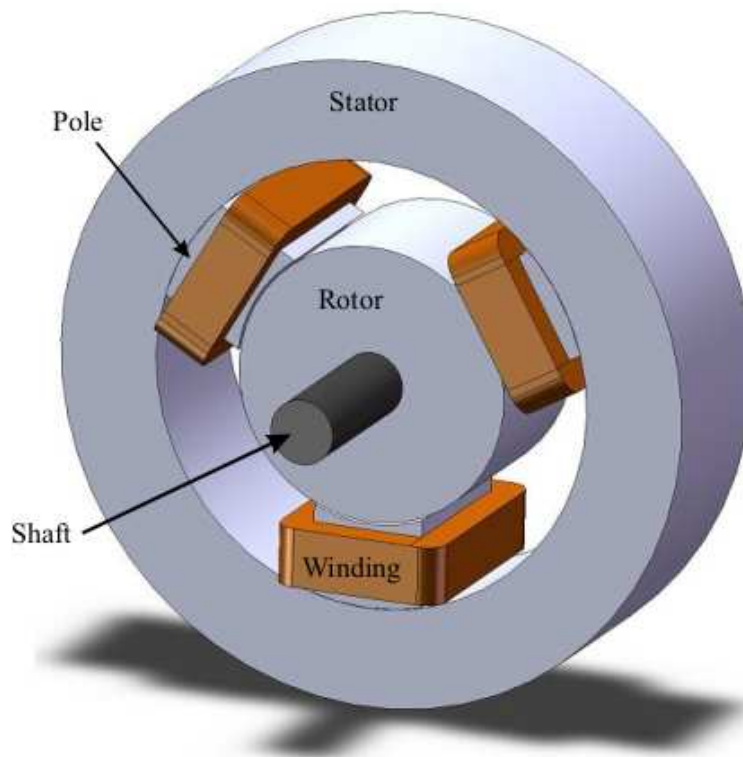


Fig. 1.3: The three-dimensional geometry of radial magnetic bearing.

The end-region field of the bearing has been studied by the 3D simulation and compare with the 2D results.

The arrangement of the three-pole radial magnetic bearing problem in two-dimensio-

nal case is shown in Fig. 1.2. The poles of the Y-shaped magnetic bearing Pole#1, Pole#2, Pole#3 are lag each other in phase by  $120^\circ$ . In the simulations, only the upper two windings has been excited by the second generator current  $I_2$ . This situation is when the rotor is in the centre of bearing, not needed the control currents. The source current density is maintained constant at  $|\vec{J}_0| = 5,1 \cdot 10^6 \text{ A/m}^2$ . The stator, the rotor and the poles are laminated, because the losses are reduced and eliminate the effect of eddy currents. The shaft is a solid iron, which is surrounding the laminated rotor.

The three-dimensional arrangement of the radial magnetic bearing is shown in Fig. 1.3. This figure shows very well the windings are longer than the core length. Mainly, the overhanging part of the windings generate the end-region field, which has an effect the inside field of the bearing.

The scope of my master thesis is to present the numerical optimization and simulation of the Y-shaped radial magnetic bearing by one of the most usable electromagnetic field computation technique, the finite element method (FEM).

In engineering point of view, the aim of the research is to build up a finite element technique based optimization procedure to design the a radial magnetic bearing, and to validated the two-dimensional optimisation results through the comparison of two-dimensional and three-dimensional finite element simulations. Furthermore, to check the correctness of the two-dimensional results of the short axial length AMB simulation with linear and nonlinear material.

The organization of my master thesis is the following.

In chapter 2 and 3, the theoretical background of the realized simulations has been described. The starting point is Maxwell's equations, from which the used potential formulation can be deduced. The finite element method is based on the weak formulation of the potential formulation, so the chapter 3 presents the deduction of the weak formulation applying mathematical rules and theorems.

Chapter 4 deals with the used nonlinear equation solvers and the polarization method. These solvers are necessary in the nonlinear finite element simulations. The solvers are the Newton-Raphson technique and the fixed point method. In this chapter, I introduce the basics of these numerical techniques, and its main steps in the finite element simulation.

In chapter 5, I describe the main steps of finite element method, the preprocessing, the computation and the postprocessing. I shortly present the two- and three dimensional finite elements, and the used solvers. In the postprocessing section I present the computation of the important quantities of magnetic bearing, i.e. the flux linkage and the electromagnetic force.

Chapter 6 contains the basics of the application of optimization methods, and the combination of these with numerical technique. In this chapter will be presents the used optimization techniques, the well known brute-force search and the Nelder-Mead simplex search algorithm. Finally, the results of the optimisation and the comparison of the used methods.

In chapter 7, the analytic computation of the force has been presented. I describe the simplifications and the deduction of the matrix equations of the force components.

Last, the comparison of the computed quantities can be found in chapter 8, and the conclusions with future works are presented in chapter 9. The main references of my research are also given at the end of my diploma.

# Chapter 2

## Equations of the Static Magnetic Field

The magnetic bearing is assumed to be a static magnetic field problem. The assumption of the problem is valid if the purpose of the lamination in the stator and in the rotor is eliminate the effect of eddy currents. The solid shaft of the rotor should be modeled as a solid iron. However, when the rotor is rotating, no magnetic flux penetrates through the solid shaft. Thus, when analyzing the bearing for the actual operation point, the shaft can be modeled as air.

The Maxwell's equations of the static magnetic field problems are presented in this chapter. The simplification of the problem, the symmetry planes, and the boundary conditions of the problem are also presented in this chapter.

### 2.1 Maxwell's Equation

In the static magnetic field problems, the magnetic field has no interaction with the electric field, because the field quantities are independent on the time variation (i.e.  $\partial/\partial t = 0$ ). However, the current  $i$  flowing in coils generate magnetic field around the coils.

The studied static magnetic field problem is separated into two parts, the magnetic material region (e.g. stator)  $\Omega_m$ , and the nonmagnetic domain (e.g. air)  $\Omega_0$ . The scheme of the analyzed two-dimensional static magnetic field problem can be seen in Fig. 2.1. The domains and regions are the same in the three-dimensional problem, only the boundaries have some differences.

To the formulation of the problem, the differential equations are the following [6–16]:

$$\nabla \times \vec{H} = \vec{J}_0, \quad \text{in } \Omega_0 \cup \Omega_m, \quad (2.1)$$

$$\nabla \cdot \vec{B} = 0, \quad \text{in } \Omega_0 \cup \Omega_m, \quad (2.2)$$

$$\nabla \cdot \vec{J}_0 = 0, \quad \text{in } \Omega_0, \quad (2.3)$$

where  $\vec{H}$  is the magnetic field intensity,  $\vec{B}$  is the magnetic flux density and  $\vec{J}_0$  is a source current density.

The source current density is determined from the known  $i$  coil current by the following relation:

$$|\vec{J}_0| = \frac{N_w i}{S_c}, \quad (2.4)$$

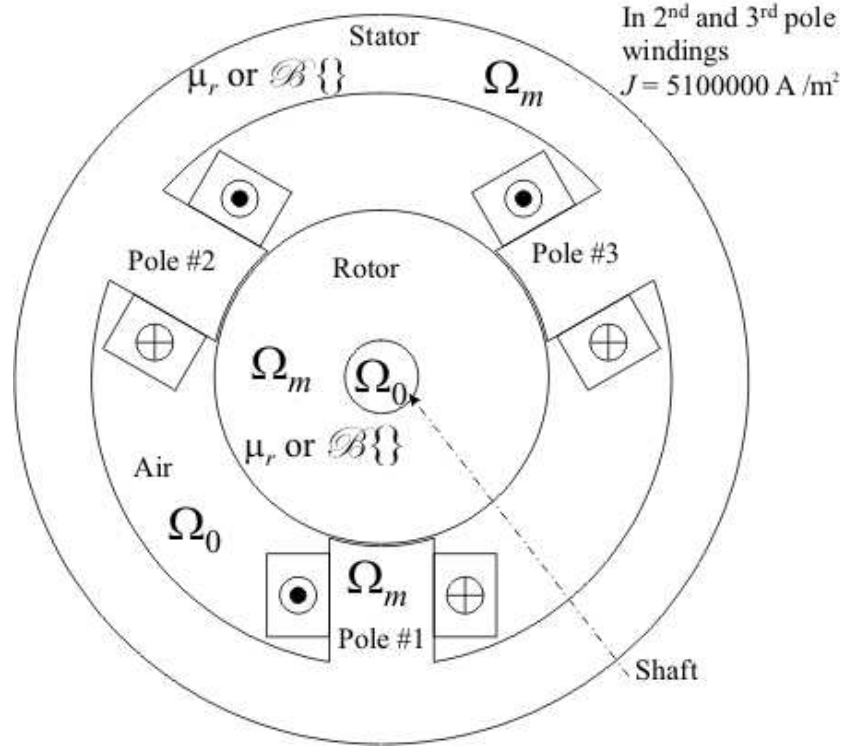


Fig. 2.1: The structure of the two-dimensional static magnetic field problem.

where  $N_w$  is the number of turns of winding and  $S_c$  is the cross section area of coil. The directions of the  $\vec{J}_0$  source current density are signed in the Fig. 2.1.

The constitutive relationship can be used in its inverse form because of the used potential formulation. The inverse constitutive relations can be written as

$$\vec{H} = \begin{cases} \nu_0 \vec{B}, & \text{in air, } \Omega_0, \\ \nu_0 \nu_r \vec{B}, & \text{in magnetically linear material, } \Omega_m, \\ \mathcal{B}^{-1}\{\vec{B}\} = \nu_o \vec{B} + \vec{I}, & \text{in magnetically nonlinear material, } \Omega_m, \end{cases} \quad (2.5)$$

where  $\nu_0 = 1/\mu_0$  is the reluctivity of vacuum and  $\nu_r$  is the relative reluctivity. The value of the relative reluctivity is  $\nu_r = 1/\mu_r = 1/3000 = 3.33 \cdot 10^{-4}$  m/H. The  $\mathcal{B}^{-1}\{\vec{B}\}$  is a hysteresis operator, which simulates the nonlinear material, in this problem this is a simple nonlinear curve. The  $\nu_o$  is the properly chosen constant, the ideal reluctivity (the "o" character in the subscript means the optimal). The  $\vec{I}$  is the residual nonlinearity, which depends on the input - output of the used nonlinear curve without hysteresis. The  $\vec{I}$  residual is a magnetic field intensity like quantity.

## 2.2 The Regions and Boundaries

Maxwell's equations are valid in the problem region  $\Omega = \Omega_m \cup \Omega_0$ . The problem region  $\Omega$  is bounded by  $\partial\Omega$ . The  $\partial\Omega$  is separated into two disjunct parts  $\Gamma_H$  and  $\Gamma_B$ , i.e.  $\partial\Omega = \Gamma_H \cup \Gamma_B$  [6, 10, 16].

The regions and boundaries of the two- and three-dimensional problem can be seen in Fig. 2.2(a). and in Fig. 2.2(b).

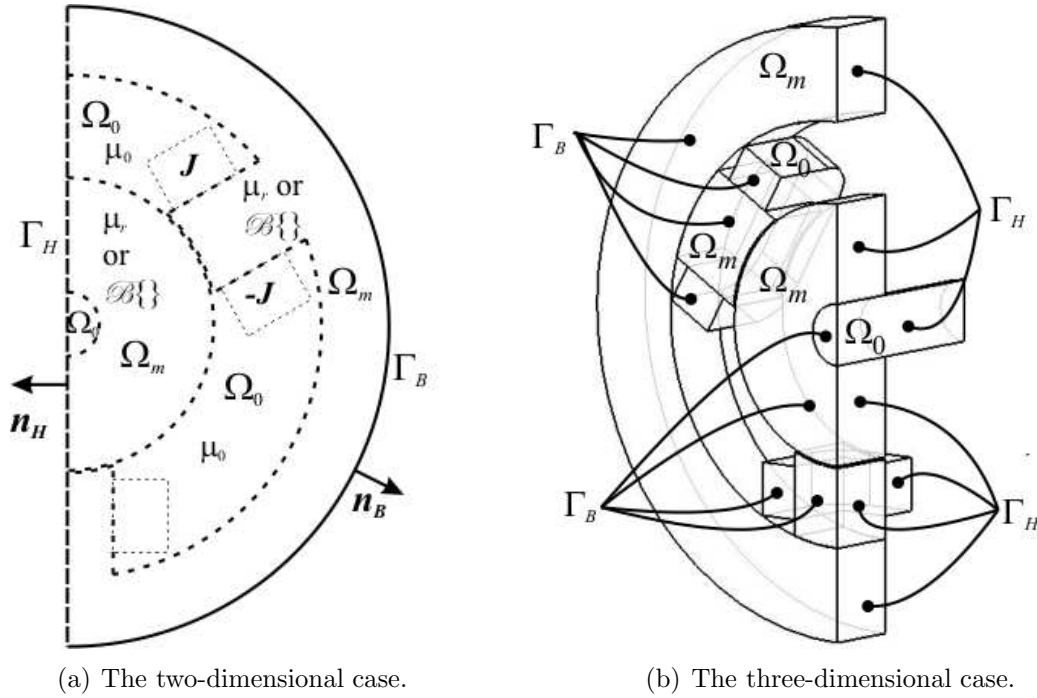


Fig. 2.2: The regions and boundaries of the simulated magnetic bearing.

$\Gamma_H$  in Fig. 2.2 denotes where the tangential component of the magnetic field intensity is given by a known surface current density  $\vec{K}$ . In this problem  $\Gamma_H$  is a symmetry plane, in this case  $\vec{K}=\vec{0}$ . The boundary  $\Gamma_B$  is usually the closing boundary or a symmetry plane of the problem region, where the normal component of the magnetic flux density is vanishing. The tangential component of the magnetic field intensity and the normal component of the magnetic flux density must be continuous on the interface between the two subregions,  $\Omega_m$  and  $\Omega_0$ . However, in this problem the continuity on this boundary condition is satisfied by the used potential formulation. This is why the  $\Gamma_{m0}$  isn't denoted in the Fig. 2.2.

The boundary conditions of the symmetry plane of the three dimensional problem is presented in Fig. 2.2(b).

In the three-dimensional simulation has not been used the outer boundary of the problem geometry as a closing boundary as against the two-dimensional case. The closing boundary of the three-dimensional problem is not shows in Fig. 2.2(b). The radii of this closing boundary is basically three times larger than the diameter of the geometry of AMB, but it is possibly better to use five - ten times radii. The boundary condition of the three-dimensional closing boundary is  $\Gamma_B$ , like in the two-dimensional problem (Fig. 2.2(a)).

These boundary conditions can be formulated as [6, 10, 16]:

$$\vec{H} \times \vec{n}_H = \vec{0}, \quad \text{on } \Gamma_H, \quad (2.6)$$

and

$$\vec{B} \cdot \vec{n}_B = 0, \quad \text{on } \Gamma_B, \quad (2.7)$$

where  $\vec{n}_H$  és  $\vec{n}_B$  are the outer normal unit vector according to the boundary of the regions.

# Chapter 3

## Potential Formulation

There are several potential formulations applicable to calculate the electromagnetic field quantities, fundamentally scalar and vector potentials can be used [6, 9–13, 16, 18, 19]. The aim of potential formulations is to reduce the solution of Maxwell's equations to the solution of different type of partial differential equations.

The investigated magnetic bearing problem is considered a static magnetic field problem. The static magnetic field is defined by Maxwell's equations (2.1), (2.2), (2.3), constitutive relations in (2.5), moreover the boundary conditions (2.6) and (2.7).

The static magnetic field can be described by the magnetic vector potential  $\vec{A}$  and the reduced magnetic scalar potential  $\Phi$  [6, 9–13, 16, 18, 19].

This section deals with the used potential formulation of magnetic bearing problem, the partial differential equations of  $\vec{A}$  - formulation. Furthermore, the weak formulation of the differential equations by the weighted residual method [20].

### 3.1 Formulation with Magnetic Vector Potential, the $\vec{A}$ - Formulation

The magnetic vector potential is defined by [6–19]:

$$\vec{B} = \nabla \times \vec{A}, \quad (3.1)$$

which satisfies (2.2) exactly, because of the identity  $\nabla \cdot \nabla \times \vec{v} \equiv 0$  for any vector function  $\vec{v} = \vec{v}(\vec{r})$ . Substituting the definition (3.1) into the first Maxwell's equation (2.1) and using the constitutive relation from (2.5), it leads to the partial differential equations [6, 9–13, 16, 18, 19]:

$$\nabla \times (\nu \nabla \times \vec{A}) = \vec{J}_0, \quad \text{in } \Omega_0 \cup \Omega_m, \text{ in linear case,} \quad (3.2)$$

and

$$\nabla \times (\nu_o \nabla \times \vec{A}) = \vec{J}_0 - \nabla \times \vec{I}, \quad \text{in } \Omega_0 \cup \Omega_m, \text{ in nonlinear case.} \quad (3.3)$$

To ensure the uniqueness of the magnetic vector potential, the divergence of it can be selected according to Coulomb gauge [6, 10, 16, 19], i.e.

$$\nabla \cdot \vec{A} = 0. \quad (3.4)$$

Gauging is satisfied automatically in 2D, but unfortunately it is not true in 3D. The origin of numerical problems is the lack of uniqueness of the magnetic vector potential in three dimensions [10, 18].

Thereinafter presents the uniqueness of the vector potential in two-dimensional problem, and a numerical technique which is not sensitive to Coulomb gauge in three-dimensional case.

### Two-dimensional case

In 2D problems Coulomb gauge  $\nabla \cdot \vec{A} = 0$  is satisfied automatically, if the source current density has only  $z$  component, the magnetic field intensity vector and the magnetic flux density vector have  $x$  and  $y$  components [6, 10, 16], i.e.

$$\vec{J}_0 = J_0(x, y)\vec{e}_z, \quad (3.5)$$

$$\vec{H} = H_x(x, y)\vec{e}_x + H_y(x, y)\vec{e}_y, \quad (3.6)$$

$$\vec{B} = B_x(x, y)\vec{e}_x + B_y(x, y)\vec{e}_y. \quad (3.7)$$

The magnetic vector potential has only  $z$  component,

$$\vec{A} = A_z(x, y)\vec{e}_z, \quad (3.8)$$

because ( $A_x = 0$ ,  $A_y = 0$  and  $A_z = A_z(x, y)$ )

$$\vec{B} = \nabla \times \vec{A} = \begin{vmatrix} \vec{e}_x & \vec{e}_y & \vec{e}_z \\ \frac{\partial}{\partial x} & \frac{\partial}{\partial y} & 0 \\ 0 & 0 & A_z \end{vmatrix} = \vec{e}_x \frac{\partial A_z}{\partial y} - \vec{e}_y \frac{\partial A_z}{\partial x}, \quad (3.9)$$

i.e.  $B_x(x, y) = \partial A_z / \partial y$  and  $B_y(x, y) = -\partial A_z / \partial x$ . The divergence of this one component vector potential is equal to zero, because

$$\nabla \cdot \vec{A} = \frac{\partial A_z(x, y)}{\partial z} = 0. \quad (3.10)$$

### Three-dimensional case

In three-dimensional problems, the uniqueness of the vector potential is not so evident. One possibility, it can be prescribed by applying a numerical technique which is not sensitive to Coulomb gauge. When using edge element approximation in the finite element approximation and taking care about the representation of source current density [6].

One of many possibilities the representation of  $\vec{J}_0$  source current density is the  $\vec{T}_0$  impressed current vector potential [6, 10, 16, 19, 22]:

$$\vec{J}_0 = \nabla \times \vec{T}_0, \quad (3.11)$$

which satisfies  $\nabla \cdot \vec{J}_0 = 0$ , furthermore the divergence of  $\vec{T}_0$  is selected zero, which satisfies the Coulomb gauge. It must be noted that,  $\vec{T}_0$  is calculated on free space, i.e.

$\mu = \mu_0$  must be set everywhere in the problem region. The used technique, the following functional can be built up, to find out the source term  $\vec{T}_0$  [6]:

$$\mathcal{F}\{\vec{T}_0\} = \int_{\Omega} |\nabla \times \vec{T}_0 - \vec{J}_0|^2 d\Omega. \quad (3.12)$$

This relationship is equivalent the partial differential equation of free space, which can be formulated as [6]

$$\nabla \times \nabla \times \vec{T}_0 = \nabla \times \vec{J}_0, \quad \text{in } \Omega_0 \cup \Omega_m, \quad (3.13)$$

and the boundary conditions of on the  $\Gamma_B$  and on the  $\Gamma_H$  boundary

$$\vec{T}_0 \cdot \vec{n}_B = 0, \quad \text{on } \Gamma_B, \quad (3.14)$$

$$\vec{T}_0 \times \vec{n}_H = \vec{0}, \quad \text{on } \Gamma_H. \quad (3.15)$$

It can be solved by a numerical field calculation procedure, which is not sensitive to Coulomb gauge. Finally  $\vec{T}_0$  can be regarded as known, because this quantity is calculated before the numerical simulation.

After these, let us define the boundary conditions of the  $\vec{A}$ -formulations, which are same in the two and three dimensions.

On the  $\Gamma_H$  boundary, the tangential component of the magnetic field intensity vector can be set by the relation [6, 10, 18, 19]

$$\vec{H} \times \vec{n}_H = \vec{0} \Rightarrow (\nu \nabla \times \vec{A}) \times \vec{n}_H = \vec{0}, \quad \text{on } \Gamma_H, \text{ in linear case,} \quad (3.16)$$

and

$$(\nu_o \nabla \times \vec{A} + \vec{I}) \times \vec{n}_H = \vec{0}, \quad \text{on } \Gamma_H, \text{ in nonlinear case.} \quad (3.17)$$

The normal component of the magnetic flux density can be set as [6, 10, 16, 18, 19]

$$\vec{B} \cdot \vec{n}_B = 0 \Rightarrow (\nabla \times \vec{A}) \cdot \vec{n}_B = 0, \quad \text{on } \Gamma_B. \quad (3.18)$$

The left-hand side of the last formulation can be chosen as [10, 18]:

$$(\nabla \times \vec{A}) \cdot \vec{n}_B = \nabla \cdot (\vec{A} \times \vec{n}_B) = 0, \quad (3.19)$$

finally

$$\nabla \cdot (\vec{n}_B \times \vec{A}) = 0, \quad (3.20)$$

i.e.

$$\vec{n}_B \times \vec{A} = \vec{0}, \quad \text{on } \Gamma_B. \quad (3.21)$$

Finally, the partial differential equations and the boundary conditions of the presented two-dimensional static magnetic field problem, which solution satisfies Coulomb gauge can be formulated as [6, 9–13, 16–19]:

$$\nabla \times (\nu \nabla \times \vec{A}) = \vec{J}_0, \quad \text{in } \Omega_0 \cup \Omega_m, \text{ in linear case,} \quad (3.22)$$

$$\nabla \times (\nu_o \nabla \times \vec{A}) = \vec{J}_0, \quad \text{in } \Omega_0 \cup \Omega_m, \text{ in nonlinear case,} \quad (3.23)$$

and the partial differential equations of the three-dimensional static magnetic field problem [6, 10, 18, 19]:

$$\nabla \times (\nu \nabla \times \vec{A}) = \nabla \times \vec{T}_0, \quad \text{in } \Omega_0 \cup \Omega_m, \text{ in linear case,} \quad (3.24)$$

$$\nabla \times (\nu_o \nabla \times \vec{A}) = \nabla \times \vec{T}_0 - \nabla \times \vec{I}, \quad \text{in } \Omega_0 \cup \Omega_m, \text{ in nonlinear case.} \quad (3.25)$$

The Neumann type ((3.26) and (3.27)) and Dirichlet type ((3.28)) boundary conditions of the static magnetic field problem [6, 9–13, 17–19]:

$$(\nu \nabla \times \vec{A}) \times \vec{n}_H = \vec{0}, \quad \text{on } \Gamma_H, \text{ in linear case,} \quad (3.26)$$

$$(\nu_o \nabla \times \vec{A} + \vec{I}) \times \vec{n}_H = \vec{0}, \quad \text{on } \Gamma_H, \text{ in nonlinear case,} \quad (3.27)$$

$$\vec{n}_B \times \vec{A} = 0, \quad \text{on } \Gamma_B. \quad (3.28)$$

When using nodal elements in the 3D finite element approximation needed some extra term for the implicit enforcement of Coulomb gauge. This method results in the gauged version of the  $\vec{A}$  - formulation. The vector element based formulation (which has been used in this work), the ungauged  $\vec{A}$  - formulation is newer than the gauged  $\vec{A}$  - formulation.

## 3.2 Weak Formulation of the $\vec{A}$ - Formulation

The finite element method is associated with variational methods [21] or residual methods [6–14, 18, 20]. The residual methods are established directly from the physical equations. It is a respectable advantage comparing with the different methods since it is relatively easier to understand and to apply. This is the main reason why nowadays most of the FEM analysis is performed by using the residual method. The Galerkin's method is a particular form of residual method and it is widely used in electromagnetism. The finite element method is based on the Galerkin's method of the weighted residual method [6–14, 18].

The weighted residual method [20] can be applied to minimize the residual of a partial differential equation. The best approximation for the potentials can be obtained when the integral of the residual of the partial differential equation multiplied by a weighting function over the problem domain is equal to zero. The weighting function can be arbitrary, but in Galerkin's method, the weighting functions are selected to be the same as those used for expansion of the approximate solution.

### 3.2.1 The Weak Formulation with Galerkin's Method

The weak formulation of the weighted residual method can be obtained when applying the rule of integration by parts to decrease the order of the differential operator in the inner product. The finite element method can be derived from this group of the weighted residual method. In the case of finite element method, the weighting function and the basis function of the approximating function are the same.

The finite element method uses the the weak formulation with Galerkin's method when the basis functions of the approximating function and the weighting function are the same. Here, the weak formulations of the potential formulations according to Galerkin's method are presented, which are appropriate in the finite element method. In the following  $\vec{W} = \vec{W}(\vec{r})$  denotes the vector weighting function as well as the basis functions of approximating function and  $N = N(\vec{r})$  denotes the scalar weighting function as well as the basis functions of approximating function [6–14, 18, 20, 21].

Vector potentials  $\vec{A} = \vec{A}(\vec{r})$  are approximated by an expansion in terms of  $J$  elements of an entire function set  $\vec{W}_j$  in 3D and  $N_j$  in 2D. Shape functions  $N_j$  and  $\vec{W}_j$  are the elements of an entire function set, which can be defined in many ways. The definition of these elements are presented in Chapter 5.

In the following  $\vec{A}^\kappa$ ,  $\vec{T}_0^\kappa$  will denote the approximated unknown potential functions and  $\vec{I}^\kappa$  will denote the approximated residual term.

The weak formulations of  $\vec{A}$  - formulations is based on the partial differential equation (3.25) and on the Neumann-type interface condition (3.27):

$$\begin{aligned} & \int_{\Omega} \vec{W}_k \cdot [\nabla \times (\nu_o \nabla \times \vec{A}^\kappa)] d\Omega \\ & + \int_{\Gamma_H} \vec{W}_k \cdot [(\nu_o \nabla \times \vec{A}^\kappa + \vec{I}^\kappa) \times \vec{n}_H] d\Gamma \\ & = \int_{\Omega} \vec{W}_k \cdot (\nabla \times \vec{T}_0^\kappa) d\Omega - \int_{\Omega} \vec{W}_k \cdot (\nabla \times \vec{I}^\kappa) d\Omega \end{aligned} \quad (3.29)$$

ahol  $k = 1, \dots, J$ .

The second order derivative in the first integral can be reduced to first order one by using the next mathematical identity:

$$\nabla \cdot (\vec{a} \times \vec{b}) = \vec{b} \cdot \nabla \times \vec{a} - \vec{a} \cdot \nabla \times \vec{b}, \quad (3.30)$$

with the notation  $\vec{a} = \vec{W}_k$  and  $\vec{b} = \nu_o \nabla \times \vec{A}^\kappa$ . The right-hand side can also be simplified by applying the same identity with the notation  $\vec{a} = \vec{W}_k$  and  $\vec{b} = \vec{T}_0^\kappa$  or  $\vec{b} = \vec{I}^\kappa$ . After using Gauss' theorem the following equation can be obtained:

$$\begin{aligned} & \int_{\Omega} \nu (\nabla \times \vec{W}_k) \cdot (\nabla \times \vec{A}^\kappa) d\Omega + \int_{\Gamma_H \cup \Gamma_B} [(\nu_o \nabla \times \vec{A}^\kappa) \times \vec{W}_k] \cdot \vec{n}_H d\Gamma \\ & + \int_{\Gamma_H} \vec{W}_k \cdot [(\nu_o \nabla \times \vec{A}^\kappa + \vec{I}^\kappa) \times \vec{n}_H] d\Gamma \\ & = \int_{\Omega} (\nabla \times \vec{W}_k) \cdot \vec{T}_0^\kappa d\Omega + \int_{\Gamma_H \cup \Gamma_B} (\vec{T}_0^\kappa \times \vec{W}_k) \cdot \vec{n}_H d\Gamma \\ & - \int_{\Omega} (\nabla \times \vec{W}_k) \cdot \vec{I}^\kappa d\Omega - \int_{\Gamma_H \cup \Gamma_B} (\vec{I}^\kappa \times \vec{W}_k) \cdot \vec{n}_H d\Gamma. \end{aligned} \quad (3.31)$$

The first surface integral can be reformulated according to

$$[(\nu_o \nabla \times \vec{A}^\kappa) \times \vec{W}_k] \cdot \vec{n}_H = [\vec{n}_H \times (\nu_o \nabla \times \vec{A}^\kappa)] \cdot \vec{W}_k = -\vec{W}_k \cdot [(\nu_o \nabla \times \vec{A}^\kappa) \times \vec{n}_H]. \quad (3.32)$$

The second and last integral on the right-hand side can be rearranged by using the identity:

$$-(\vec{I}^\kappa \times \vec{W}_k) \cdot \vec{n}_H = -(\vec{n}_H \times \vec{I}^\kappa) \cdot \vec{W}_k = \vec{W}_k \cdot (\vec{I}^\kappa \times \vec{n}_H), \quad (3.33)$$

$$(\vec{T}_0^\kappa \times \vec{W}_k) \cdot \vec{n}_H = (\vec{n}_H \times \vec{T}_0^\kappa) \cdot \vec{W}_k = (\vec{W}_k \times \vec{n}_H) \cdot \vec{T}_0^\kappa = -(\vec{n}_H \times \vec{W}_k) \cdot \vec{T}_0^\kappa, \quad (3.34)$$

after these, the equation is the following:

$$\begin{aligned}
& \int_{\Omega} \nu (\nabla \times \vec{W}_k) \cdot (\nabla \times \vec{A}^\kappa) \, d\Omega - \int_{\Gamma_H \cup \Gamma_B} \vec{W}_k \cdot [(\nu_o \nabla \times \vec{A}^\kappa) \times \vec{n}_H] \, d\Gamma \\
& + \int_{\Gamma_H} \vec{W}_k \cdot [(\nu_o \nabla \times \vec{A}^\kappa + \vec{I}^\kappa) \times \vec{n}_H] \, d\Gamma \\
& = \int_{\Omega} (\nabla \times \vec{W}_k) \cdot \vec{T}_0^\kappa \, d\Omega + \int_{\Gamma_H \cup \Gamma_B} (\vec{T}_0^\kappa \times \vec{W}_k) \cdot \vec{n}_H \, d\Gamma \\
& - \int_{\Omega} (\nabla \times \vec{W}_k) \cdot \vec{I}^\kappa \, d\Omega + \int_{\Gamma_H \cup \Gamma_B} \vec{W}_k \cdot (\vec{I}^\kappa \times \vec{n}_H) \, d\Gamma.
\end{aligned} \tag{3.35}$$

It is easy to see that the first and the last surface integral are vanishing on  $\Gamma_H$ , because the second surface integral. The rest terms on  $\Gamma_B$  is reformulate,

$$\vec{W}_k \cdot [(\nu_o \nabla \times \vec{A}^\kappa) \times \vec{n}_H] = (\nu_o \nabla \times \vec{A}^\kappa) \cdot (\vec{n}_H \times \vec{W}_k), \tag{3.36}$$

and

$$\vec{W}_k \cdot (\vec{I}^\kappa \times \vec{n}_H) = \vec{I}^\kappa \cdot (\vec{n}_H \times \vec{W}_k), \tag{3.37}$$

and the Dirichlet boundary condition (3.28) must be satisfied, i.e.  $\vec{n}_H \times \vec{W}_k = \vec{0}$ . The third surface integral is reformulate:

$$(\vec{T}_0^\kappa \times \vec{W}_k) \cdot \vec{n}_H = (\vec{n}_H \times \vec{T}_0^\kappa) \cdot \vec{W}_k = (\vec{W}_k \times \vec{n}_H) \cdot \vec{T}_0^\kappa = -(\vec{n}_H \times \vec{W}_k) \cdot \vec{T}_0^\kappa, \tag{3.38}$$

where the second term is vanishing on  $\Gamma_H$  because of the Dirichlet boundary condition 3.15 so  $\vec{W}_k \cdot \vec{n}_H = 0$ , and it is evident that the last term is vanishing on  $\Gamma_B$ .

Finally, the weak formulation of the  $\vec{A}$  - formulation, which msut be realized by a numerical technique, which is not sensitive to Coulomb gauge is as follows:

$$\begin{aligned}
\int_{\Omega} \nu (\nabla \times \vec{W}_k) \cdot (\nabla \times \vec{A}^\kappa) \, d\Omega &= \int_{\Omega} (\nabla \times \vec{W}_k) \cdot \vec{T}_0^\kappa \, d\Omega \\
&- \int_{\Omega} (\nabla \times \vec{W}_k) \cdot \vec{I}^\kappa \, d\Omega,
\end{aligned} \tag{3.39}$$

where  $k = 1, \dots, J$ . In the laminated parts  $\nu = \nu_o$  and in the air region  $\nu = \nu_0$ .

In the two-dimensional case the weighting function and the basis functions of approximating function of the  $\vec{A}$  magnetic vector potential is the  $N = N(\vec{r})$  scalar weighting function, because magnetic vector potential has only one component ( $z$ ), thus the vector potential is a scalar in 2D.

# Chapter 4

## Nonlinear Equation Solvers

The prediction of the magnetic behaviour is an important role in the working condition in many electromagnetic devices (e.g. transformers, motors, etc.). The hysteresis of magnetic materials influencing not only the distribution of the magnetic field intensity, but also the related electromagnetic quantities, like electromagnetic force. Hence, the prediction of the electromagnetic behaviour is an important tool for the design of electrical apparatus.

In this problem, a single-valued nonlinear curve has been used, instead of the hysteresis loop. The half of the used single-valued nonlinear curve can be seen in Fig. 4.1.

The used potential formulation, and the weak formulations of  $\vec{A}$  - formulation are presented in the last chapter. The used numerical method is the Finite Element Method (FEM) [6, 9–14, 16–19, 22, 26–38], which has been used to solve a partial differential equations. However, the implementation of the hysteresis characteristic into the FEM procedure, the partial differential equations are generally nonlinear because of the non-

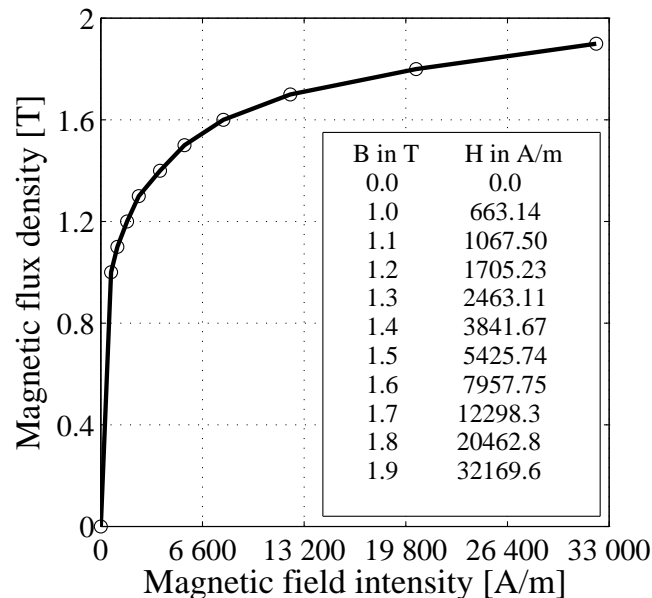


Fig. 4.1: The magnetization curve of the laminated parts.

linear characteristic of ferromagnetic material. In this case necessary to used a numerical technique for handling the nonlinearity.

There are two main groups of methods to handle nonlinear characteristics of ferromagnetic materials in electromagnetic field computation and a technique to solve the resulting system of nonlinear equations. One of these groups is the successive approximation based method and the others techniques are based on Newton's method. From these groups, the fixed point technique [6, 16, 23–25, 29, 31–38] and the Newton-Raphson method [9, 12, 13, 23–28, 30, 31] have been used in this work.

The used nonlinear solvers are presented in this chapter. The Newton-Raphson method has been used in the two-dimensional case, and the fixed point technique has been used in three-dimensional case.

First, the Newton-Raphson method has been used in the three-dimensional problem, too. However, it has a problem with the convergence. This is why the fixed point method has been used in three-dimensional case. The convergence of the Newton-Raphson method is one of the basic research themes of the Laboratory of Electromagnetic Field.

## 4.1 Newton-Raphson Method

The Newton-Raphson method is a popular algorithm for finding the roots of the equations [9, 12, 13, 23–28, 30, 31].

The nonlinear equation is the following form [23–25]

$$f(x) = 0, \quad (4.1)$$

where  $f(x)$  function is uniqueness and continuous in the  $a < x < b$  finite or infinite interval. Every  $c$  value, where  $f(x)$  function equal zero, i.e.  $f(c) = 0$ , the roots of (4.1) equation, i.e. the zero of  $f(x)$  function.

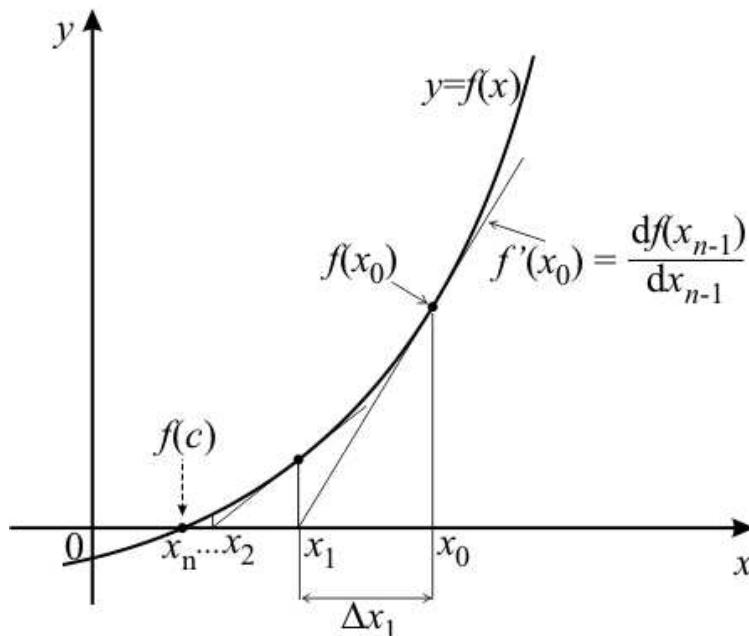


Fig. 4.2: The geometrical construction of Newton-Raphson method.

Suppose that the iteration step  $k - 1$  has resulted in an incorrect solution  $x_{n-1}$  for which  $f(x_{n-1}) \neq 0$ . This is why used a correction at the iteration step  $k$  by the  $\Delta x_n$  term:

$$x_n = x_{n-1} + \Delta x_n, \quad (4.2)$$

and assuming that the  $f(x_n) \approx 0$ . The function  $f(x_n)$  can be expanded in Taylor's series near  $x_{n-1}$ :

$$f(x_n) = f(x_{n-1} + \Delta x_n) = f(x_{n-1}) + \frac{df(x_{n-1})}{dx_{n-1}} \Delta x_n + \dots = 0. \quad (4.3)$$

The high order derivatives of the above Taylor's series are neglected, keeping only the linear terms (constant and first derivative term) and reformulation gives the following result:

$$-\frac{df(x_{n-1})}{dx_{n-1}} \Delta x_n = f(x_{n-1}). \quad (4.4)$$

The meaning of this equation can be seen in Fig. 4.2. At the starting point  $x_0$  determines the  $f(x_0)$  function value and the line tangent to the curve at the point  $(x_0, f(x_0))$ . Define  $x_1$  to be the point of intersection of the line tangent and the  $x$ -axis. The point of intersection  $x_1$  determines the function value  $f(x_1)$  and the line tangent to the curve at the point  $(x_1, f(x_1))$ , and the new point of intersection  $x_2$ . These steps are repeated until found the zero of  $f(x)$ , the  $f(c)$  point.

Reformulate the above equation and substitute in the equation (4.2), gives the well known formula of the Newton-Raphson method [23–25]:

$$x_n = x_{n-1} - \frac{f(x_{n-1})}{\frac{df(x_{n-1})}{dx_{n-1}}}. \quad (4.5)$$

The system of nonlinear equations with several variables is the follows:

$$\mathbf{f}(\mathbf{x}_n) = \mathbf{0}, \quad (n = 1, 2, \dots), \quad (4.6)$$

and the multidimensional expansion in Taylor's series near  $\mathbf{x}_{n-1}$  is:

$$\mathbf{f}(\mathbf{x}_n) = \mathbf{f}(\mathbf{x}_{n-1} + \Delta \mathbf{x}_n) = \mathbf{f}(\mathbf{x}_{n-1}) + \mathbf{J}_{|\mathbf{x}_{n-1}} \Delta \mathbf{x}_n + \dots = \mathbf{0}, \quad (4.7)$$

where  $\mathbf{J}$  is a Jacobian matrix,

$$\mathbf{J} = \frac{\partial \mathbf{f}(\mathbf{x}_{n-1})}{\partial \mathbf{x}_{n-1}}. \quad (4.8)$$

The general form of system of equations of nonlinear finite element method is the follows [12, 13, 29]:

$$\mathbf{S}(\mathbf{A})\mathbf{A} = \mathbf{u}, \quad (4.9)$$

where  $\mathbf{A} = [A_1 \dots A_n]^T$  the vector of unknown vector potentials,  $\mathbf{S}$  is a system matrix [6, 12, 13],

$$\mathbf{S} = S_{ij} = \int_{\Omega} \nu(\nabla N_i) \cdot (\nabla N_j) d\Omega, \quad (i, j = 1, \dots, n), \quad (4.10)$$

where  $N_i$  and  $N_j$  is a shape functions of nodal elements and  $n$  is the number of nodes. The  $\mathbf{u}$  is a vector with entries [6, 12, 13]

$$\mathbf{u} = u_i = \int_{\Omega} \vec{J}_0 \cdot (\nabla N_i) d\Omega, \quad (i = 1, \dots, n). \quad (4.11)$$

Reformulate the (4.9) equation results the system of residuum equations,

$$\mathbf{r}(\mathbf{A}) = \mathbf{S}(\mathbf{A})\mathbf{A} - \mathbf{u} = \mathbf{0}, \quad (4.12)$$

which has been handled like the (4.6) equation.

The residual term is gives like at the (4.4) equations, which can be written as:

$$\Delta \mathbf{A}_n = \mathbf{J}_{|\mathbf{A}_{n-1}}^{-1} \mathbf{r}(\mathbf{A}_{n-1}). \quad (4.13)$$

The equation (4.13) has to be used, the solution of  $\mathbf{A}_n$  is the following:

$$\mathbf{A}_n = \mathbf{A}_{n-1} + \Delta \mathbf{A}_n = \mathbf{A}_{n-1} + \mathbf{J}_{|\mathbf{A}_{n-1}}^{-1} \mathbf{r}(\mathbf{A}_{n-1}). \quad (4.14)$$

However, the Jacobian matrix  $\mathbf{J}$  never explicitly inverted in practical computing, because very difficult and lengthy. The nonlinear problem is thus converted to successive linear problems. At the step  $n$  of iteration, matrix  $\mathbf{J}$  is evaluated using the nodal values  $\mathbf{A}_{n-1}$  obtained at the preceding step.

The Jacobian matrix  $\mathbf{J}$  of the static magnetic field problem is obtained by differentiating the residual vector in 4.12 [12, 13],

$$\mathbf{J} = \frac{\partial \mathbf{r}(\mathbf{A})}{\partial \mathbf{A}} = \mathbf{S}(\mathbf{A}) + \frac{\partial \mathbf{S}(\mathbf{A})}{\partial \mathbf{A}} \mathbf{A}. \quad (4.15)$$

The Jacobian matrix from the above equations after some mathematical transformation is given by [12, 13]:

$$J_{ij} = S_{ij} + 2 \int_{\Omega} \frac{\partial \nu(B^2)}{\partial B^2} \left[ \nabla N_i \left( \sum_{l=1}^3 \vec{B}_l \right) \right] \left[ \nabla N_j \left( \sum_{m=1}^3 \vec{B}_m \right) \right] d\Omega. \quad (4.16)$$

The inverse of  $\mathbf{J}$  Jacobian matrix is more practical from the above system of linear equations.

The steps of one Newton-Raphson iteration, which can be shows Fig. 4.3 are:

- The initial condition of the method, when  $\vec{A} = \vec{0}$ ,  $\vec{B} = \vec{0}$  and  $\nu(B^2) = 0$ ;
- Assembling the system matrix  $\mathbf{S}$  and Jacobian matrix  $\mathbf{J}$  from the equation (4.16);
- Determine the residual term  $\Delta \mathbf{A}_n$  from the equation (4.13) by the gradient method [23, 25];
- Compute the vector  $\mathbf{A}_n$ , which contain the unknown potentials, from the equation (4.14);
- Calculate the  $B_x$  and  $B_y$  the components of magnetic flux density based on equation (3.1), determine the components of magnetic field intensity  $\vec{H}$  and reluctivity  $\nu_r$  from the nonlinear curve (Fig. 4.4). The MATLAB `interp1` [39] function has been used to determine the  $\nu_r$ ;

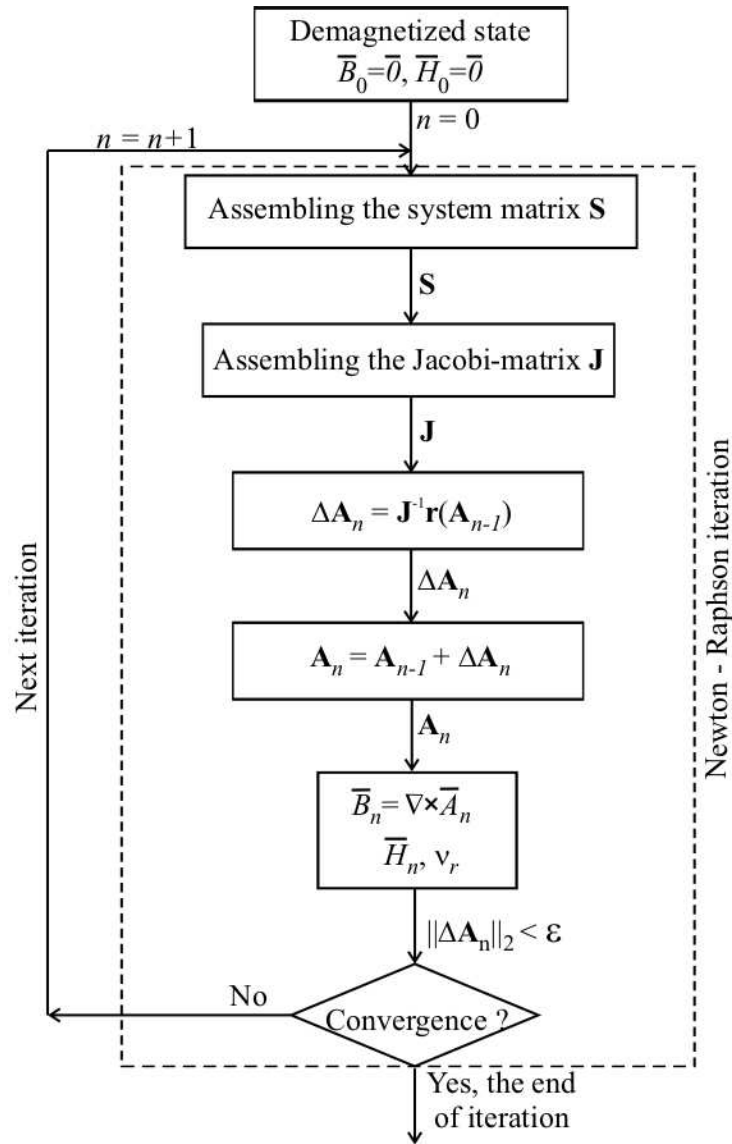


Fig. 4.3: Flowchart of the Newton-Raphson method.

- The iteration is repeated from the second step until the error is small enough. The value of the imposed error is  $\varepsilon = 10^{-6}$ . The error is computed from the vector norm of  $\Delta \mathbf{A}_n$ ,  $\|\Delta \mathbf{A}_n\|_2 < \varepsilon$ .

The convergence of the Newton-Raphson method is quadratic close to the solution of the nonlinear equations, this is why less than ten iteration are required for adequate precision. The nonlinear curve is monotonously increasing and its first derivative is continuous and monotonously decreasing, this is the minimal condition of the convergence of this method. These conditions are satisfied as you can see in Fig. 4.4.

## 4.2 The Polarization Method

The polarization method is shortly presented in this section, one can find more about this method in the publications: [6, 16, 26–29, 31–38]. This method is widely used in the

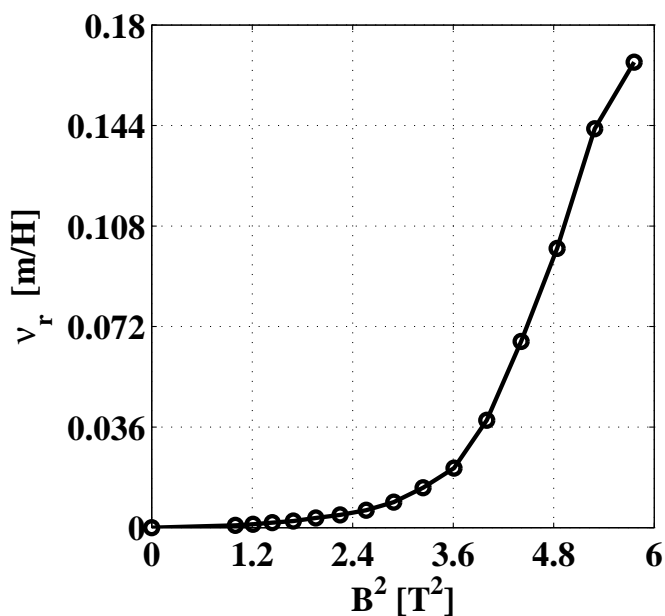


Fig. 4.4: The  $\nu_r$  relative reluctivity as a function of the  $B^2$  square magnetic flux density.

nonlinear electromagnetic field problems.

According to the polarization method, the magnetic flux density can be split into two parts as [6]

$$\vec{B} = \mathcal{B}\{\vec{H}\} = \mu_o\vec{H} + \beta, \tag{4.17}$$

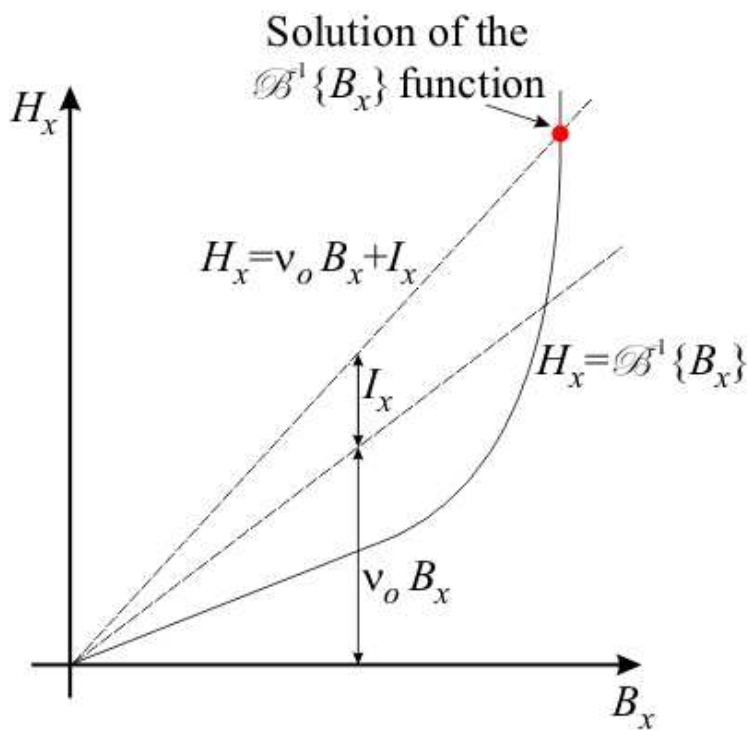


Fig. 4.5: The graphical form of the polarization method.

where  $\mu_o \vec{H}$  is a linear term, because  $\mu_o$  is supposed to be constant and nonlinearity is hidden in the second term  $\beta$ . The  $\beta$  nonlinear term is a magnetic flux density like quantity.

Multiply the relation (4.17) by  $\nu_o = 1/\mu_o$ , which results the equation  $\nu_o \vec{B} = \vec{H} - \nu_o \beta$ . The second, nonlinear term  $-\nu_o \beta$  is denoted by  $\vec{I}$  results the follows  $\nu_o \vec{B} = \vec{H} + \vec{I}$ . Reformulate of this relation gives the following [6, 26, 27, 29, 31, 34, 37]

$$\vec{H} = \nu_o \vec{B} + \vec{I} \quad (4.18)$$

constitutive relation. The denotation of this equation can be seen in Fig. (4.5).

Than mentioned in the chapter 2, the  $\nu_o$  reluctivity is the properly chosen constant, the optimal value of reluctivity. The value of  $\nu_o$  reluctivity [6, 33, 34, 37, 38]

$$\nu_o = \frac{\nu_{max} + \nu_{min}}{2} \quad (4.19)$$

where  $\nu_{max}$  and  $\nu_{min}$  are the maximum and minimum slope of the inverse nonlinear curve. It is evident that  $\mu_{max}$  and  $\mu_{min}$  are the maximum and minimum slope of the nonlinear curve (Fig. 4.1), where  $\nu_{max}=1/\mu_{min}$  and  $\nu_{min}=1/\mu_{max}$ .

### 4.3 Fixed Point Method

The fixed point method (or another name successive approximation) with polarization method has been used to solve the nonlinear partial differential equations of three-dimensional problem [6, 23–25, 29, 31–38].

The convergence of the fixed point technique is stable and robust, however much slower than the convergence of the Newton-Raphson method.

The fixed point method is based on the following form of nonlinear equation, which has been equivalent the equation (4.1) [6, 16, 23–25]

$$x = h(x), \quad (4.20)$$

which is usually called the fixed point from of nonlinear equation. The system of nonlinear equations can be represented by the vector valued function  $\mathbf{x}=h(\mathbf{x})$ .

In Fig. 4.6 the operation of the fixed point iterations is illustrated. In the figure, the fixed point equation  $x=h(x)$  is approximated by a simple function  $y=h(x)=x$ . The point denoted by  $c$ , where  $c=h(c)$ , is called fixed point, which is the solution of the nonlinear equation and it is the intersection point of the functions  $y=x$  and  $y=h(x)$ . The iteration can be started by any arbitrary point, for instance  $x_0$ , where  $y_0=h(x_0)$  can be calculated by using the function  $h(x)$ . Value  $y_0$  is the input of the second step of iteration, i.e.  $x_1=y_0=h(x_0)$ . This results in  $y_1=f(x_1)$  and  $x_2=y_1=h(x_1)$ . This iteration scheme can be generalized as

$$x_n = y_{n-1} = h(x_{n-1}), \quad (n = 1, 2, \dots). \quad (4.21)$$

The fixed point iteration is convergent, if the distance  $|x_n - x_{n-1}|$  is decreasing by increasing the index  $n$ . The condition

$$|x_n - x_{n-1}| < \varepsilon, \quad (4.22)$$

can be used to stop the iteration, where  $\varepsilon$  is a small positive real number.

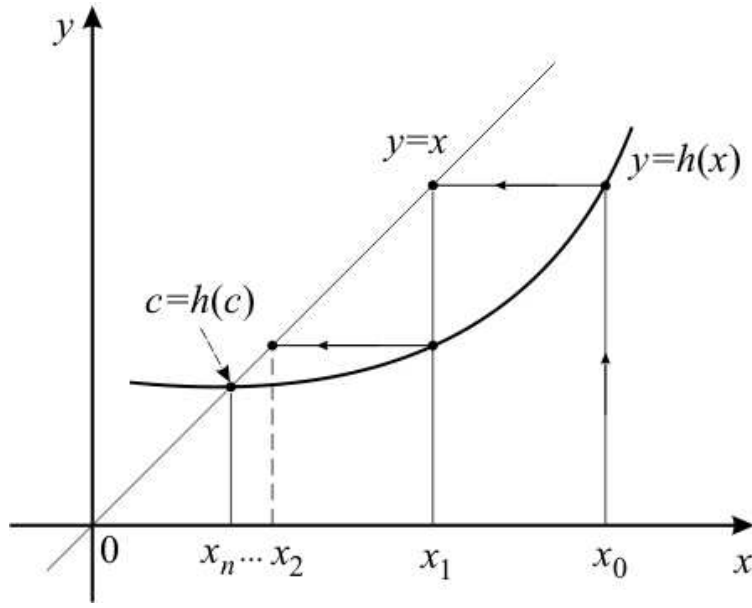


Fig. 4.6: The geometrical construction of fixed point method.

The fixed point scheme must satisfy some criteria for the convergence. The conditions of stable convergence of the fixed point iteration [6, 16, 23–25]:

The function  $h(x)$  of equation (4.20) is differentiable on the set of  $\mathbb{I}$ , which is the input (argument) of the function  $h$ , and differentiable on the set of  $\mathbb{O}$ , which is the output (value) of the function  $h$  and  $\mathbb{O}$  is the subset of  $\mathbb{I}$ , i.e.  $\mathbb{O} \subset \mathbb{I}$ . Furthermore, exist constant  $q < 1$ , which  $|h'(x)| \leq q$  for every  $x \in \mathbb{I}$ . In this case, the series (4.21) composed by starting  $x_0 \in \mathbb{I}$  point converged to the fixed point of the equation (4.20) in the set  $\mathbb{I}$ .

The presented fixed point method is the following in the finite element method for the simulated problem. The argument of the  $\vec{x}$  is the  $\vec{B}$  magnetic flux density and the functions is the  $\mathcal{B}^{-1}\{\cdot\}$  hysteresis operator. In this problem, the polarization method combined the fixed point scheme has been used to the approximation of the solution of the nonlinear equations.

The initial condition of the fixed point technique are as follows:  $\vec{B} = \vec{0}$ ,  $\vec{I} = \vec{0}$  and  $\vec{H} = \vec{0}$ . This is the demagnetized state of the magnetic material. Starting from this point, the magnetic flux density  $\vec{B}$  and the residual term  $\vec{I}$  can be determined using the iterative procedure, and by the hysteresis curve determine the  $\vec{H}$  magnetic field intensity.

In Fig. 4.7 the steps of fixed point scheme are shown, which as follows:

- Generate and solve the system of linear equations,  $\mathbf{SA} = \mathbf{u}$ , and determine the value of  $\vec{T}_0$  for all finite elements;
- Over again generate and solve the actual system of linear equations,  $\mathbf{SA} = \mathbf{u}$ . The constant system matrix  $\mathbf{S}$  is not changing during the iteration process, it is enough to calculate it once. The vector  $\mathbf{A}$  contains the nodal value of unknown potential;
- Determine the components of magnetic flux density ( $B_x, B_y, B_z$ ) of all finite elements by the equation (3.1);
- The components of magnetic field intensity of all finite elements can be obtained by the nonlinear curve in the Gaussian points. The MATLAB `interp1` [39] function

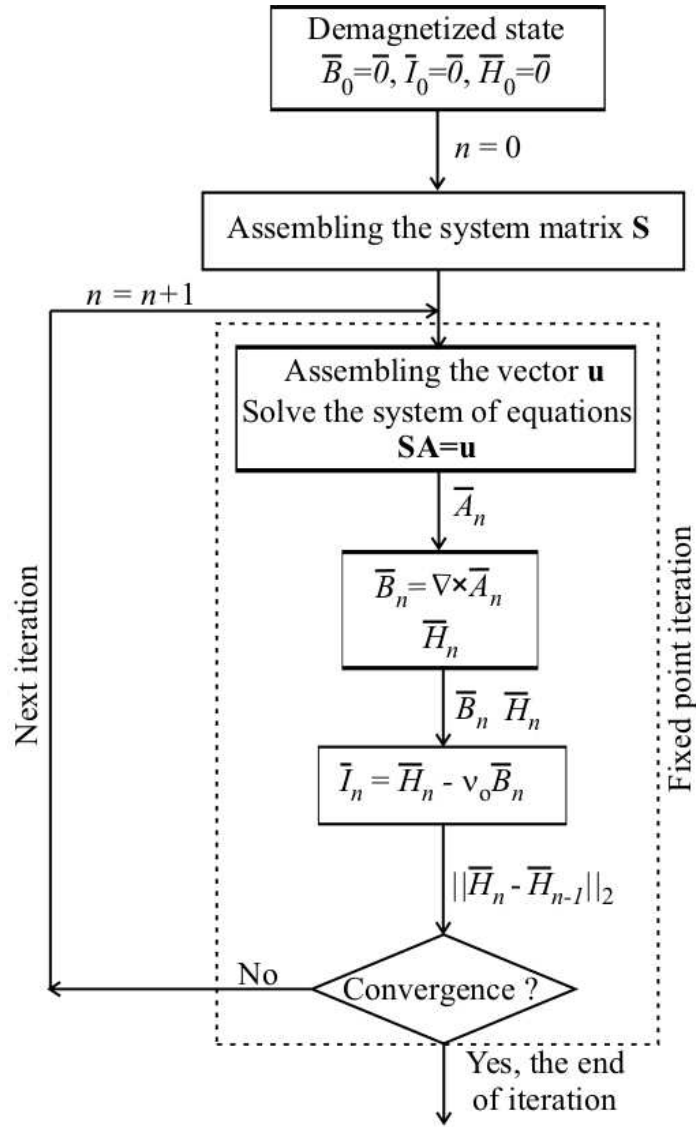


Fig. 4.7: Flowchart of the fixed point technique.

has been used to determine the components of  $\vec{H}$  from the nonlinear curve (Fig. 4.1);

- Determine the components of the nonlinear residual term  $\vec{I}$  in every finite element in the nonlinear region by the  $I_p = H_p - \nu_o B_p$  relations, where  $p = x, y, z$ ;
- Determine the error of the computation. The difference of the components of magnetic field intensity in the last two iteration steps is calculated in each finite elements and its vector norm is the error  $\varepsilon$ ,  $\|H_{p,n} - H_{p,n-1}\|_2 < \varepsilon$ , where  $p = x, y, z$ ;
- The iteration is repeated from the second step until the error is small enough. The value of the imposed error is  $\varepsilon = 10^{-6}$ , like in the Newton-Raphson method;

The value of the  $\nu_o$  optimal reluctivity is constant from the equation (4.19) through every iteration.

# Chapter 5

## The Finite Element Method

The basis of numerical techniques is to reduce the partial differential equations by using scalar and vector potentials to algebraic ones. These algebraic equations can be solved by numerical methods e.g. (3.39) [6–14, 16–18, 21]. This reduction can be done by discretizing the partial differential equations in time if necessary and in space. The potential functions, the approximation method and the generated mesh distinguish the numerical field solvers.

The Finite Element Method (FEM) is the most popular and the most flexible numerical technique to determine the approximate solution of the partial differential equations in engineering. For example, commercially available FEM software package is COMSOL Multiphysics [40] and the public domain program FEMM (Finite Element Method Magnetics) [41] for 2D fields which have been used in this work.

The COMSOL Multiphysics FEM software has the advantage that the weak formulation of a problem can be inserted easily and it is not necessary to implement mesh generators, solvers and postprocessors. These properties are very useful from the point of view of research, because the time consuming programming task can be eliminated.

### 5.1 Fundamentals of FEM

This section summarizes the FEM as a computer-aided design (CAD) technique in engineering sciences to obtain the electromagnetic field quantities in the case of static magnetic field problems. Here, I show the main steps of simulation with FEM. The main steps of simulation with FEM are illustrated in Fig. 5.1.

#### 5.1.1 Preprocessing

##### A. Model Specification

Firstly, in the model specification phase, the model of the problem, which simulation requires electromagnetic field calculations must be set up, i.e. the scientists of engineers have to find out the partial differential equations, which must be solved with prescribed boundary and continuity conditions. We have to find out, whether it is a nonmagnetic region, where the linear static magnetic field equations has been used, and which one is a magnetically nonlinear media region where has been used the nonlinear field equations, and how the characteristics of the materials look like. After selecting potentials, the

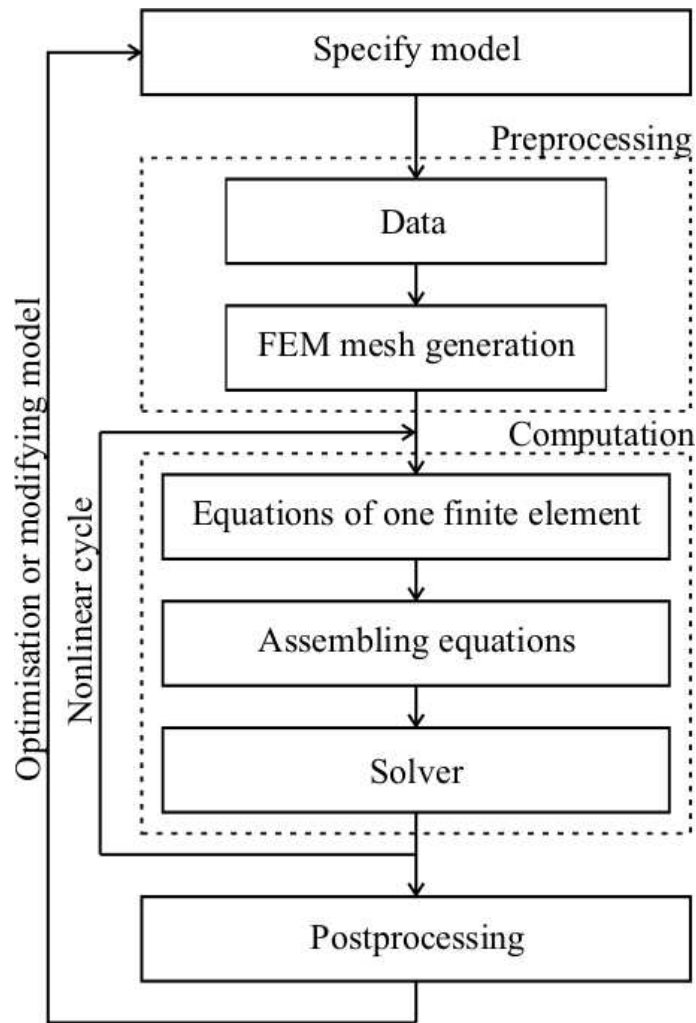


Fig. 5.1: Steps of simulation by finite element method.

weak formulation of these partial differential equations must be worked out as well. It is depending on the problem, of course, but the chosen mathematical model of the arrangement should be adequate to calculate electromagnetic field quantities in the given accuracy. The geometry of the problem must be defined by a CAD software tool.

The next step is the preprocessing task. Here, the values of different parameters have been given, such as the material properties, i.e. the relative permeability or reluctivity, the excitation signal like source current density  $\vec{J}_0$ . The geometry can be simplified according to symmetries or axial symmetries. In this work the symmetry plane has been used. The 2D problem is enough to simulate the half of the bearing, and in the 3D problem is enough to simulate the fourth of the arrangement because of symmetry plane.

This step is shown in Fig. 5.2. In this figure shows the three-dimensional radial magnetic bearing in the frame of COMSOL Multiphysics. Inside the geometry the magnetic flux density vectors can be seen. Right hand side of the geometry, the **Subdomain Settings** and the **Free Mesh Parameters** windows can be seen. In these windows the weak form of partial differential equations, the size of the mesh elements or mesh density can be set. The upper menu window show the important tool of postprocessing the **Plot Parameters** window, where the simulated data and electromagnetic quantities obtained from the potentials can also be simulated and plotted easily.

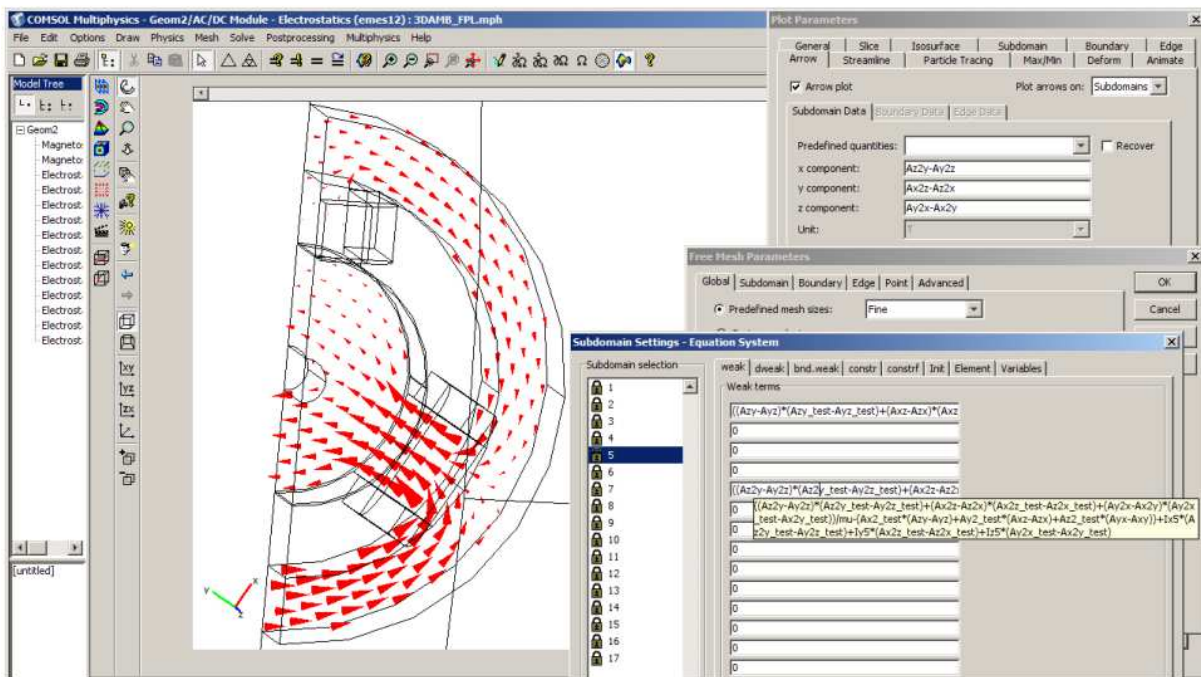


Fig. 5.2: The model specification in COMSOL Multiphysics.

### B. 2D Finite Element Mesh

In the preprocessing task the geometry of the problem must be discretized by a finite element mesh. The fundamental idea of FEM is to divide the problem region to be analyzed into smaller finite elements with given shape. A finite element can be triangles or quadrangles in two dimensions.

Fig. 5.3 and Fig. 5.4 shows the typical two-dimensional finite elements. In the figures denotes the normal numbers is the nodals, and the bold italic number is a edges. A linear triangular element (Fig. 5.3(a)) has three nodes 1, 2 and 3, here numbered anticlockwise and it has three edges. A quadratic triangular element (Fig. 5.4(a)) has six nodes and nine edges. The linear quadrangle element (Fig. 5.3(b)) has four nodes and four edges and the quadratic case has eight nodes and ten edges [6, 9–12].

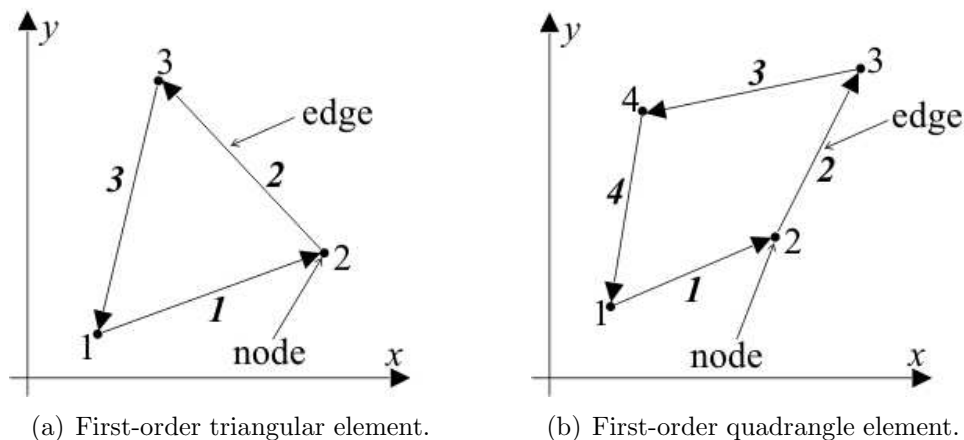


Fig. 5.3: Linear (first order) finite elements in the two-dimensional  $x - y$  plane.

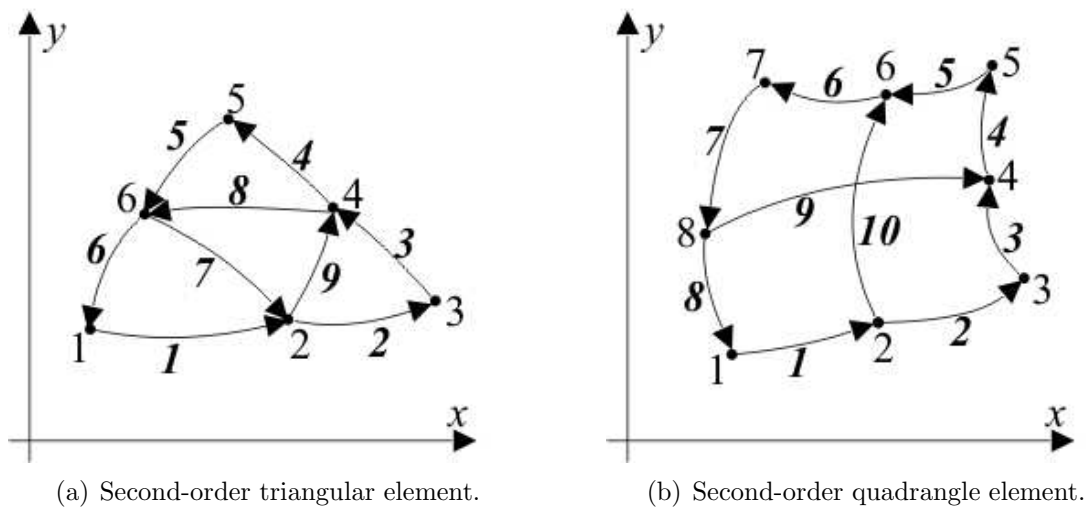


Fig. 5.4: Quadratic (second-order) finite elements in the two-dimensional  $x - y$  plane.

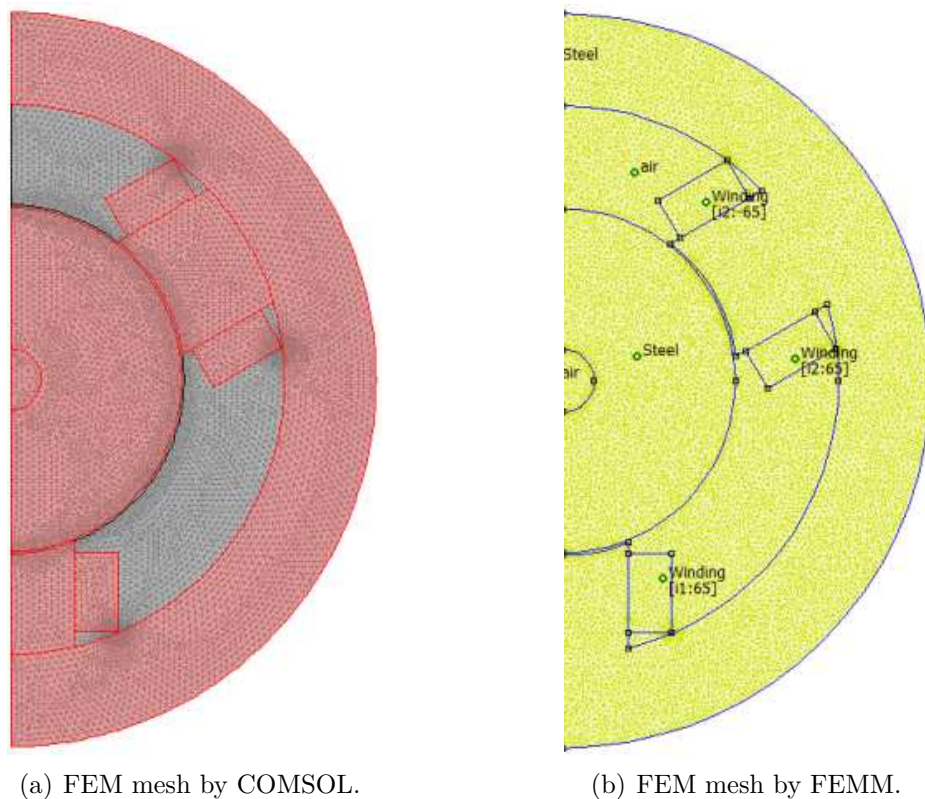


Fig. 5.5: The triangular discretization of the 2D magnetic bearing geometry.

FEM mesh, as illustration, generated by COMSOL multiphysics can be seen in Fig. 5.5(a). Fig 5.5(b) is illustrated the triangular FEM mesh generated by FEMM. Fig. 5.6 and Fig. 5.5. the enlarged regions of the magnetic bearing are shown. The arrangement of magnetic bearing has been discretized by a triangular elements as it is shown in Fig. 5.6. Fig. 5.6(b) shows the used five-layer mesh in the air gap, which has necessary for the better force calculation.

All the simulations have been studied using the same mesh in COMSOL Multiphysics,

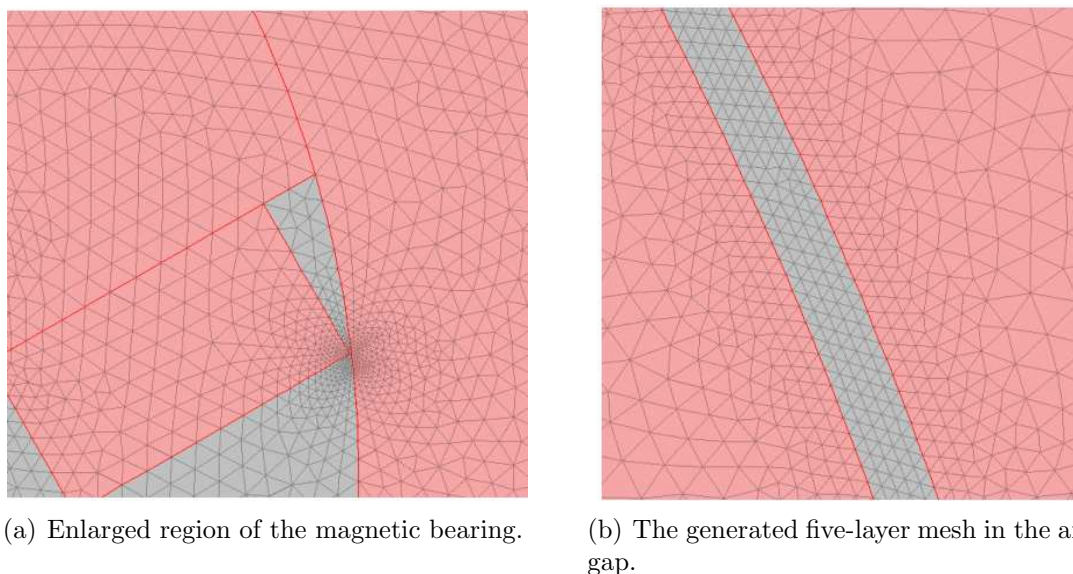


Fig. 5.6: Enlargement of the discretization.

which consists of 15829 second-order triangular elements as it can be seen on the left hand side of Fig. 5.6. Fig. 5.6 shows the half of the used mesh in the FEMM for the calculation which consists of 17387 second order triangular elements. The number of unknowns is 31930 and 34290 at COMSOL and FEMM respectively.

### C. 3D Finite Element Mesh

A finite element can be tetrahedron or hexahedron in three dimensions.

Fig. 5.7 shows the typical three-dimensional finite elements. A linear tetrahedron element(Fig. 5.7(a)) has four nodes and six edges. A linear hexahedron element (Fig. 5.4(a)) has eight nodes and twelve edges. In this work the quadratic form of tetrahedron elements has been used, which has ten nodes and twenty-four edges. Fig. 5.8 shows the discretization of the three-dimensional radial bearing geometry by quadratic tetrahedron elements.

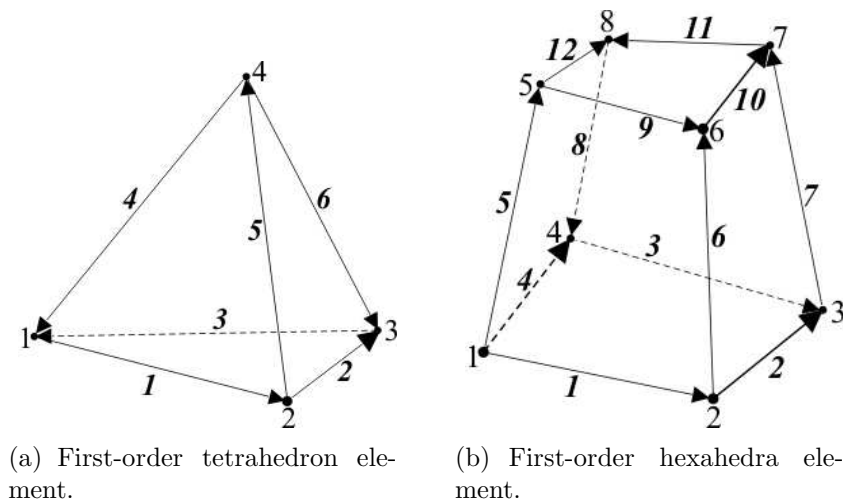


Fig. 5.7: Linear (first-order) finite elements in three dimensions.

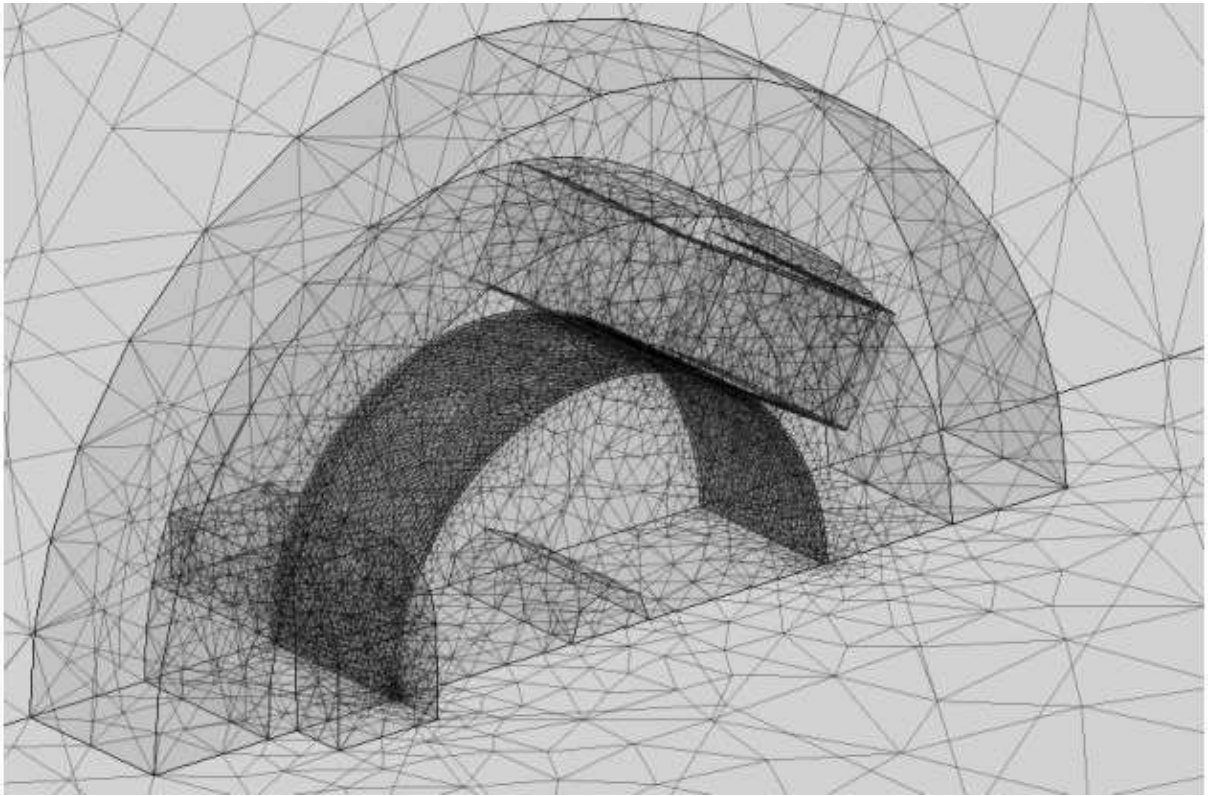


Fig. 5.8: The three-dimensional discretization of the bearing geometry.

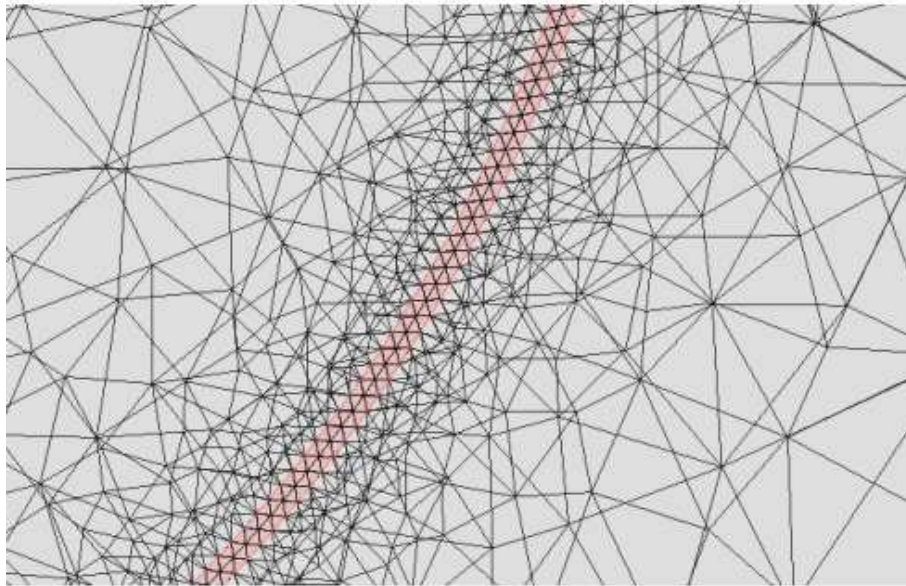


Fig. 5.9: The generated two-layer mesh in the air gap.

The used two-layer mesh in the air gap in three dimensions can be seen in Fig. 5.9. In the three-dimensional case the two-layer mesh is enough, because the calculated force using two- and three-layer mesh is nearly the same. However, the number of unknown is very high, if the three-layer mesh has been used in the air gap.

All the simulations have been studied using the same mesh in three dimensions. The

three-dimensional mesh consist of 86339 second-order tetrahedron elements, and the number of unknowns is 563528.

### 5.1.2 Shape Functions

The presented potential functions can be scalar valued, e.g. the 2D magnetic vector potential, or vector valued, e.g. the 3D magnetic vector potential  $\vec{A}$ , or the impressed current vector potential  $\vec{T}_0$ .

The scalar potential functions can be approximated by the so-called nodal shape functions  $N = N(\vec{r})$  and the vector potential functions can be approximated by either nodal or so-called vector shape functions, also called edge shape functions  $\vec{W} = \vec{W}(\vec{r})$ .

Generally, a shape function is a simple continuous polynomial function defined in a finite element and it is depending on the type of the used finite element.

Each shape function is defined in the entire problem region, and a scalar shape function corresponds to just one nodal point and each vector shape function corresponds to just one edge. Each scalar shape function is nonzero over just those finite elements that contain its nodal point and equals to zero over all other elements and each vector shape function is nonzero over just those finite elements that contain its edge and equals to zero over all other elements. Furthermore, the scalar shape function has a value unity at its nodal point and zero at all the other nodal points, and the line integral of a vector shape function is equal to one along its edge and the line integral of it is equal to zero along the other edges. Moreover the shape functions are linearly independent, i.e. no shape function equals a linear combination of the other shape functions.

The accuracy of solution obtained by FEM can be increased in three ways. The first one is called  $h$ -FEM, it is increasing the number of finite elements, i.e. decreasing the element size. The second way is called  $p$ -FEM, it is to increase the degree of polynomials building up a shape function. The third way is called  $hp$ -FEM, it is the mixture of the previous methods.

You can find more about the shape functions the next publications [6, 9–13, 18]

The 2D magnetic vector potential  $\vec{A}$  and source current density  $\vec{J}_0$  has been approximated by second order nodal shape function, and the 3D vector potentials, like  $\vec{A}$ ,  $\vec{T}_0$  have been approximated by second order edge shape function in this study.

### 5.1.3 Finite Element Simulation

The next step in FEM simulations is solving the problem. The FEM equations, based on the weak formulations [6, 10–13, 16], must be set up in the level of one finite element, then these equations must be assembled through the FEM mesh. Assembling means that the global system of equations is built up, which solution is the approximation of the introduced potential. The obtained global system of algebraic equations is linear, depending on the medium to be analyzed. Then this global system of equations must be solved by a solver. The computation may contain iteration, if the constitutive relations are nonlinear. This is the situation when simulating ferromagnetic materials with nonlinear characteristics. Iteration means that the system of equations must be set up and must be solved step by step until convergence is reached.

If the constitutive relations are nonlinear, the numerical computations were performed using computer programs developed under MATLAB environment using the

```

6 load Source.m;
7 load Hourve.m;
8
9 mu0 = 4*pi*1e-7;
10 mumax = 0.0015;
11 mumin = 7.5398e-6;
12 muopt = (mumax + mumin)/2;
13 nuopt = 1/muopt;
14 nu = 1/(1000*4*pi*1e-7);
15
16 fem.const(26) = num2str(1/nuopt);
17 fem.const(4) = num2str(5);
18
19 rng_Ix2 = find(asseminit(fem,'Init','Ix',1), 'Out','U');
20 rng_Iy2 = find(asseminit(fem,'Init','Iy',1), 'Out','U');
21 rng_Is2 = find(asseminit(fem,'Init','Is',1), 'Out','U');
22 rng_Ix5 = find(asseminit(fem,'Init','Ix5',1), 'Out','U');
23 rng_Iy5 = find(asseminit(fem,'Init','Iy5',1), 'Out','U');
24 rng_Is5 = find(asseminit(fem,'Init','Is5',1), 'Out','U');
25 rng_Ix8 = find(asseminit(fem,'Init','Ix8',1), 'Out','U');
26 rng_Iy8 = find(asseminit(fem,'Init','Iy8',1), 'Out','U');
27 rng_Is8 = find(asseminit(fem,'Init','Is8',1), 'Out','U');
28 rng_Ix15 = find(asseminit(fem,'Init','Ix15',1), 'Out','U');
29 rng_Iy15 = find(asseminit(fem,'Init','Iy15',1), 'Out','U');
30 rng_Is15 = find(asseminit(fem,'Init','Is15',1), 'Out','U');
31 rng_Ix = [rng_Ix2:rng_Ix5:rng_Ix8:rng_Ix15];
32 rng_Iy = [rng_Iy2:rng_Iy5:rng_Iy8:rng_Iy15];
33 rng_Is = [rng_Is2:rng_Is5:rng_Is8:rng_Is15];
34
35 Hxlast = zeros(length(rng_Ix),1);
36 Hylast = Hxlast;
37 Hzlast = Hxlast;
38
39 A = xmeshinfo(fem);
40 rng_xyz2 = find(A.nameinds==1);
41 xyz_specimen2 = A.coords(:,rng_xyz2);

```

Fig. 5.10: One part of the script of the fixed point technique.

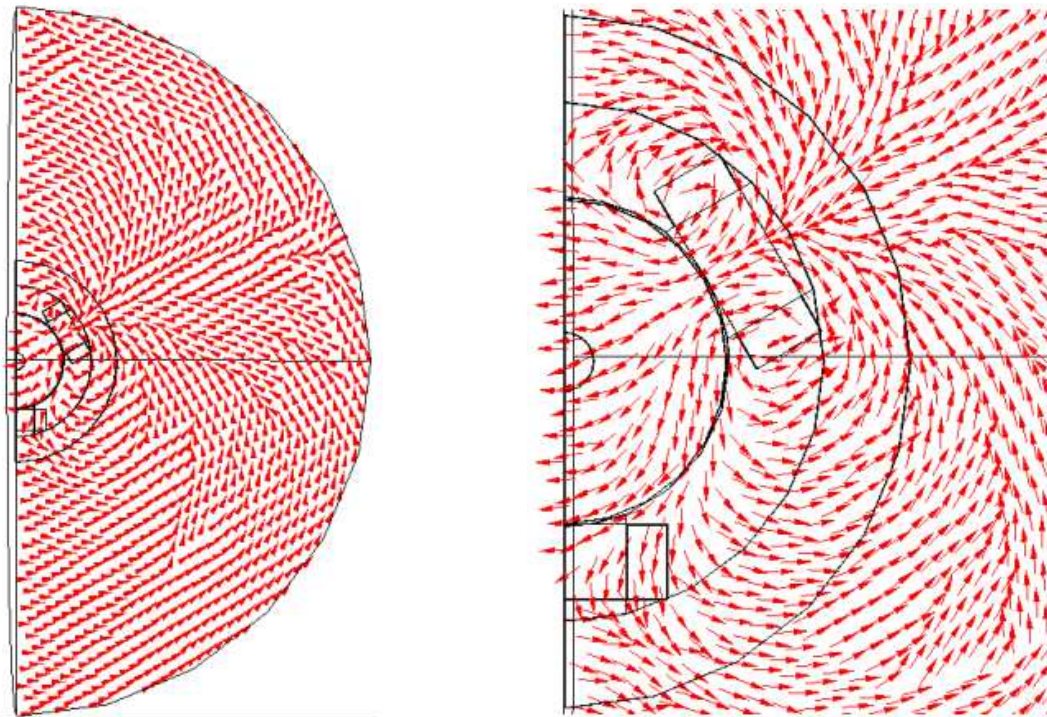
COMSOL script language. Fig. 5.10 shows one part of the nonlinear iteration script of the fixed point technique.

## A. Solvers

Generally, computation programs take into account the symmetry of the global matrix, and storing only the half of this matrix in the memory, because the system matrix  $\mathbf{S}$  is symmetrical.

In the two-dimensional linear  $\vec{A}$  - potential formulation, the vector potential function  $\vec{A}$  has been approximated by nodal shape function, i.e. the problem based on nodal finite elements have been solved by the direct solver UMFPACK (Unsymmetric MultiFrontal PACKage) solver [40, 42]. The nonlinear problem has been solved by the direct solver SPOOLES (SParse Object Oriented Linear Equations Solver) [40, 43].

In the three-dimensional  $\vec{A}$  - potential formulation, the current density  $\vec{J}_0$  of winding has been represented by the impressed current vector potential  $\vec{T}_0$  approximated by edge shape functions. The edge shape functions have been approximated by vector elements, and the iterative solver GMRES (Generalized Minimum Residual Method) solver [40, 44] with SSOR (Symmetric Successive Over-Relaxation) preconditioner [40, 45] has been applied. In Fig. 5.11 the normalized impressed current vector potential in the whole problem and in the magnetic bearing can be seen. In the three-dimensional case, the approximated vector potential function  $\vec{A}$  has been solved by the direct solver SPOOLES (SParse Object Oriented Linear Equations Solver) with linear and nonlinear  $\vec{B} - \vec{H}$  relationship. This solver used, because of the UMFPACK has been used much more memory than the SPOOLES, and as mentioned above, the number of unknowns in 3D, is more than 2D.



(a) The normalized  $\vec{T}_0$  in the whole problem.

(b) The normalized  $\vec{T}_0$  in the radial magnetic bearing.

Fig. 5.11: Representation of the impressed current vector potential  $\vec{T}_0$ .

The FEMM software has been used the Successive Approximation [9, 41] in linear case. In nonlinear case, the Conjugate Gradient [23, 41] with Newton-Raphson method has been used.

### 5.1.4 Postprocessing

The result of computations is the approximated potential values in the FEM mesh. Any electromagnetic field quantity (e.g. magnetic field intensity, magnetic flux density, etc.) can be calculated by using the potentials at the postprocessing stage. Loss, inductance, energy, force and other quantities can also be calculated. The postprocessing gives a chance to modify the geometry, the material parameters or the FEM mesh to get more accurate result.

In the  $\vec{A}$ -formulation the magnetic flux density  $\vec{B}$  is the primer quantity. The primer quantity coupled with e.g. constitutive relations gives the other quantities.

This section deals with the determination of the flux linkage and the electromagnetic force of the radial magnetic bearing in 2D and 3D.

#### A. Flux Linkage

The flux linkage  $\Psi$  is more useable in electrical machines (e.g. induction motor) than the flux  $\Phi$ .

The definition of flux  $\Phi$ : the surface integral of the perpendicular component of flux

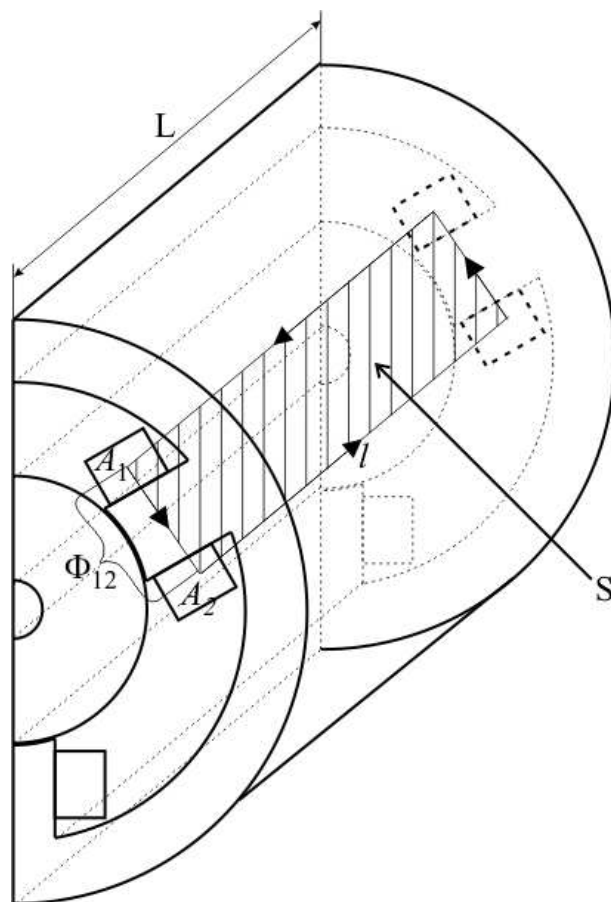


Fig. 5.12: The computation of flux linkage of magnetic bearing.

lines through an arbitrary area is the flux [7–9, 12, 15]:

$$\Phi = \int_S \vec{B} \cdot d\vec{S}, \quad (5.1)$$

namely the flux is given if the induction vector is integrated over the surface.

If the winding comprises  $N_w$  turns, and  $\Phi$  flux lines link with each turn, the product  $N_w \Phi$  is called flux linkage [7–9, 12, 15, 46], i.e.

$$\Psi = N_w \Phi = N_w \int_S \vec{B} \cdot d\vec{S}, \quad (5.2)$$

where  $N_w$  the number of turns of winding. After using the Stokes' theorem, the following equation can be obtained:

$$\Psi = N_w \int_S \vec{B} \cdot d\vec{S} = N_w \int_S (\nabla \times \vec{A}) \cdot d\vec{S} = N_w \oint_l \vec{A} \cdot d\vec{l}, \quad (5.3)$$

i.e. a line integral around the contour  $\vec{l}$  of the surface  $\vec{S}$ . This is shown in Fig. 5.12. However, the contribution of the ends to the integral zero, and the vector potential is constant in the axial direction. Thus, we have in 2D [12] :

$$\Phi_{12} = L (A_1 - A_2) \Rightarrow \Psi = N_w L (A_1 - A_2), \quad (5.4)$$

where  $L$  is the axial length of the bearing, which equals the equivalent core length of the bearing. The  $A_1$  and  $A_2$  denote the average values of the magnetic vector potential for the particular coil-end.

In the three-dimensional problem the equation (5.2) has been used the flux linkage computation.

## B. Electromagnetic Force

A precise analysis of a radial magnetic bearing requires the study of the interaction between mechanical and electrical quantities. The electromagnetic force plays a fundamental role in the corresponding energy conversation.

There are different methods, based in several formulations, to evaluate the force. One of these method the Maxwell's stress tensor method [9, 12, 17, 35, 47–49]. This is commonly used in the calculation of forces and torques in the numerical analysis of electrical devices.

The electromagnetic force is obtained as a surface integral, but in two-dimensional case the surface integral is reduced to a line integral along the air gap.

For the practical application of Maxwell's stress tensor, suppose that the magnetic field intensity  $\vec{H}$  is known on the surface  $S$  enclosing the rotor. It is also required that this body is located in air or within a material with permeability  $\mu = \mu_0$ . Fig. 5.13 shows the magnetic bearing, where  $\Gamma$  is a line along the air gap,  $\vec{n}$  is a unit vector. In 3D the  $\Gamma$  line is the  $S$  surface. The right hand side of Fig. 5.13 shows the force effect of an arbitrary elementary surface.

In the linear, isotropic material the matrix form of the Maxwell's stress tensor is the following [7, 8, 12, 15]

$$\bar{\bar{\mathbf{T}}}_m = \vec{H} \circ \vec{B} - \frac{1}{2}(\vec{H}\vec{B})\mathbf{1} = \begin{vmatrix} \mu H_x^2 - \frac{1}{2}\mu H^2 & \mu H_x H_y & \mu H_x H_z \\ \mu H_y H_x & \mu H_y^2 - \frac{1}{2}\mu H^2 & \mu H_y H_z \\ \mu H_z H_x & \mu H_z H_y & \mu H_z^2 - \frac{1}{2}\mu H^2 \end{vmatrix}, \quad (5.5)$$

where  $\bar{\bar{\mathbf{T}}}_m$  is a Maxwell's stress tensor,  $\vec{H} \circ \vec{B}$  is a dyadic multiplication of the two vectors  $\vec{H}$  and  $\vec{B}$ , while  $\mathbf{1}$  is a unit dyad (third-order identity matrix). From the formula (5.5), the force on the arbitrary oriented surface is the following:

$$\vec{\sigma} = \bar{\bar{\mathbf{T}}}_m \cdot \vec{n} = \mu_0(\vec{H} \cdot \vec{n})\vec{H} - 2\mu_0 H^2 \vec{n}, \quad (5.6)$$

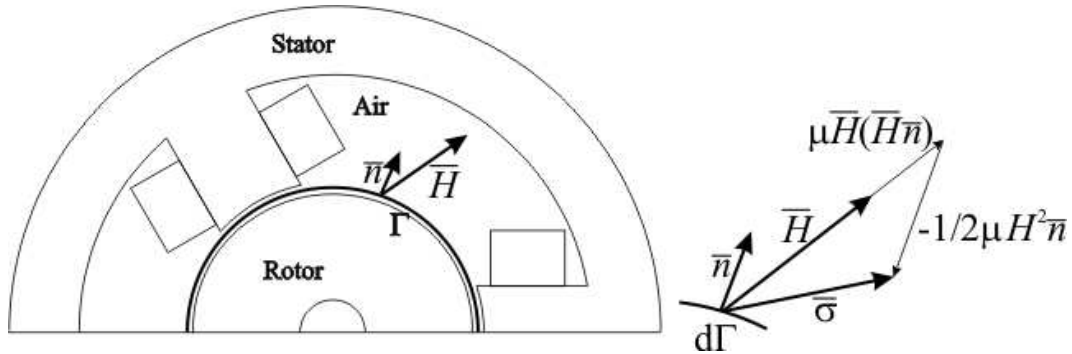


Fig. 5.13: The rotor under magnetic field surrounded by the surface  $\Gamma$  and the vector diagram of  $\vec{\sigma}$  stress tensor.

where  $\vec{\sigma}$  is the force,  $\vec{H}$  is the magnetic field intensity,  $H = |\vec{H}|$  is the length of the magnetic field intensity vector and  $\vec{n}$  is the unit normal vector of the arbitrary oriented surface (see in Fig. 5.13).

Substituting the relation  $\vec{H} = 1/\mu_0 \vec{B}$  into the equation (5.6) results in

$$\vec{\sigma} = \frac{1}{\mu_0}(\vec{B} \cdot \vec{n})\vec{B} - \frac{1}{2\mu_0}B^2\vec{n}, \quad (5.7)$$

where  $\vec{B}$  is the magnetic flux density and  $B = |\vec{B}|$  is the length of the magnetic flux density vector.

In the three-dimensional model the electromagnetic force is obtained as a surface integral over the surface in the airgap, around the rotor as [9, 12, 35, 47, 48]:

$$\vec{F} = \oint_S \vec{\sigma} dS = \oint_S \left[ \frac{1}{\mu_0}(\vec{B} \cdot \vec{n})\vec{B} - \frac{1}{2\mu_0}B^2\vec{n} \right] dS. \quad (5.8)$$

In the two-dimensional case the surface integral is reduced to a line integral along the air gap. In Fig. 5.13 shows this line as  $\Gamma$ . The formula of electromagnetic force in two dimensions is [9, 12, 17, 47, 48]:

$$\vec{F} = L \int_{\Gamma} \vec{\sigma} d\Gamma = L \int_{\Gamma} \left[ \frac{1}{\mu_0}(\vec{B} \cdot \vec{n})\vec{B} - \frac{1}{2\mu_0}B^2\vec{n} \right] d\Gamma, \quad (5.9)$$

where  $L$  is the axial length (the equivalent core length of the bearing). The axial length is  $L = 49.21$  mm.

# Chapter 6

## Numerical Optimization

Design of the radial magnetic bearing with the electromagnetic force over a given geometry parameters range is an example of an optimization problem. Rather than finding a single solution, optimization implies finding many solutions then selecting the best one. Optimization is an inherently slow, difficult procedure, but it is extremely useful when well done. The difficult problem of optimizing an electromagnetics design has only recently received extensive attention.

Usually the problem has a lot of local minima and only one global minima or local maxima and global maximum, it is depends to the problem. The optimization methods usually have been found a local minimum, and rarely the first global minimum. This is why very difficult to find the global minimum and very slowly the optimization procedure.

Different type optimization methods and its modifications has been used in the engineering sciences. Basicly, the genetic algorithm and its modifications have been used in geometry optimization technique in the machine design [4, 51, 52], however, there are a lot of another optimization techniques for the geometry design. One of these methods is the Nelder-Mead simplex search method (downhill simplex method or amoeba method) [53–59], which is a commonly used nonlinear optimization technique.

In this work the well known brute-force search and the above mentioned Nelder-Mead method have been used combining it with the finite element method for the geometry optimization of magnetic bearing.

Brute-force search is also useful as a basic method when benchmarking other algorithms, than now. The brute-force or exhaustive search combined with finite element analysis one of the simplest numerical way of the numerical geometry design. This problem-solving technique that consists of systematically enumerating all possible candidates for the solution and checking whether each candidate satisfies the statement of the problem. This method is simple to implement, and always found the solution. However, its computational cost is grow very quickly as the size of the problem increases, thus very slow.

First, in the next section the Nelder-Mead method presented, and after this the short description of the finite element based optimization for the magnetic bearing problem. In the end of this chapter the results of optimizations are presented and compared.

## 6.1 Nelder-Mead Simplex Search Algorithm

A Nelder-Mead simplex optimization algorithm is used in order to optimize the objective function. The simplex algorithm does not need a derivative, only a numerical evaluation of the objective function is required [53–59]. However, the convergence of the Nelder-Mead method is extremely sensitive to the selected starting point [55].

Its starting point is a simplex of dimension  $n + 1$  where  $n$  is the dimension of the problem. A simplex is a Euclidean geometric spatial element having the minimum number of boundary points, such as a line segment in one-dimensional space, a triangle in two-dimensional space or a tetrahedron in three-dimensional space. The algorithm can be implemented in  $n$  variables ( $n$ -dimensional), where simplex is a hypercube with  $n + 1$  vertex points. At every point the objective function is evaluated such as:  $f(x_1) < f(x_2) < \dots < f(x_{n+1})$ . The point where  $f(x_i)$  is the highest numerical value (worst vertex) of all three points is perpendicularly mirrored against the opposite plain segment. This called a reflection. The reflection can be accompanied with an expansion to take large steps or with a contraction to shrink the simplex where an optimization valley floor is reached. The optimization procedure continues until the termination criteria are met. The termination criterion is usually the maximum number of reflections with contractions or a tolerance for optimization variables [54, 56, 57].

In the next, the effect of the different operations of Nelder-Mead method are presented for a two-dimensional function based on [54, 57] as you can see Fig. 6.1.

### The Initial Trinagle

Let be  $f(x, y)$  the two-dimensional function that is to be minimize. Let gives the three vertices of a trinagle such as:  $\mathbf{B} = (x_1, y_1)$ ,  $\mathbf{G} = (x_2, y_2)$ ,  $\mathbf{W} = (x_3, y_3)$ , where  $\mathbf{B}$  is the best vertex,  $\mathbf{G}$  is a good vertex,  $\mathbf{W}$  is a worst vertex.

- ① *Midpoint of the Good Side:* The construction process uses the midpoint of the line segment joining  $\mathbf{B}$  and  $\mathbf{G}$ . It is found by averaging the coordinates:

$$\mathbf{M} = \frac{\mathbf{B} + \mathbf{G}}{2} = \left( \frac{x_1 + x_2}{2}, \frac{y_1 + y_2}{2} \right). \quad (6.1)$$

- ② *Reflection:* The function decreases when move along the side of the trinagle from  $\mathbf{W}$  to  $\mathbf{B}$ , and from  $\mathbf{W}$  to  $\mathbf{G}$ . Hence it is feasible that  $f(x, y)$  takes on smaller values at points that lie away from  $\mathbf{W}$  on the opposite side on the line between  $\mathbf{B}$  and  $\mathbf{G}$ . Let choose the test point  $\mathbf{R}$  (Reflection). To determine  $\mathbf{R}$ , we first find the midpoint  $\mathbf{M}$ . The draw the line segment from  $\mathbf{W}$  to  $\mathbf{M}$  and call its length  $d$ . This last segment is extended a distance  $d$  throught  $\mathbf{M}$  to locate the point  $\mathbf{R}$  (see Fig. 6.1(a)). The vector formula of reflection:

$$\mathbf{R} = \mathbf{M} + (\mathbf{M} - \mathbf{W}) = 2\mathbf{M} - \mathbf{W}. \quad (6.2)$$

- ③ *Expansion:* If the function value of  $\mathbf{R}$  is smaller than the function value at  $\mathbf{W}$ , then we have moved in the correct direction toward the minimum. Perhaps the minimum just a bit farther than the point  $\mathbf{R}$ . So we extended the line segment through  $\mathbf{M}$  and  $\mathbf{R}$  to the point  $\mathbf{E}$  (Expansion) (see Fig. 6.1(b)). This form an expanded triangle  $\mathbf{BGE}$ . The point  $\mathbf{E}$  is found by moving an additional distance

$d$  along the line joining  $\mathbf{M}$  and  $\mathbf{R}$ . If the function value at  $\mathbf{E}$  is less than the function value at  $\mathbf{R}$ , then  $\mathbf{E}$  is a better vertex point than  $\mathbf{R}$ . The vector formula of expansion:

$$\mathbf{E} = \mathbf{R} + (\mathbf{R} - \mathbf{M}) = 2\mathbf{R} - \mathbf{M}. \tag{6.3}$$

- ④ *Contraction*: If the  $\mathbf{R}$  and  $\mathbf{W}$  vertex points are the same, another point must be tested. Perhaps the function is smaller at  $\mathbf{M}$ , but cannot replace  $\mathbf{W}$  with  $\mathbf{M}$ , because it must have a triangle. Consider the two midpoint  $\mathbf{C}_1$  and  $\mathbf{C}_2$  of the line segments  $\mathbf{WM}$  and  $\mathbf{MR}$  respectively. The point with the smaller function value is called  $\mathbf{C}$  (Contraction), and the new triangle is  $\mathbf{BGC}$  (see Fig. 6.1(c)). If  $\mathbf{C}=\mathbf{C}_1$ , this is the inside contraction, if  $\mathbf{C}=\mathbf{C}_2$  is the outside contraction.
- ⑤ *Shrink*: If the function value at  $\mathbf{C}$  is not less than the value at  $\mathbf{W}$ , the points  $\mathbf{G}$  and  $\mathbf{W}$  must be shrunk toward  $\mathbf{B}$  (see Fig. 6.1(d)). The point  $\mathbf{G}$  is replaced with  $\mathbf{M}$ , and  $\mathbf{W}$  is replaced with  $\mathbf{S}$ , which is the midpoint of the line segment joining  $\mathbf{B}$  with  $\mathbf{W}$ .

A computation efficient algorithm should perform function evaluation only it needed.

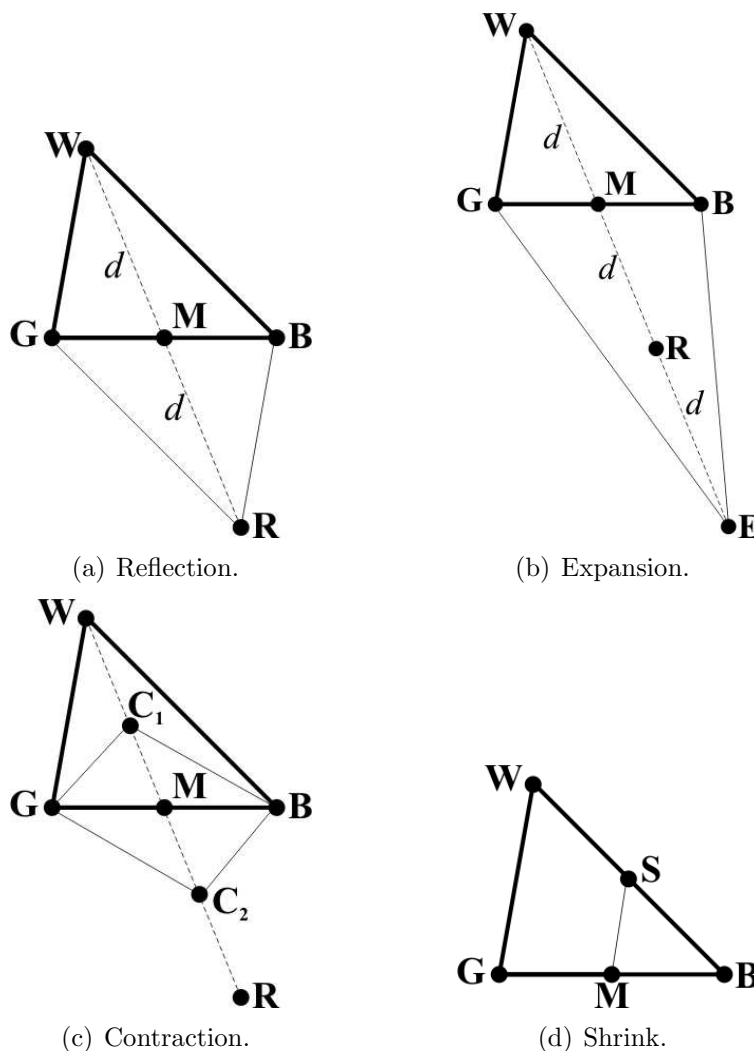


Fig. 6.1: Main operations of Nelder-Mead algorithm for a two-dimensional problem.

In each step, a new vertex is found, which replaces  $\mathbf{W}$ . The basic of used MATLAB program code of Nelder-Mead simplex method for a bi-dimensional function can be found in [54]

## 6.2 The FEM-Based Numerical Optimization

In this problem the  $n$  number of variables is five, i.e. the simplex is a hypercube with six vertex. The variables are the geometry parameters of magnetic bearing, the stator inner radius  $r_c$ , the stator yoke  $s_y$ , the rotor yoke  $r_y$ , the leg width  $w$  and the axial length  $L$ . This can be seen in Fig. 6.2.

The design of the radial magnetic bearing should satisfy the required performances and design constraints. The values which Table 6.1 presents are determined by an analytical approach and several empirically determined geometrical parameters. The numerical implementation of the equations and the relations of the analytical approach are very easy. The analytical approach is not present in this work, because not enough space and not of this main theme of this thesis. The analytical approach is based on the next publications, [4, 50, 60–62].

The assumptions that give rise to the error of analytical obtained results, but analytical results are very useful as initial design condition for the numerical optimization of the magnetic bearing geometry. The initial conditions of the numerical optimization methods shown in Table 6.1 have been used. The maximal bearing force  $\vec{F}_{max}$  is reached, when the currents  $I_2 = 10A$ ,  $I_1 = 0$ .

The FEM-based numerical optimizations described in the following steps:

- The geometry of the bearing is described parametrically and the initial parameter values. The bearing geometry parameters are: the stator inner radius  $r_c$  and stator

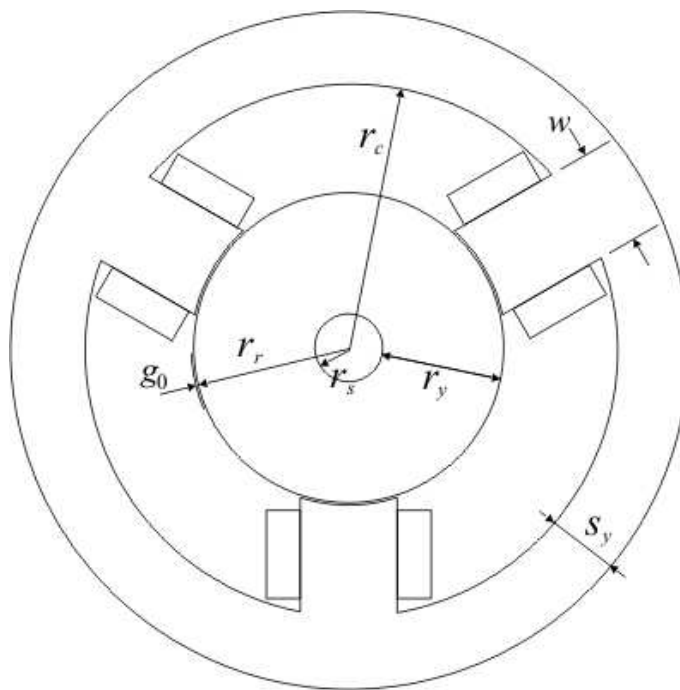


Fig. 6.2: The optimized parameter of the magnetic bearing.

Table 6.1: Required Performances and Design Constrains.

Parameters	Value
Maximal bearing force $\vec{F}_{max}$ [N]	780
Root mean square load force $\vec{F}_{RMS}$ [N]	250
Nominal air gap $g_0$ [mm]	0.5
Maximal stator radius $r_{s,max}$ [mm]	75
Shaft radius $r_s$ [mm]	7.5
Bias current $I_0$ [A]	5

yoke  $s_y$  the rotor yoke  $r_y$ , the leg width  $w$  (all shown in Fig. 6.2) and the bearing axial length  $L$ .

- The new parameter values are determined by the optimization method. The rotor position is at the bearing centre ( $x = 0$ ,  $y = 0$ ). The electromagnets are supplied in such a way that the RMS (root mean square) force is reached, i.e. by currents  $I_2 = 5A$ ,  $I_1 = 0$ .
- The bearing geometry, the material, the source current density and the boundary condition are defined. The procedure continues with Step 2 if the parameters of the bearing are outside the geometrical constraints.
- First, the FEM mesh is generated. Then the nonlinear solution of the magnetic vector potential by the 2D FEM computation is obtained using UMFPACK (Unsymmetric MultiFrontal PACKage) solver and Newton-Raphson method.
- The electromagnetic force is calculated by Maxwell's stress tensor method, (5.9).
- The value of the objective function is minimized in the optimization procedure. The optimization proceeds with Step 2 until the termination criteria is reached or found the best geometrical parameter values.

These steps have been used the brute-force search and the Nelder-Mead method combined by finite element method in the numerical geometry design of radial AMB. These steps shows the geometry optimization with nonlinear materials, but in the linear case only the forth step is difference. In linear case the solution of the magnetic vector potential by the 2D FEM computation is obtained using UMFPACK.

### 6.3 Optimization Results

Table 6.2 presents a comparison between geometry parameter values of the analytical, the brute-force (BF) search and the Nelder-Mead (NM) method. All design parameters are rounded off to one hundredth of a millimetre. The initial values are obtained from the analytical computation.

In linear case, the axial length is smaller when applying the brute-force search, and at the same time, the stator radius, stator yoke and leg width is smaller in the case of NM technique. The computation time of the Nelder-Mead method is far smaller, 3570 sec

Table 6.2: Data of the Optimized Design Parameters.

Parameters	Initial value	Linear		Nonlinear	
		BF	NM	BF	NM
Stator radius $r_s$ [mm]	82.0	75.0	72.04	75.00	71.09
Stator yoke $s_y$ [mm]	24.0	23.0	20.40	23.00	17.81
Rotor yoke $r_y$ [mm]	30.5	24.5	24.50	24.50	25.73
Leg width $w$ [mm]	26.0	25.0	21.80	23.10	21.26
Axial length $L$ [mm]	52.0	40.0	46.10	51.65	49.21
Maximal bearing force $\vec{F}_{max}$ [N]	780	830	806	783	780.3

than brute-force search computation time, 491820 sec. The Nelder-Mead method after 81 iterations found the solution, while the brute-force method has been repeated 138932 times, i.e. 44 and 3.54 second one iteration of the Nelder-Mead and the brute-force search method, respectively.

In nonlinear case, the rotor yoke is smaller when applying the brute-force search, and at the same time, the stator radius, stator yoke, leg width and axial length is smaller in the case of NM technique. Furthermore, the computation time of the Nelder-Mead method is far smaller, 14207 sec than brute-force search computation time, 240086 sec. The Nelder-Mead method after 209 iterations found the solution, while the brute-force method has been repeated 47190 times. One iteration of the NM method is nearly 68 second, and of the brute-force search is 5.08 second.

In linear and nonlinear case, the time of one iteration of NM method is larger, than brute-force search, however the number of iterations of NM method is less than the number of iterations of other method, namely the total computation time of NM method is much smaller, than BF search.

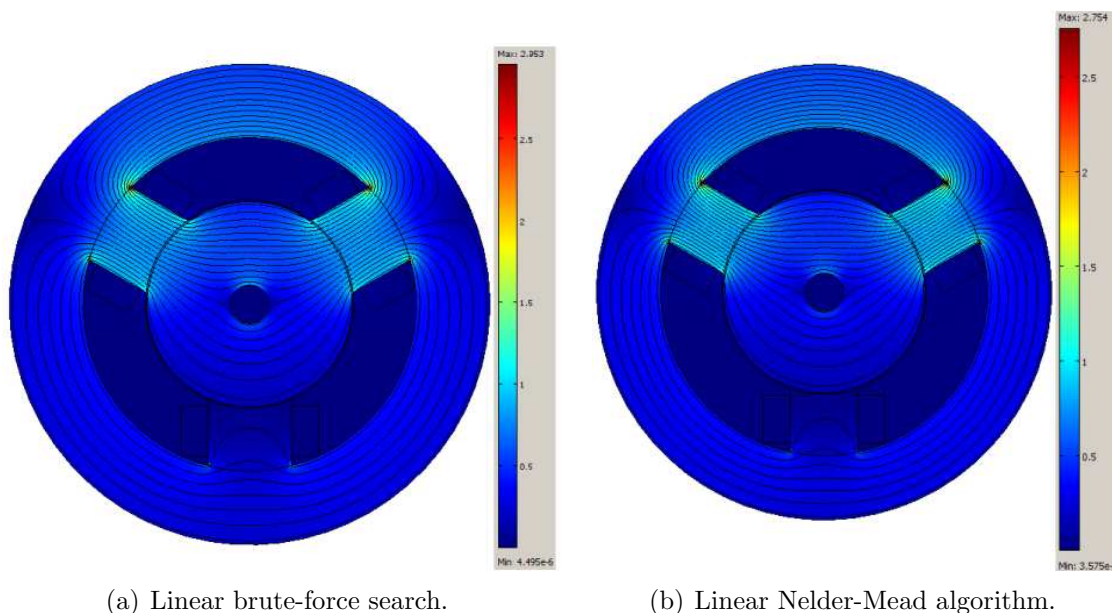


Fig. 6.3: Field plot of the result of the optimization methods in linear case.

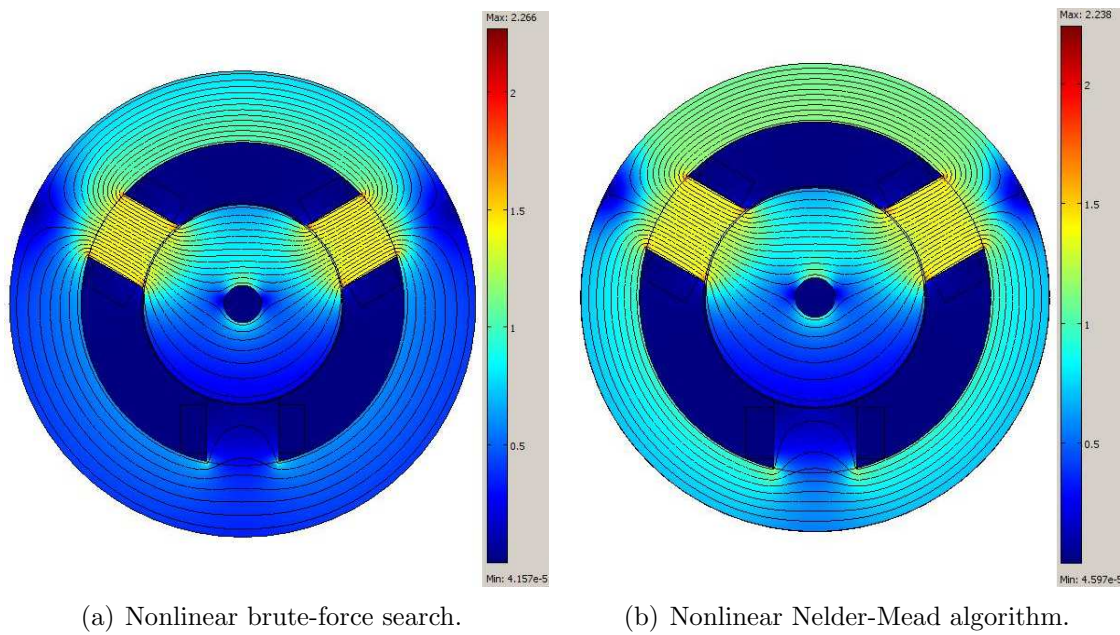


Fig. 6.4: Field plot of the result of the optimization methods in nonlinear case.

The results of the brute-force search method and Nelder-Mead optimization algorithm are illustrated in Fig. 6.3 and Fig. 6.4, respectively. These figures show the computed equipotential lines of the magnetic vector potential and surface distribution of the magnetic flux density in the radial magnetic bearing.

The further FEM simulations and analyses the forth magnetic bearing geometry has been used (see in Fig. 6.4(b)), which has been optimized by the Nelder-Mead algorithm with nonlinear media. On the whole, the geometry parameters of this bearing geometry is the best, because three geometry parameters is the smallest at this bearing, than the initial values, for example the  $r_s$  outer radius.

# Chapter 7

## Analytic Analysis of the Force

Faraday imagined that the effect of each magnet on the other could be represented by lines of magnetic force (i.e. magnetic field line) and that the attractive force was equivalent tension force along these lines. Thus one replaces the force acting between the bodies by stresses acting in the field between them. The total force on the surface given by the integration of these stresses over the  $S$  surface [1, 2, 61]:

$$\vec{F} \approx \int_S \frac{|\vec{B}|^2}{2\mu_0} d\vec{S}, \quad (7.1)$$

where  $\vec{B}$  is the magnetic flux density and  $|\vec{B}|$  is the length of the magnetic flux density vector.

This approximation is fine if the rotor material is highly permeable. The source of error comes from that component of the magnetic field which is not orthogonal to the surface of the ferromagnetic body.

The analytic calculation of these force is based on the lumped model of force. In the assumption, the  $S$  surface can be broken into  $a$  small parts, and  $\vec{B}$  is constant in each of these parts [1, 2, 61],

$$\vec{F} \approx \frac{1}{2\mu_0} \sum_{i=1}^a B_i^2 \vec{S}_i, \quad (7.2)$$

where  $\vec{S}_i$  is the outer normal vector of the  $i^{th}$  small part with magnitude equal to its area.

The analysis of force is generally performed using a fairly simple one-dimensional representation of the magnetic structure of the bearing. This approach is referred to as magnetic circuit analysis. Analogue to electrical circuit analysis [63], the approach simulates the iron elements as essentially waveguides from the magnetic fields established by the windings of magnetic bearing.

As such, this analysis tends to miss some effect, especially that part of the magnetic field which lies outside of the iron of the magnetic bearing. It also assumes field uniformity within large elements of the bearing. By making the assumptions that give rise to these errors, the analysis becomes very simple and quick, making it suitable for analytic evaluation and rapid design iteration. However, the predictions made with a magnetic circuit analysis have to be checked using a more detailed approach like finite element analysis [1, 61].

## 7.1 Lumped Model of Force

The analytical analysis of the force is based on the loop and node method [50,61]. The first step is identified the  $n_l$  independent flux loops and independent flux conservation nodes  $n_n$ . The number of independent equations is  $n_l + n_n = n_e$ . This is shown in Fig. 7.1.

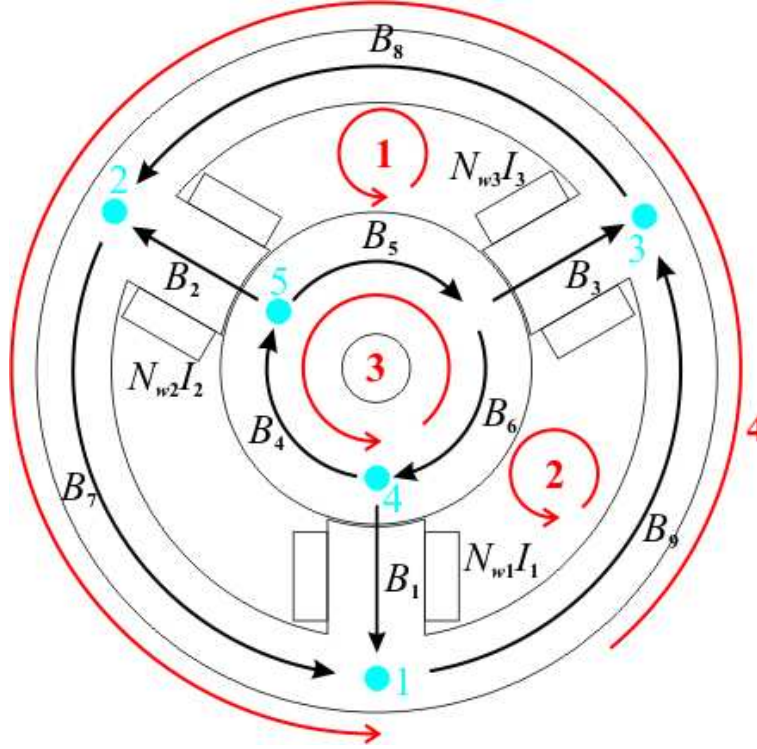


Fig. 7.1: Independent loops and nodes of Y-shaped magnetic bearing.

The number of independent loops is  $n_l=4$  (denoted by line in Fig 7.1). The four independent loop equations are the following [50]:

$$-B_2 \frac{g_2}{\mu_0} - B_2 \frac{l_2}{\mu_0 \mu_r} + B_5 \frac{l_5}{\mu_0 \mu_r} + B_3 \frac{g_3}{\mu_0} + B_3 \frac{l_3}{\mu_0 \mu_r} + B_8 \frac{l_8}{\mu_0 \mu_r} = N_{w2} I_2 - N_{w3} I_3, \quad (7.3)$$

$$-B_3 \frac{g_3}{\mu_0} - B_3 \frac{l_3}{\mu_0 \mu_r} + B_6 \frac{l_6}{\mu_0 \mu_r} + B_1 \frac{g_1}{\mu_0} + B_1 \frac{l_1}{\mu_0 \mu_r} + B_9 \frac{l_9}{\mu_0 \mu_r} = N_{w3} I_3 - N_{w1} I_1, \quad (7.4)$$

$$B_4 \frac{l_4}{\mu_0 \mu_r} + B_5 \frac{l_6}{\mu_0 \mu_r} + B_6 \frac{l_6}{\mu_0 \mu_r} = 0, \quad (7.5)$$

$$B_7 \frac{l_7}{\mu_0 \mu_r} + B_8 \frac{l_8}{\mu_0 \mu_r} + B_9 \frac{l_9}{\mu_0 \mu_r} = 0, \quad (7.6)$$

where  $B_i$  is the unknown magnetic flux density value,  $g_j$  are the air gaps,  $l_i$  is the flux flow length of the iron part,  $N_{wj}$  is the number of turns of winding and  $I_j$  is the current ( $i = 1, \dots, 9$ ,  $j = 1, 2, 3$ ).

The determination of the nine unknowns magnetic flux  $B_i$  ( $i = 1, \dots, 9$ ) into the system of equations consist of nine equations. This is why the five independent flux

conservation nodes are needed. The independent flux conservation nodes denoted by point in Fig. 7.1. The node equations are the following [50]:

$$-B_1 S_1 - B_7 S_7 + B_9 S_9 = 0, \quad (7.7)$$

$$-B_2 S_2 - B_8 S_8 + B_7 S_7 = 0, \quad (7.8)$$

$$-B_3 S_3 - B_9 S_9 + B_8 S_8 = 0, \quad (7.9)$$

$$-B_6 S_6 + B_4 S_4 + B_1 S_1 = 0, \quad (7.10)$$

$$-B_4 S_4 + B_2 S_2 + B_5 S_5 = 0, \quad (7.11)$$

where  $S_i$  is a surface patch, where the magnetic flux density assumed to be constant, e.g.  $S_1 = L \cdot w_1$ , where  $L$  is the axial length and  $w_1$  is the width of Pole # 1 ( $i = 1, \dots, 9$ ).

Summarize the loop and node equations in the form of  $\mathcal{R}$  impedance and  $\mathcal{N}$  linkage matrices [50, 61]:

$$\mathcal{R} = \frac{1}{\mu_0} \begin{bmatrix} 0 & -g_2 - \frac{l_2}{\mu_r} & g_3 + \frac{l_3}{\mu_r} & 0 & \frac{l_5}{\mu_r} & 0 & 0 & \frac{l_8}{\mu_r} & 0 \\ g_1 + \frac{l_1}{\mu_r} & 0 & -g_3 - \frac{l_3}{\mu_r} & 0 & 0 & \frac{l_6}{\mu_r} & 0 & 0 & \frac{l_9}{\mu_r} \\ 0 & 0 & 0 & \frac{l_4}{\mu_r} & \frac{l_5}{\mu_r} & \frac{l_6}{\mu_r} & 0 & 0 & 0 \\ 0 & 0 & 0 & 0 & 0 & 0 & \frac{l_7}{\mu_r} & \frac{l_8}{\mu_r} & \frac{l_9}{\mu_r} \\ -S_1 & 0 & 0 & 0 & 0 & 0 & -S_7 & 0 & S_9 \\ 0 & -S_2 & 0 & 0 & 0 & 0 & S_7 & -S_8 & 0 \\ 0 & 0 & -S_3 & 0 & 0 & 0 & 0 & S_8 & -S_9 \\ S_1 & 0 & 0 & S_4 & 0 & -S_6 & 0 & 0 & 0 \\ 0 & S_2 & 0 & -S_4 & S_5 & 0 & 0 & 0 & 0 \end{bmatrix}$$

$$\mathcal{N} = \begin{bmatrix} 0 & N_{w2} & -N_{w3} \\ -N_{w1} & 0 & N_{w3} \\ 0 & 0 & 0 \\ 0 & 0 & 0 \\ 0 & 0 & 0 \\ 0 & 0 & 0 \\ 0 & 0 & 0 \\ 0 & 0 & 0 \\ 0 & 0 & 0 \end{bmatrix}$$

From the  $\mathcal{R}$  impedance matrix emphasized the  $1/\mu_0$ , because the division by  $\mu_0$  does not change the value of node equations.

The unknowns magnetic fluxes gives the following matrix equation [50, 61]:

$$\underline{B} = \mathcal{R}^{-1} \mathcal{N} \underline{I}, \quad (7.14)$$

where  $\underline{B}$  is the column vector of unknown magnetic fluxes,  $\underline{I}$  is the column vector of currents and  $\mathcal{R}^{-1}$  is the inverse of  $\mathcal{R}$  impedance matrix.

After these, the  $\mathcal{A}_x$  and  $\mathcal{A}_y$  force summation matrices must be constructed. Fig. 7.2 shows the forces generated by the electromagnets of bearing. The force  $\mathbf{F}_2$  and force  $\mathbf{F}_3$

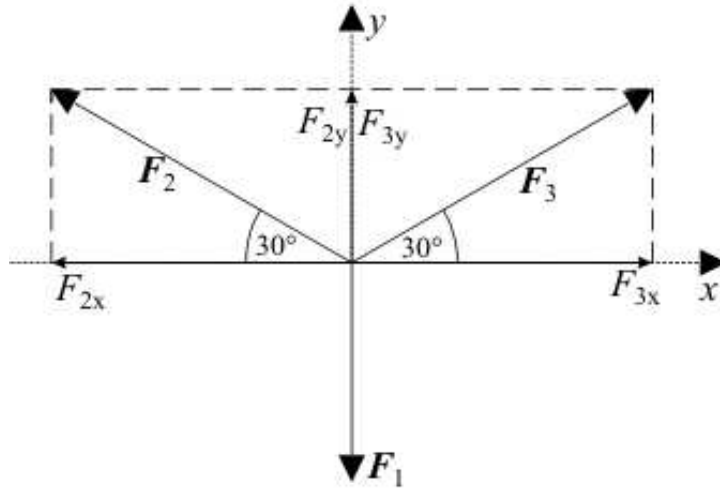


Fig. 7.2: The force vectors and its components of magnetic bearing.

must be decomposed into the  $x$  and  $y$  components. These components are very easy to determine by the sine and cosine function.

The  $x$  directed force can be generated by the second and the third pole. These forces are taken in the properly place in the  $\mathcal{A}_x$  matrix, like the  $F_{x2}$  force take in the second column of the second row:

$$\mathcal{A}_x = \frac{1}{2\mu_0} \begin{bmatrix} 0 & 0 & 0 & 0 & 0 & 0 & 0 & 0 & 0 \\ 0 & -S_2 \cos(30^\circ) & 0 & 0 & 0 & 0 & 0 & 0 & 0 \\ 0 & 0 & S_3 \cos(30^\circ) & 0 & 0 & 0 & 0 & 0 & 0 \\ 0 & 0 & 0 & 0 & 0 & 0 & 0 & 0 & 0 \\ 0 & 0 & 0 & 0 & 0 & 0 & 0 & 0 & 0 \\ 0 & 0 & 0 & 0 & 0 & 0 & 0 & 0 & 0 \\ 0 & 0 & 0 & 0 & 0 & 0 & 0 & 0 & 0 \\ 0 & 0 & 0 & 0 & 0 & 0 & 0 & 0 & 0 \\ 0 & 0 & 0 & 0 & 0 & 0 & 0 & 0 & 0 \end{bmatrix}$$

The  $\mathcal{A}_y$  matrix contain the  $y$  components of the force:

$$\mathcal{A}_y = \frac{1}{2\mu_0} \begin{bmatrix} -S_1 & 0 & 0 & 0 & 0 & 0 & 0 & 0 & 0 \\ 0 & S_2 \sin(30^\circ) & 0 & 0 & 0 & 0 & 0 & 0 & 0 \\ 0 & 0 & S_3 \sin(30^\circ) & 0 & 0 & 0 & 0 & 0 & 0 \\ 0 & 0 & 0 & 0 & 0 & 0 & 0 & 0 & 0 \\ 0 & 0 & 0 & 0 & 0 & 0 & 0 & 0 & 0 \\ 0 & 0 & 0 & 0 & 0 & 0 & 0 & 0 & 0 \\ 0 & 0 & 0 & 0 & 0 & 0 & 0 & 0 & 0 \\ 0 & 0 & 0 & 0 & 0 & 0 & 0 & 0 & 0 \\ 0 & 0 & 0 & 0 & 0 & 0 & 0 & 0 & 0 \end{bmatrix}$$

The  $1/2\mu_0$  term is needed because of the equation (7.2). The matrix equations of the  $x$  and  $y$  components of the force are the following [50, 61]:

$$f_x = \underline{B}^T \mathcal{A}_x \underline{B}, \quad (7.17)$$

$$f_y = \underline{B}^T \mathcal{A}_y \underline{B}, \quad (7.18)$$

where  $\underline{B}^T$  is the transposed of the  $\underline{B}$  matrix. Furthermore, here  $f_x$  and  $f_y$  are the scalar value.

The next step is establish the relationship between the air gaps and the rotor positions. The relationships are the follows [50, 61]:

$$g_1 = g_0 + y, \quad (7.19)$$

$$g_2 = g_0 + \cos(30^\circ)x - \sin(30^\circ)y, \quad (7.20)$$

$$g_3 = g_0 - \cos(30^\circ)x - \sin(30^\circ)y, \quad (7.21)$$

where  $g_0$  is a nominal air gap,  $x$  and  $y$  is the excursion of the rotor in the  $x$ ,  $y$  direction.

Lets take some simplification the above defined matrices. That the areas are equal at the poles  $S_1 = S_2 = S_3 = S_I$ , at the rotor  $S_4 = S_5 = S_6 = S_{II}$  and at the stator  $S_7 = S_8 = S_9 = S_{III}$ . Further, the coils all have the same number of turns  $N_{w1} = N_{w2} = N_{w3} = N_w$ . Finally, that the iron length in the back iron is same at the poles  $l_1 = l_2 = l_3 = l_I$ , at the rotor  $l_4 = l_5 = l_6 = l_{II}$  and at the stator  $l_7 = l_8 = l_9 = l_{III}$ . However, these equalities is not unconditionally in the magteic bearing. For example, the turns of windings are not same or the area of poles are different.

Forasmuch, the number of turns are the same, hence the  $N_w$  emphasize from the  $\mathcal{N}$  linkage matrix:

$$\mathcal{N} = N_w \begin{bmatrix} 0 & 1 & -1 \\ -1 & 0 & 1 \\ 0 & 0 & 0 \\ 0 & 0 & 0 \\ 0 & 0 & 0 \\ 0 & 0 & 0 \\ 0 & 0 & 0 \\ 0 & 0 & 0 \\ 0 & 0 & 0 \end{bmatrix}$$

The  $\mathcal{A}_x$  and  $\mathcal{A}_y$  force summation matrices are possible simplifying. The  $S_I$  term and the reults of the sine and cosine function ( $\cos(30^\circ) = \sqrt{3}/2$  and  $\sin(30^\circ) = 1/2$ ) emphasize from the matrices:

$$\mathcal{A}_x = \frac{S_I \sqrt{3}}{4\mu_0} \begin{bmatrix} 0 & 0 & 0 & 0 & 0 & 0 & 0 & 0 & 0 \\ 0 & -1 & 0 & 0 & 0 & 0 & 0 & 0 & 0 \\ 0 & 0 & 1 & 0 & 0 & 0 & 0 & 0 & 0 \\ 0 & 0 & 0 & 0 & 0 & 0 & 0 & 0 & 0 \\ 0 & 0 & 0 & 0 & 0 & 0 & 0 & 0 & 0 \\ 0 & 0 & 0 & 0 & 0 & 0 & 0 & 0 & 0 \\ 0 & 0 & 0 & 0 & 0 & 0 & 0 & 0 & 0 \\ 0 & 0 & 0 & 0 & 0 & 0 & 0 & 0 & 0 \\ 0 & 0 & 0 & 0 & 0 & 0 & 0 & 0 & 0 \end{bmatrix}$$

$$\mathcal{A}_y = \frac{S_I}{4\mu_0} \begin{bmatrix} -2 & 0 & 0 & 0 & 0 & 0 & 0 & 0 & 0 \\ 0 & 1 & 0 & 0 & 0 & 0 & 0 & 0 & 0 \\ 0 & 0 & 1 & 0 & 0 & 0 & 0 & 0 & 0 \\ 0 & 0 & 0 & 0 & 0 & 0 & 0 & 0 & 0 \\ 0 & 0 & 0 & 0 & 0 & 0 & 0 & 0 & 0 \\ 0 & 0 & 0 & 0 & 0 & 0 & 0 & 0 & 0 \\ 0 & 0 & 0 & 0 & 0 & 0 & 0 & 0 & 0 \\ 0 & 0 & 0 & 0 & 0 & 0 & 0 & 0 & 0 \\ 0 & 0 & 0 & 0 & 0 & 0 & 0 & 0 & 0 \end{bmatrix}$$

The  $\underline{I}$  current vectors is define as the follows:

$$\underline{I} = \mathcal{C}\hat{\underline{I}} = \mathcal{C} \begin{bmatrix} i_{ex} \\ i_{ey} \\ i_b \end{bmatrix}$$

where  $I_b$  is the bias current,  $i_{ex}$  is the control current of  $x$  direction and  $i_{ey}$  is the control current of  $y$  direction, respectively. The  $\mathcal{C}$  current selection matrix is the following [50]:

$$\mathcal{C} = \begin{bmatrix} 0 & 1 & 0 \\ \cos(30^\circ) & -\sin(30^\circ) & 1 \\ -\cos(30^\circ) & -\sin(30^\circ) & -1 \end{bmatrix}$$

which is unequivocally results from the  $\mathcal{A}_x$  and  $\mathcal{A}_y$  matrix.

The matrix equations of the forces substitute the equation (7.14) into the equation (7.17) and into the equation (7.18) are the followings [50,61]:

$$f_x = \underline{I}^T \mathcal{N}^T \mathcal{R}^{-T} \mathcal{A}_x \mathcal{R}^{-1} \mathcal{N} \underline{I}, \quad (7.27)$$

$$f_y = \underline{I}^T \mathcal{N}^T \mathcal{R}^{-T} \mathcal{A}_y \mathcal{R}^{-1} \mathcal{N} \underline{I}. \quad (7.28)$$

From these equations the forces can be easily determined. If according the geometry parameters of radial bearing, because the forces are the only unknowns in these relations.

The equations which are presented in this chapter are very easy and fast to implemented in a computer procedure or script like into MATLAB function [39]. The implemented script is very useful in the geometry optimisation of the magnetic bearing. However, the simplifications of the equations necessary check the result by a more detailed approach like finite element analysis.

# Chapter 8

## Solution of the Problem

The above sections show the used potential formulation, and its weak formulation, the used nonlinear equation solvers and the computation of the secondary quantities, like flux linkage and electromagnetic force in two and three dimensions.

After the problem solution, the results evaluation, visualization, e.g. the postprocessing follow. In this chapter the results of simulations have been compared with each other. First, the linear, after the nonlinear results are introduced. For the comparison of the two- and three-dimensional results, the value of magnetic flux density along the line inside the simulated magnetic bearing. The computed flux linkage and electromagnetic force are represent the function of current and of the displacement of the rotor. The flux linkage and electromagnetic force, which are computed by the 2D finite element software, FEMM as a two-dimensional reference solution have been compared, too. Further, the numerically computed electromagnetic force has been compared by an analytical one.

The main principles of the analytical force computation, which based on the loop and node method are presented in chapter 7. Further information about this method can be found in [50, 61].

The results have been compared only the linear region of the single-valued nonlinear curve (see in Fig. 4.1), e.g.  $I_{2,max} = 5A$ . The simulations in the linear range is enough, because the magnetic bearing is mainly operated in this range. In the saturation part of nonlinear curve is not too advantageous used the AMB, because the losses of bearing is increased, and the bearing load force is saturated.

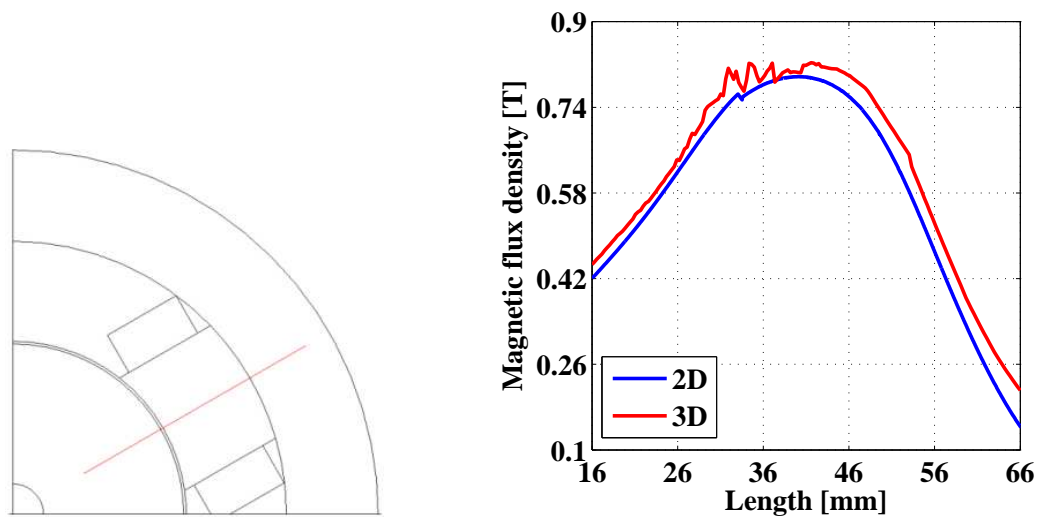
Furthermore, studied the difference of the two- and three-dimensional results, because of the end-region field effect of this short axial length magnetic bearing. If the 2D and 3D results will show a good agreement, its enough the two-dimensional simulation of this bearing, and the 2D optimisation is correct.

### 8.1 Results of the Linear Simulations

In this section the linear simulation results are presented, as well as the computing quantities of the radial magnetic bearing by some field plot and figures to compare the different results.

First, the primary quantity is studied, e.g. the magnetic flux density  $\vec{B}$ . After the primary quantity, the computed flux linkage has been compared. The flux linkage results by the FEMM has been used as a reference, because this quantity has been computed automatically. Finally, one of the most important quantity of magnetic bearings, the

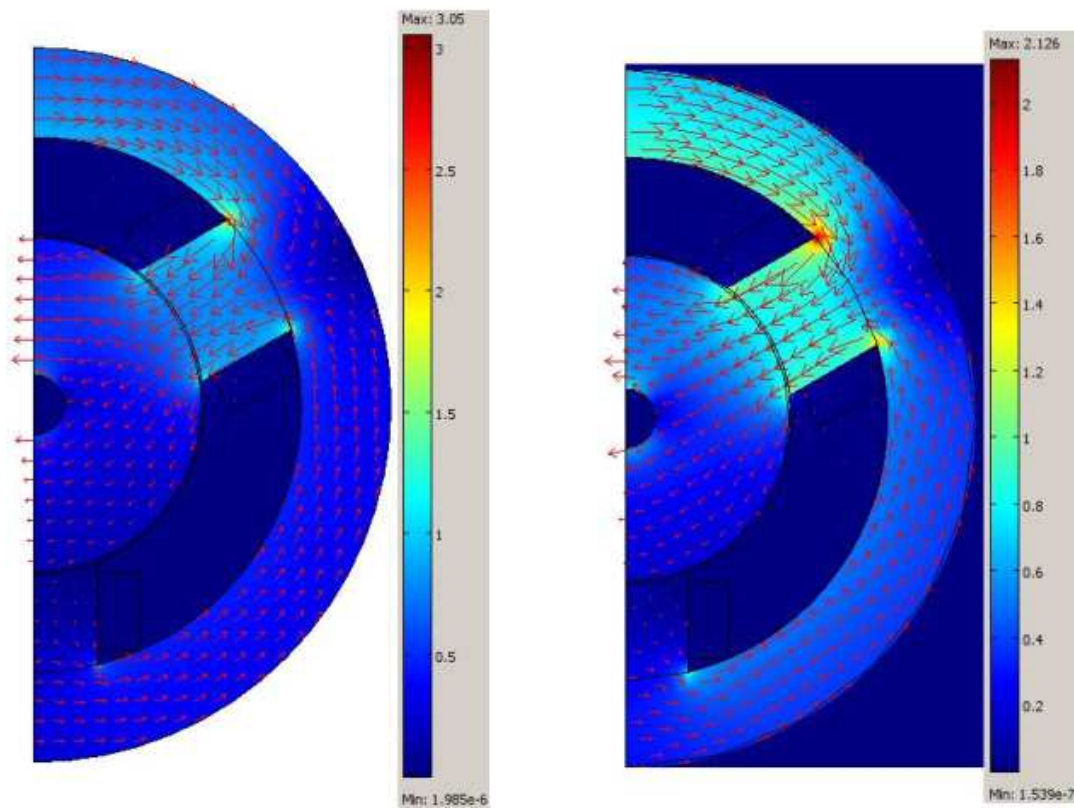
electromagnetic force have been compared. The numerical computed force is compared with the analytical computed force.



(a) The line, where shows the magnetic flux density.

(b) The value of the magnetic flux density.

Fig. 8.1: The magnetic flux density inside the magnetic bearing.



(a) Two-dimensional linear case.

(b) Three-dimensional linear case.

Fig. 8.2: The surface plot and vectors of magnetic flux density inside the magnetic bearing with linear material.

The line, where shows the value of magnetic flux density can be seen in Fig. 8.1(a). The primary quantity is compared along this line, because in this case, its shows the value of magnetic flux density inside the rotor, the pole and the stator. Fig. 8.1(b) shows the magnetic flux density along the line inside the radial bearing. The value of magnetic flux density nearly same in the figure in 2D and 3D case.

The magnetic flux density distribution and magnetic flux density vectors inside the magnetic bearing can be seen in Fig. 8.2. In this case, the excitation of the windings is the bias current, i.e.  $I_2=5\text{A}$ . The scale of figures are not same in 2D and 3D, because the flux density is higher in 2D. The main reason of it can be that the third dimension is neglected. In this simulation the length of the third dimension ( $z$ -axis) has been considered infinite. This infinite  $z$ -length has been resulted the variant behavior of magnetic flux in the corner of connection of pole and stator. If the maximum of the scale of Fig. 8.2(a) is set 2.126 T, then the flux distribution is same in the two cases. This shows the Fig. 8.3. The distribution and vectors of magnetic field intensity  $\vec{H}$  are same, because in this case has been linear relation between  $\vec{B}$  and  $\vec{H}$ , ( $\mu_r=3000$ ).

The results of computed flux linkage are presented the next figures. Fig. 8.4 shows the flux linkage in linear computations. In this case, the rotor is in the center position of the bearing, i.e. the air gap is nominal,  $g_0=0.5\text{ mm}$ . In this figure the two finite element approaches (2D and FEMM) are practically the same. The difference between the 3D finite element and the two 2D finite element results is increasing with the increase of

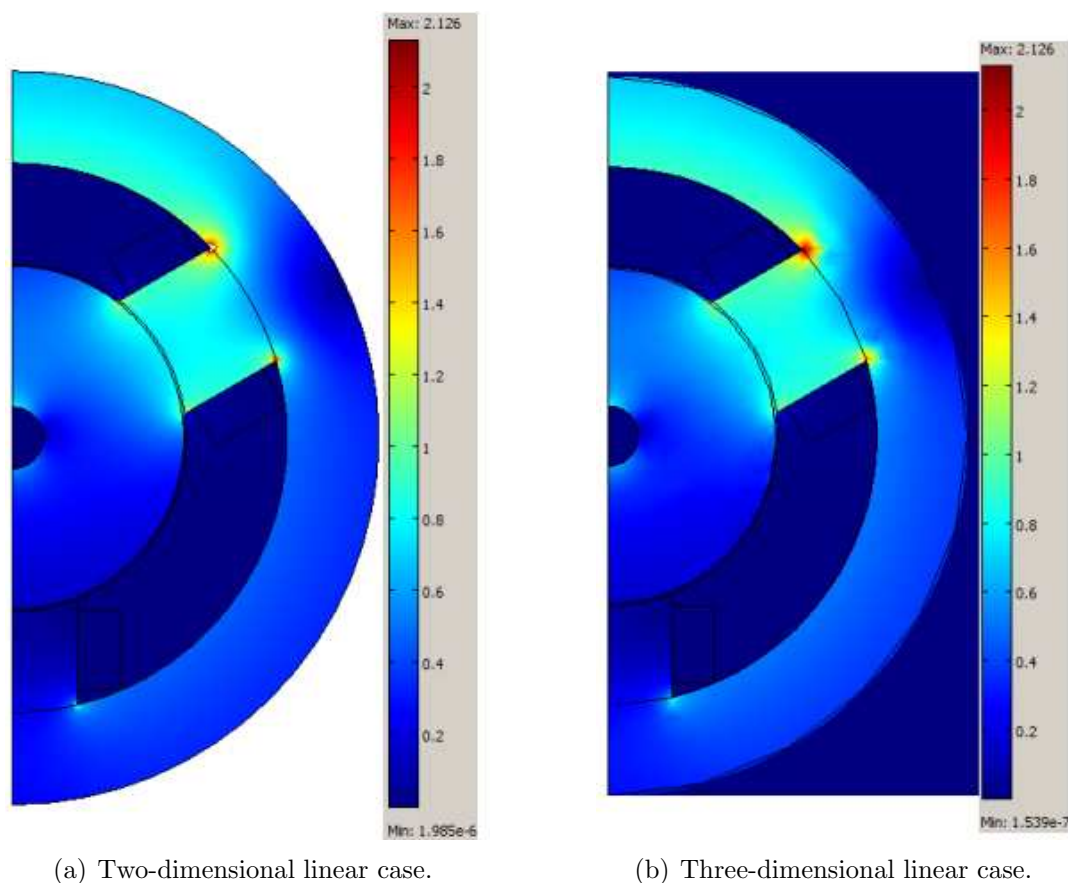


Fig. 8.3: The surface plot of magnetic flux density inside the magnetic bearing at same maximum value of the scale.

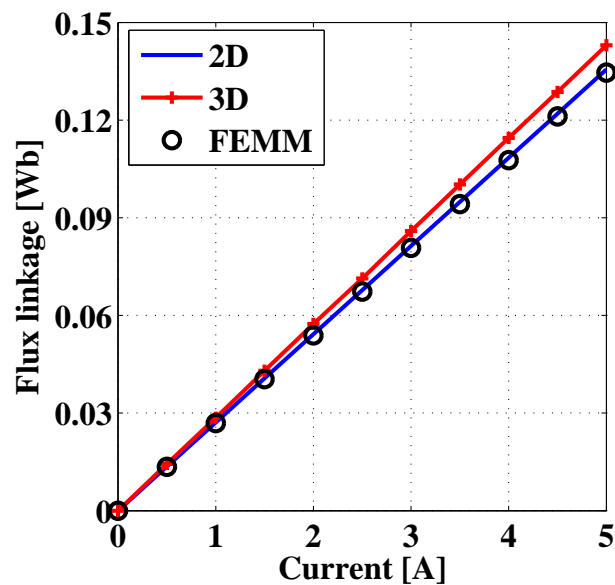


Fig. 8.4: The flux linkage - current characteristic at nominal air gap.

current of winding. Nevertheless, the maximum of the difference between 2D and 3D results is less than 5% at  $I_2=5\text{A}$ . Thus, adequately good the two-dimensional results for this quantity.

In the further figures, Fig. 8.5, Fig. 8.6 and Fig. 8.7 the flux linkage the function of the displacement of the rotor and of the variation of windings' current shows. The

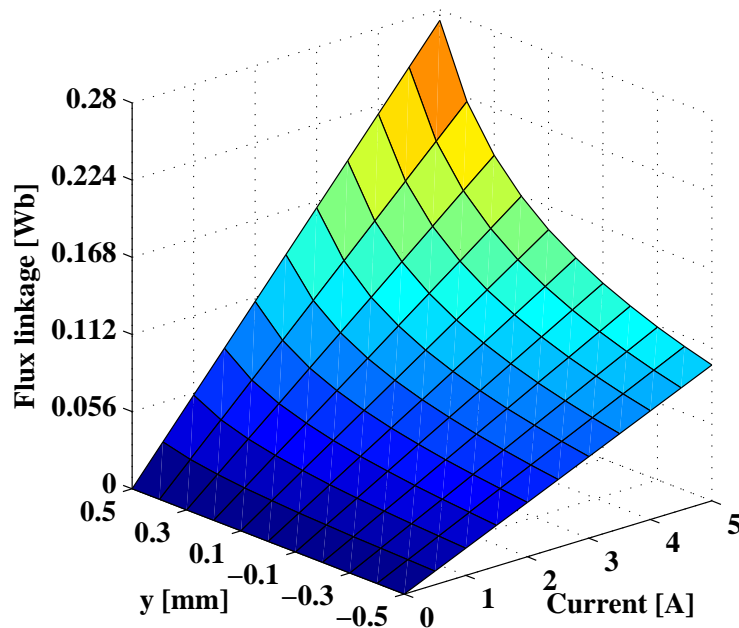


Fig. 8.5: The flux linkage the function of the  $y$ -directed displacement of the rotor and of the variation of the current in two-dimensional case.

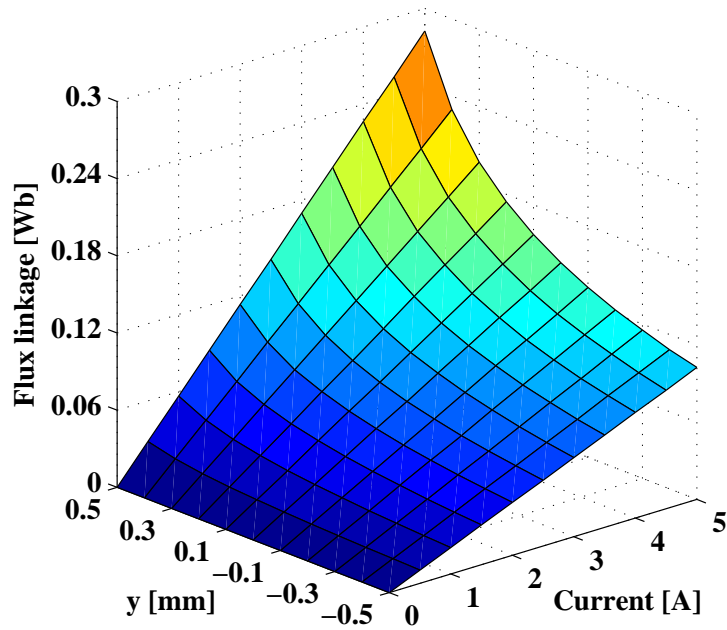


Fig. 8.6: The flux linkage the function of the  $y$ -directed displacement of the rotor and of the variation of the current in three-dimensional case.

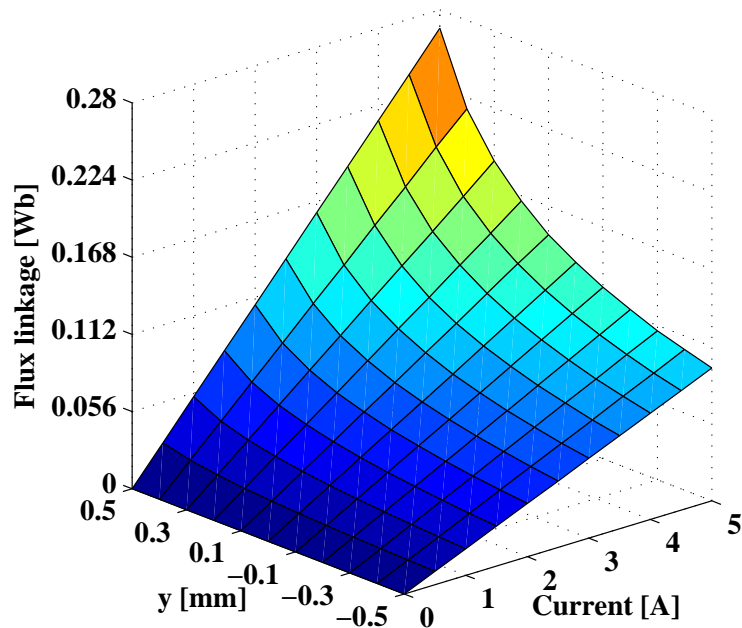


Fig. 8.7: The flux linkage the function of the  $y$ -directed displacement of the rotor and of the variation of the current by the FEMM.

displacement of the rotor is the  $y$ -direction displacement. In these figures shows same results as an above mentioned. The computed flux linkage is a little bit higher in three

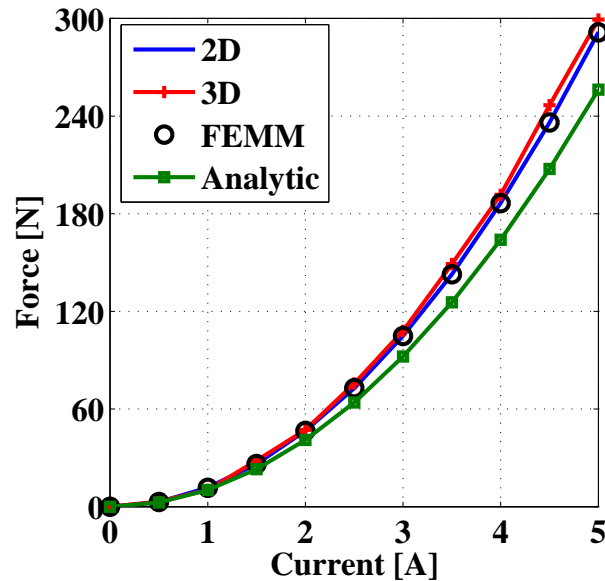


Fig. 8.8: The electromagnetic force - current characteristic at nominal air gap.

dimensions, than in two dimensions, and the 2D and FEMM results seems to be equal at all currents and rotor positions. The maximum of difference is less than 5%. The main reason of the difference of the 2D and 3D results can be that in the 3D case the whole winding simulated, whereas in 2D case the windings are infinite, and the end windings has been neglected. However, the results of flux linkage shows good agreement between 2D and 3D FEM computations.

After flux linkage, the next is the presentation and comparison of the results of the computed electromagnetic force. The electromagnetic force the function of the current can be seen in Fig. 8.8. In this figure, the forces have reference to the rotor center position. This figure shows the three numerical computation results and in addition to the analytical results, too. The two-dimensional (2D) and the FEMM results are the same, because the black circles which are presented the FEMM results are perfectly accomodate to the blue line, the results of the two-dimensional computation. The electromagnetic force of 3D computation is a quiet larger than at the flux linkage. However, the difference of the 2D and 3D results at this quantity is not higher than 5% at the used current range of the simulations. Furthermore, the difference between the curve of analytic results and of FEM results is much higher, and the difference is decreased when the current becomes higher. The maximum of the difference is less than 15%. Thus, the analytical computation is perfect and suitable for the evaluation of the electromagnetic force of the bearing and quick design iteration. However, than the figure is shows, necessary a more accurate computation for the magnetic field intensity or the electromagnetic force, like finite element analysis after the analytical computations.

Fig. 8.9, Fig. 8.10, Fig. 8.11, Fig. 8.12 show the flux linkage the function of the  $y$ -directed displacement of the rotor and of the variation of current of windings. The results in Fig. 8.9 and Fig. 8.11 are practically same, because the difference of the two-dimensional finite element computations is less than 1%. The difference of three-dimensional and two-dimensional computations is less than 5%, which difference is acceptable in the case of numerical calculation methods. However, the correctness of the

analytical results in this case is worse. The reason of this the motion of the rotor, because the analytical matrix equations are can not be correctly described the physical meaning

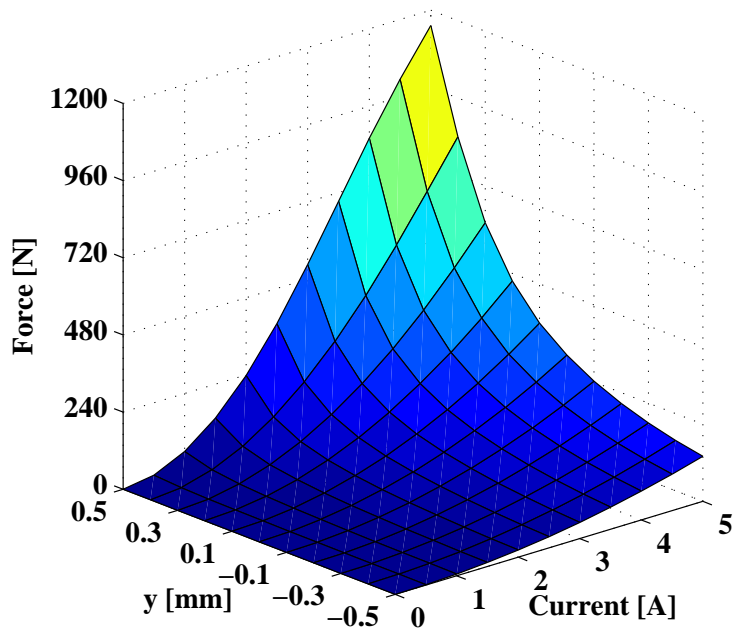


Fig. 8.9: The electromagnetic force the function of the  $y$ -directed displacement of the rotor and of the variation of the current in two-dimensional case.

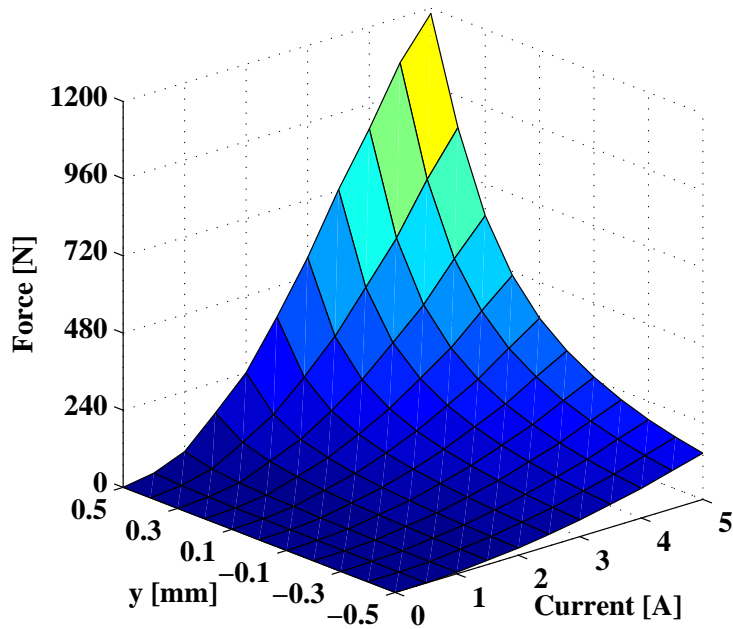


Fig. 8.10: The electromagnetic force the function of the  $y$ -directed displacement of the rotor and of the variation of current in three-dimensional case.

of the motion. The maximal difference of the analytical and the 3D finite element results is 28.3%.

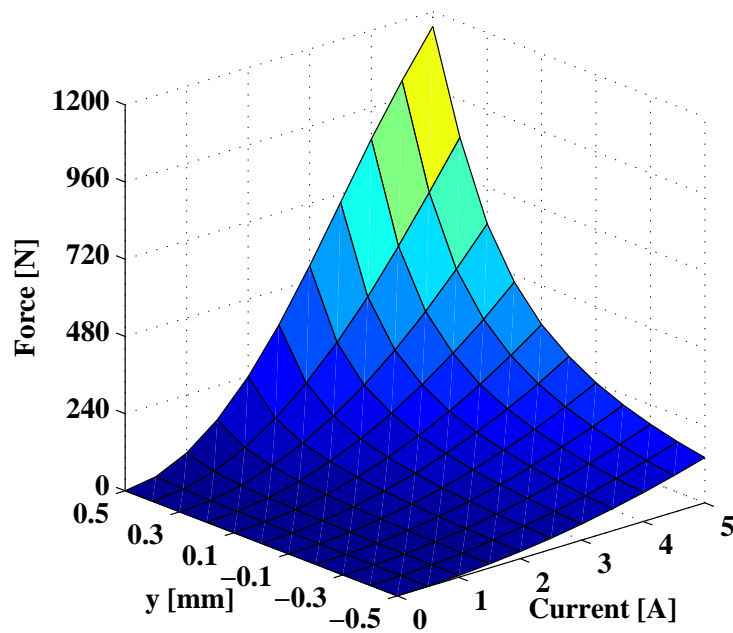


Fig. 8.11: The electromagnetic force the function of the  $y$ -directed displacement of the rotor and of the variation of the current by the FEMM.

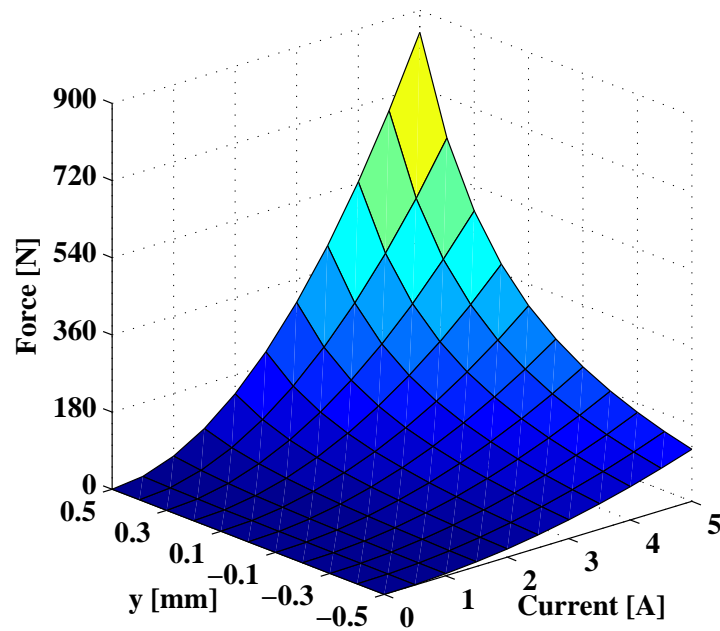


Fig. 8.12: The electromagnetic force the function of the  $y$ -directed displacement of the rotor and of the variation of the current by the analytic computation.

The difference of the computed quantities of the two-dimensional and three-dimensional finite element analyses is less than 5% with linear  $\vec{B}$  -  $\vec{H}$  relationship. Thus, its enough the 2D FEM computation for the magnetic bearing analysis in the linear case.

## 8.2 Results of the Nonlinear Simulations

In this section the results of the nonlinear computations have been presented and compared. However, ere the primary and secondary quantities have been presented, the nonlinear equation solvers, the Newton-Raphson method and the fixed point technique have been compared. The comparison is focused on the number of iterations, the convergence and the computation time of the nonlinear equation solvers.

Table 8.1 presents the computation time consumption and the number of iterations of the used nonlinear equation solvers. The values which presents the table shows that one case when the rotor is fixed in the bearing centre. The comparison of the time consumption is not feasible. In the table, at  $I_2=0\text{A}$  current the computation time of one fixed point iteration is nearly hundred times bigger than the time of one iteration of Newton-Raphson method. This great difference in the time is follow from the number of unknowns. The fixed point technique is solved a more larger equation system, because of the number of unknowns is higher in the three-dimansional case (see in section 5.1.1.). Furthermore, the impressed current vector potential  $\vec{T}_0$  has been computed when the edge element based  $\vec{A}$  - formulation with fixed point technique is applied, and this add about 25s in every computation turn. However, it is possible to conclude the speed and the computation time from the number of iteration. If the time of one iteration is the same in the two methods, the Newton-Raphson technique is faster, because of the less iteration number.

The number of iterations of the techniques is comparable. The number of iterations

Table 8.1: The computation time and the number of iterations of the nonlinear equation solvers.

Current [A]	Newton-Raphson method		Fixed point technique	
	Number of iterations	Time [s]	Number of iterations	Time [s]
0.0	1	0.900	1	114.27
0.5	2	1.625	14	1649.696
1.0	2	1.589	14	1625.487
1.5	2	1.741	14	1630.848
2.0	3	2.245	14	1640.902
2.5	5	3.653	14	1649.973
3.0	6	4.761	14	1664.150
3.5	7	5.123	14	1653.296
4.0	8	6.192	14	1633.527
4.5	9	6.696	19	2203.341
5.0	9	6.830	65	7595.440

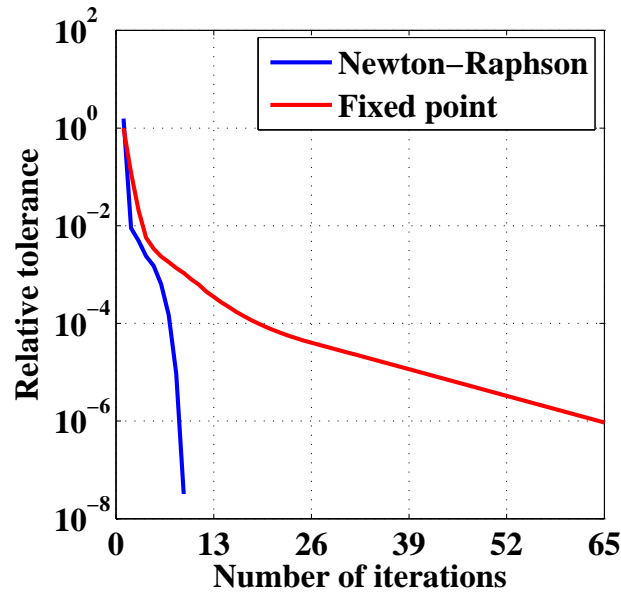


Fig. 8.13: The relative tolerance the function of the number of iterations at  $I_2=5A$  current.

of Newton-Raphson method is progressively increased with increasing with the current. As against of it, the number of iterations of fixed point method almost 14, only the first and the last two numbers of iterations are different. At the last two, mainly at the last current value  $I_2=5A$ , the number of iterations is shows why Newton-Raphson technique is used. If necessary a fast nonlinear equation solver, this method usually few iterations are required for adequate precision. Whereas, the fixed point method is slower, lot of iterations are needed for the adequate precision, however the convergence is more stable than in the case of Newton-Raphson method.

The relative tolerance the function of the number of iterations can be seen in Fig. 8.13, at the simulation where the current is  $I_2=5A$ . The computation formulas of the relative tolerance are presented in the used nonlinear equation solver methods in the chapter 4. This figure also shows the convergent of fixed point technique, and it is much slower than the other method. The fixed point method after 65 iterations achieved the predefined error ( $\varepsilon=10^{-6}$ ), it is due to the error is slower decreased at a single iteration. The relative tolerant curve of Newton-Raphson method shows the quadratic convergence i.e. the quadratically decreased the error.

The left hand side in the figure of the Fig 8.14 shows the line, where studied the value of magnetic flux density inside the magnetic bearing. The value of magnetic flux density along the line in Fig. 8.14(b) shows a better agreement than in linear case (see in Fig. 8.1(b)). This good agreement can be seen the next figure, the Fig. 8.15 as well.

The magnetic flux density distribution and magnetic flux density vectors inside the magnetic bearing can be seen in Fig. 8.15 at the simulation with  $I_2=5A$ . The above mentioned good agreement shows this field plot figures, because the magnetic flux density distribution of the two figures (8.15(a) and 8.15(b)) are perfectly same. This is verified in the scale of the figures, where the maxima are nearly same,  $B_{max} \approx 1.42T$ . The length of the magnetic flux vectors are almost same in the same parts of the magnetic bearing.

After the primary quantity  $\vec{B}$ , the next is the presentation and comparison of the

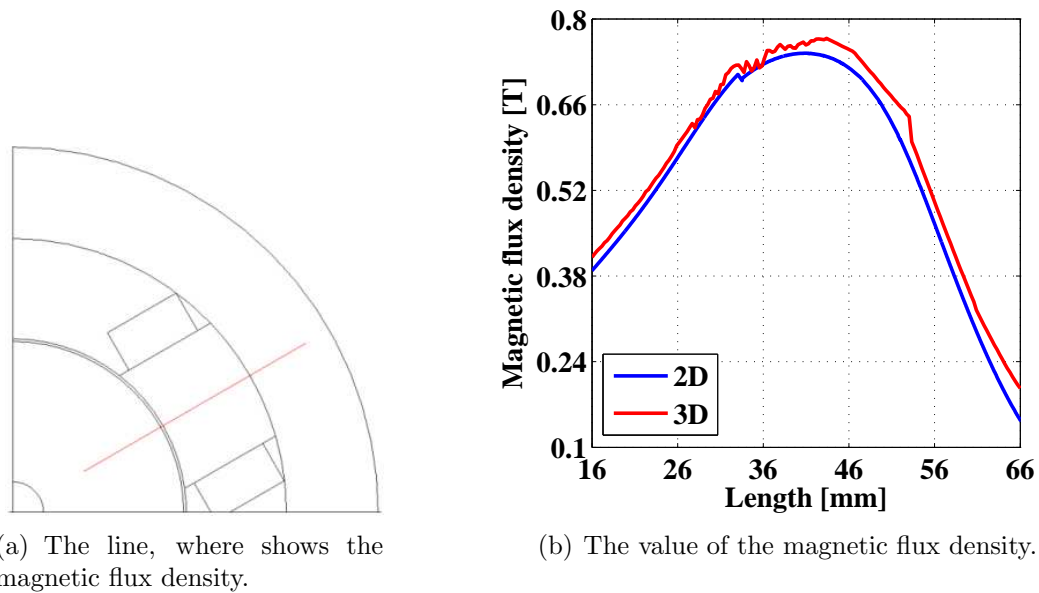


Fig. 8.14: The magnetic flux density inside the magnetic bearing.

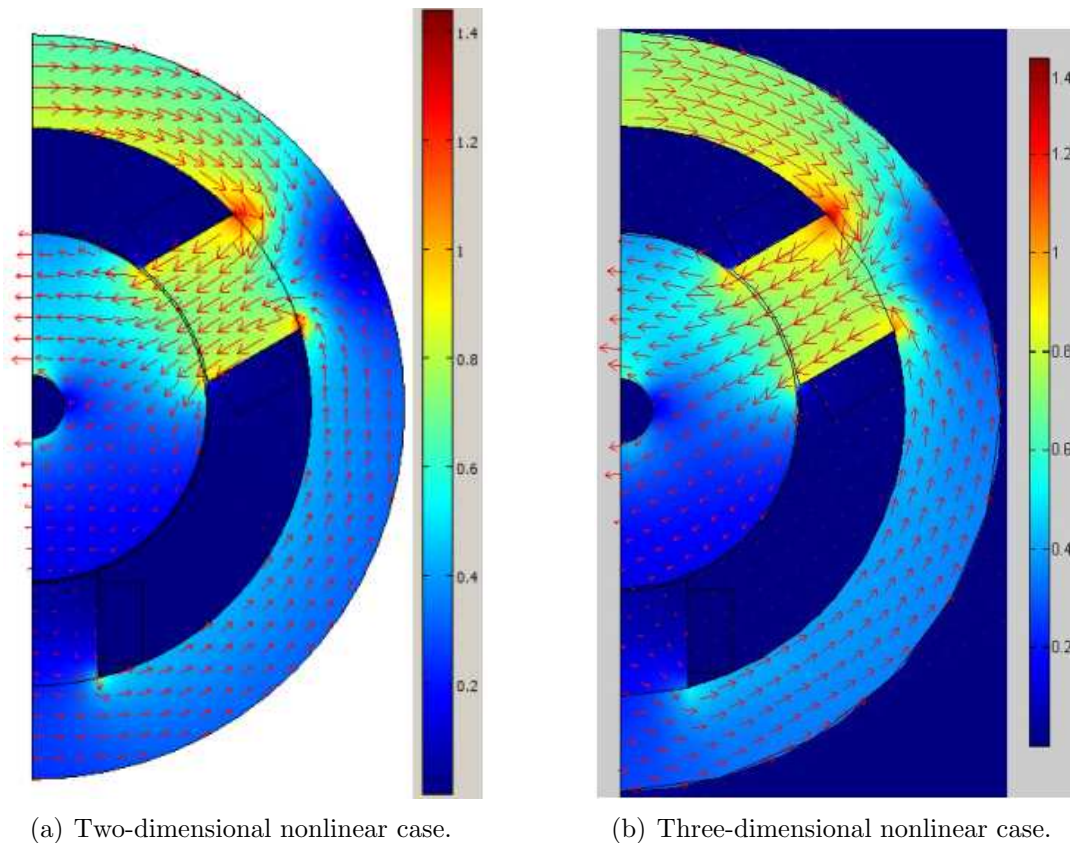


Fig. 8.15: The surface plot and vectors of magnetic flux density inside the magnetic bearing with nonlinear material.

secondary quantities again, the flux linkage and the electromagnetic force of the radial magnetic bearing.

The computed flux linkage  $\Psi$  by the three different nonlinear finite element ap-

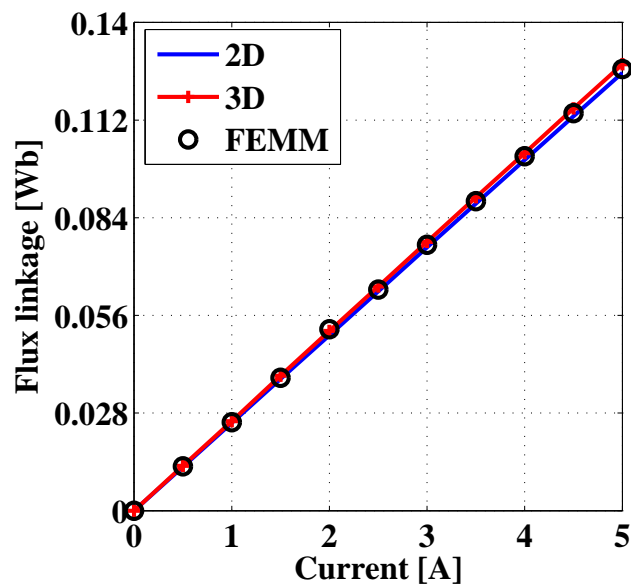


Fig. 8.16: The flux linkage - current characteristic at nominal air gap.

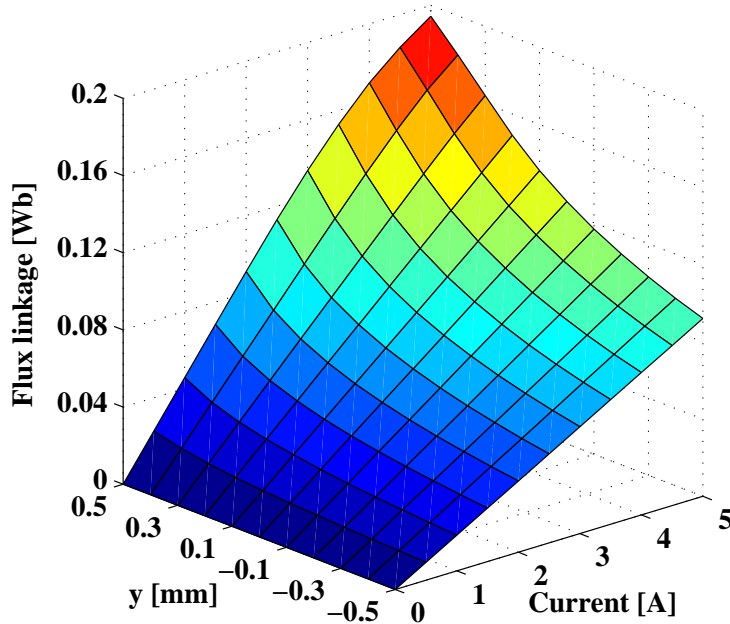


Fig. 8.17: The flux linkage the function of the  $y$ -directed displacement of the rotor and of the variation of the current in two-dimensional case.

proaches can be seen in Fig. 8.16. The results of this figure shows when the rotor is fixed in the centre of the bearing. In this figure, the results are close to each other. The results of the two- (2D) and the three-dimensional (3D) simulations the maximum of the difference is less than 2%. The results of the FEMM software are located between the two others. This quantity is shown in a good agreement, likewise at the magnetic flux density vectors and distribution.

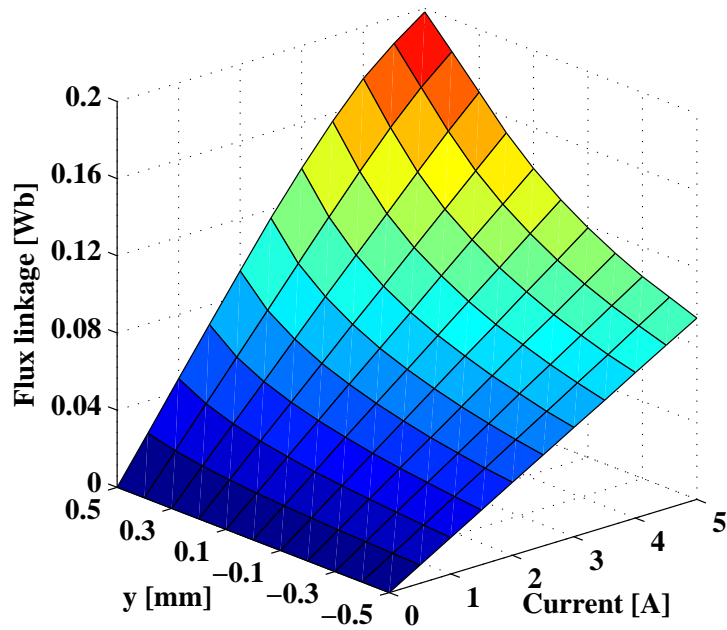


Fig. 8.18: The flux linkage the function of the  $y$ -directed displacement of the rotor and of the variation of the current in three-dimensional case.

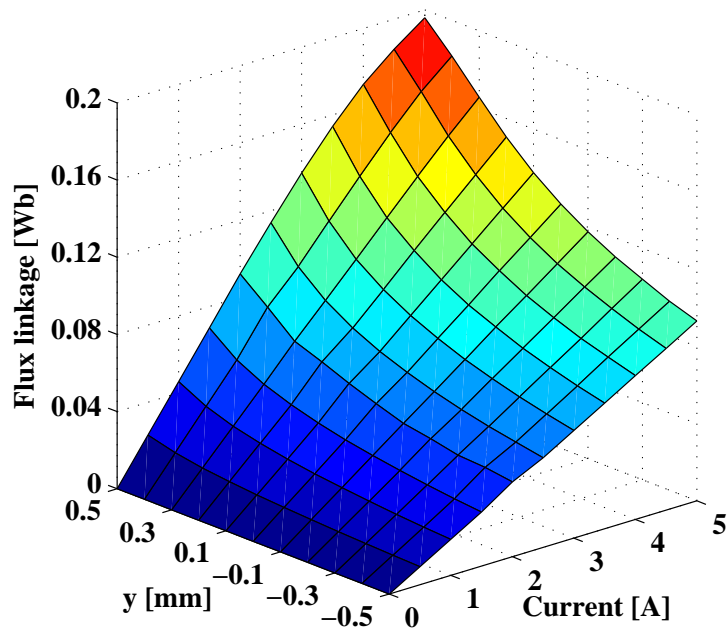


Fig. 8.19: The flux linkage the function of the  $y$ -directed displacement of the rotor and of the variation of the current by the FEMM.

Fig. 8.17, Fig. 8.18 and Fig. 8.19 show the variation of the flux linkage the function of the  $y$ -directed displacement of the rotor and of the variation of current of windings.

These figures seem to be nearly the same in the different rotor positions and currents. These show the maximum of the flux linkage, at the 0.5mm displacement and at the 5A winding current, because the maximums are 0.198Wb and 0.199Wb in 2D and 3D, respectively. The difference of these results is less than 2%.

The last quantity of this chapter is the electromagnetic force obtained by the non-linear simulations. The numerically computed electromagnetic force versus the function

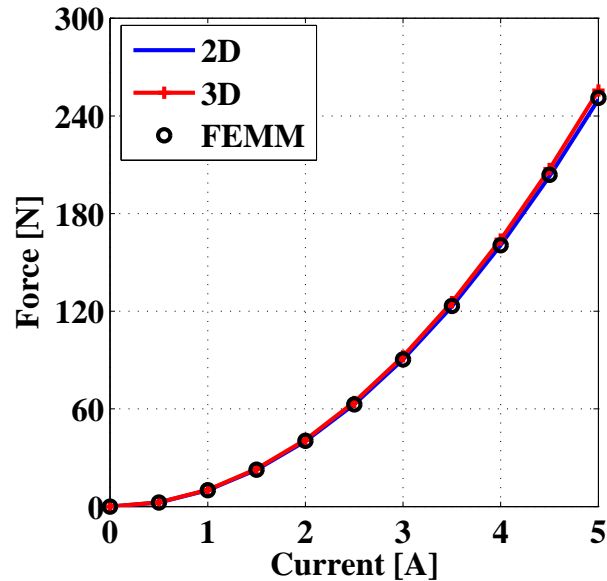


Fig. 8.20: The electromagnetic force - current characteristic at nominal air gap.

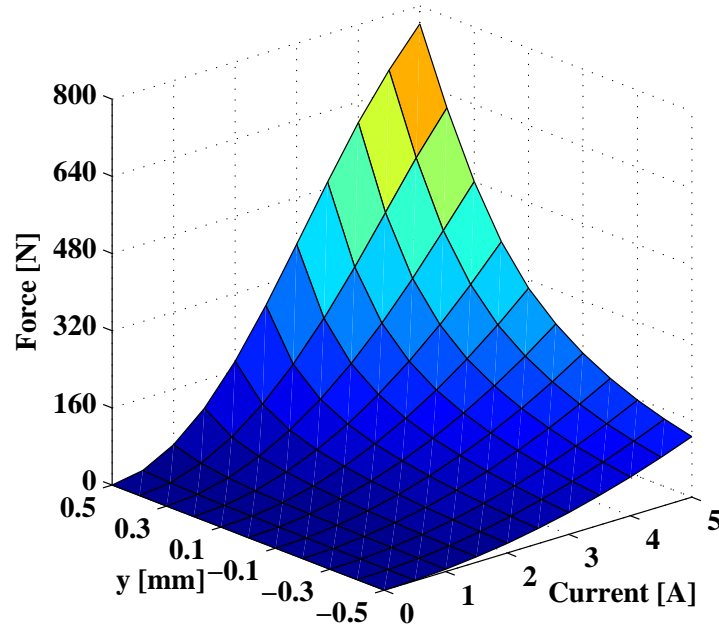


Fig. 8.21: The electromagnetic force the function of the  $y$ -directed displacement of the rotor and of the variation of the current in two-dimensional case.

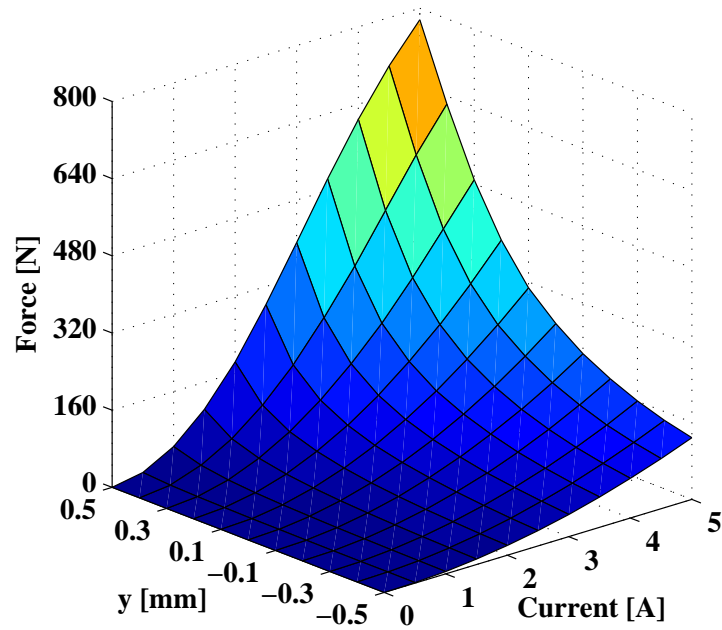


Fig. 8.22: The electromagnetic force the function of the  $y$ -directed displacement of the rotor and of the variation of the current in three-dimensional case.

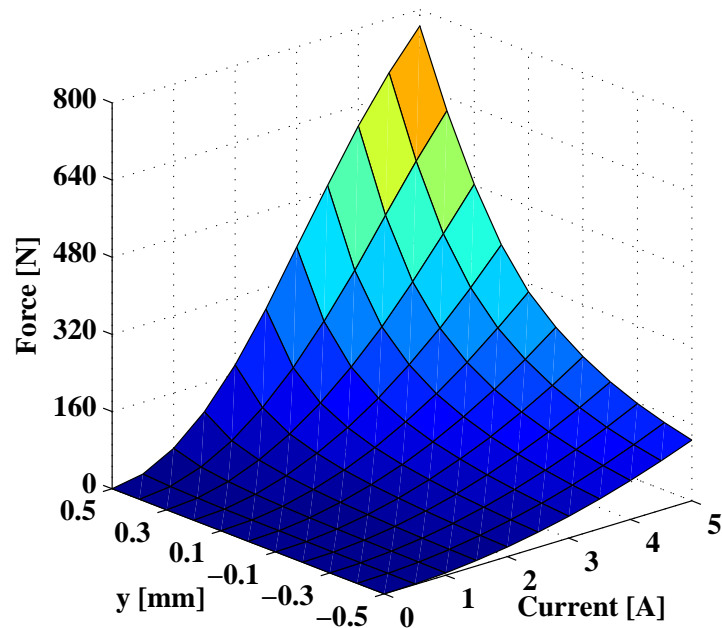


Fig. 8.23: The electromagnetic force the function of the  $y$ -directed displacement of the rotor and of the variation of the current by the FEMM.

of the current can be seen in Fig. 8.20. These results have reference to the fixed rotor position in the center, than in the linear case. The obtained results are practically the

same. The other presented quantities which are due to the nonlinear simulations this good agreement show. The difference is less than 2% when comparing this quantity.

Let's note here that the analytically computed electromagnetic force is closer to the force obtained from the nonlinear simulations than from the linear simulations, as than it can be seen in Fig. 8.8. However, it is coincidence at this problem. One of the simplifications of the analytical computation is the neglitation of the nonlinearity of material, because the magnetic bearing is operating in the linear range of the nonlinear curve of the material. Thus, linear results are given from the analytical computation.

The further figures (Fig. 8.21, Fig. 8.22 and Fig. 8.23) shows the variation of the electromagnetic force the function of the  $y$ -directed displacement of the rotor and of the variation of current of windings. The agreement of the results at the difference rotor positions and winding currents are almost same like in the Fig. 8.20. The maximum of the difference of the results is less than 2%, which can be seen in Fig. 8.21, Fig. 8.22 and Fig. 8.23. The three different nonlinear simulations gives a same electromagnetic force. Thus, its enough to use the 2D FEM computation for the magnetic bearing analysis not only in the linear case, but in the nonlinear case, too.

# Chapter 9

## Conclusions and future works

### Conclusions

In this master thesis, the computer-aided design and the numerical analysis of a Y-shaped radial magnetic bearing was presented. The one of aims of this work is the implementation of a two-dimensional numerical design of a three-pole radial magnetic bearing. After a numerical design, the second aim of this work is the verification of the designed bearing. Its enough the two-dimensional simulation of this short axial length magnetic bearing with the neglitation of the end-region field effect. The importance of this thesis is the implementation of the fast and easy application tool for the computer-aided magnetic bearing design and analysis.

In this work, the weak form of the  $\vec{A}$  - potential formulation to solve the presented problems has been implemented from the basic physical equations of the magnetic bearing, the Maxwell's equations of the static magnetic field problem. I introduced the main steps of the finite element method, the computation of the flux linkage and the electromagnetic force in two- and three-dimensional cases. Further, the finite element analysis has been implemented to solve the problem with linear and nonlinear material. Because of the nonlinearity, the used nonlinear equation solvers, the Newton-Raphson method and the fixed point technique have been shortly presented. Finally, the used optimization method, the Nelder-Mead simplex search algorithm and the steps of the finite element based optimization method have been presented.

The best bearing geometry has been chosen from the results of optimization, and has been accomplished the numerical analysis of the chosen magnetic bearing. The simulation procedures have been compared by computed quantities. These simulation procedures are the two-dimensional and the three-dimensional magnetic field computation with linear and nonlinear materials. Further of these, the two-dimensional linear and nonlinear finite element computations have been implemented by the free finite element software, FEMM, as a reference numerical computation. The compared quantities are the above mentioned flux linkage  $\Psi$  and electromagnetic force  $\vec{F}$ . The electromagnetic force has been computed by analytical computation, too.

In chapter 8, the results have been presented, and these results shows its enough the two-dimensional finite element design and simulation for the short axial length magnetic bearing. The maximum of the difference of the computed quantities is 5% and 2% in the linear and in the nonlinear case, respectively. Thus, the two-dimensional finite element method has been given properly good results.

## Future works

I am going to continuing this work, and redesign this bearing by genetic algorithm, because basically the Nelder-Mead (NM) method has been found the local minima, whereas the genetic algorithm (GA) should been find the global minimum [64]. The results of GA and of NM method will be compared.

The main future research work is to build up the prototype of the numerical designed Y-shaped radial bearing fed by two amplifier. Because of the high nonlinearity, the design of a nonlinear controllers for this three-pole bearing to the properly operation is a future task. The one of the nonlinear controllers is based on the classical control theory like PID controller, and the other one is based on the modern soft computing theory like fuzzy system, neural network, genetic algorithm or these combination [6, 65, 66].

I would like to continue my studies in the doctoral school. The above mentioned future works and plans are my Ph.D. theses.

To write this document the L<sup>A</sup>T<sub>E</sub>X word processor (<http://www.miktex.org/>) have been used.

# Chapter 10

## Acknowledgement

This work was carried out in the Laboratory of Electromagnetic Fields at Széchenyi Istvan University.

I would like to take the opportunity to express my gratitude to Dr. Miklós Kuczmann, Ph.D., associate professor, Head of the Laboratory of Electromagnetic Field for all years we spent together as supervisor and student, for his calmness and for all the knowledge he shared with me. I am also very grateful to Dr. Péter Kis, Ph.D., associate professor for the help of this work, as well as a lot of signature.

Special thanks to Professor Herbert De Gersem for lectorate of my bachelor and master thesis. Special thanks go to Professor Oszkár Bíró, Professor Amália Iványi and Professor Marko Jesenik for helpful and valuable comments for my presentations.

I wish to thanks the Department of Telecommunication for the place of the laboratory.

Last but not least, I would like thank my family, my parents, my sister and my girlfriend, Klára Sümegi for constant understanding, encouragement and support.

The financial support of the János Bolyai Research Scholarship of the Hungarian Academy of Sceince (BO/00064/06), the Széchenyi Istvan University (12-3210-02) and the Hungarian Scientific Research Fund, OTKA PD73242.

Dániel Marcsa  
Győr, 30<sup>th</sup> November 2010

# Bibliography

- [1] G. Schwitzer, E. H. Maslen (Eds.). *Magnetic Bearings - Theory, Design, and Application to Rotating Machinery*. Springer, Berlin, 2009.
- [2] F. C. Moon, P. Chang. *Superconducting Levitation - Applications to Bearings and Magnetic Transportation*. Wiley-VCH, Weinheim, 2004.
- [3] T. A. Lembke. *Design and Analysis of a Novel Low Loss Homopolar Electrodynamic Bearing*. Ph.D. Thesis, KTH Royal Institute of Technology, Stockholm, 2005.
- [4] B. Polajzer. *Design and Analysis of an Active Magnetic Bearing Experimental System*. Ph.D. Thesis, University of Maribor, Maribor, 2003.
- [5] M. Antila, E. Lantto, A. Arkkio. Determination of Forces and Linearized Parameters of Radial Active Magnetic Bearings by Finite Element Technique. *IEEE Transactions on Magnetics*, 34:684694, 1998.
- [6] M. Kuczmann, A. Iványi. *The Finite Element Method in Magnetics*. Akadémiai Kiadó, Budapest, 2008.
- [7] J. D. Jackson. *Classical Electrodynamics*. 3rd Edition, John Wiley, 1999.
- [8] J. A. Stratton. *Electromagnetic Theory*. McGraw Hill, London, 1941.
- [9] J. P. A. Bastos, N. Sadowski. *Electromagnetic Modeling by Finite Element Methods*. Marcel Dekker Inc., New York, 2003.
- [10] O. Bíró, K. R. Richter. CAD in electromagnetism. *In Series Advances in Electronics and Electron Physics*, Academic Press, New York, 1991, pp. 82.
- [11] J. Jin. *The Finite Element Method in Electromagnetics*. JohnWiley and Sons, New York, 2002.
- [12] J. Luomi. *Finite Element Methods for Electrical Machines (lecture Notes for postgraduate course in electrical machines)*. Chalmers University of Technology, Göteborg, 1993.
- [13] P. P. Silvester and R. L. Ferrari. *Finite Elements for Electrical Engineers*. Cambridge University Press, Cambridge, 1983.
- [14] O. C. Zienkiewicz and R. Taylor. *The Finite Element Method*. McGraw-Hill, Maidenhead, 1991.

- [15] K. Simonyi and L. Zombory. *Theoretical Electromagnetics (in Hungarian)*. Műszaki Könyvkiadó, Budapest, 2000.
- [16] P. Kis. *Jiles-Atherton Model Implementation to Edge Finite Element Method*. Ph.D. Thesis, Budapest, Budapest University of Technology and Economics, 2007.
- [17] D. Marcsa. *Induction Motors Simulation by Finite Element Method and Different Potential Formulations with Motion Voltage Term*. B.Sc. Thesis, Széchenyi István University, Győr, 2009.
- [18] O. Bíró. *Potential Functions in Eddy Current Field Analysis by the Finite Element Method (in Hungarian)*. Hungarian Academy of Sciences, 2003.
- [19] O. Bíró, K. Preis, K. R. Richter. On the use of the magnetic vector potential in the nodal and edge finite element analysis of 3D magnetostatic problems. *IEEE Transactions on Magnetics*, 32:651654, 1996.
- [20] A. Iványi. *Continuous and Discrete Simulation in Electrodynamics (in Hungarian)*. Akadémiai Kiadó, Budapest, 2003.
- [21] A. Iványi. *Magnetic Field Computation with R-functions*. Akadémiai Kiadó, Budapest, 1998.
- [22] O. Bíró, K. Preis, G. Vrisk, K. R. Richter, I. Tícar. Computation of 3-D magnetostatic fields using a reduced scalar potential. *IEEE Transactions on Magnetics*, 29:13291332, 1993.
- [23] A. Ralston. *A First Course in Numerical Analysis: Second Edition*. Dover Publications, 2001.
- [24] O. Kis, M. Kovács. *Numerical Methods (in Hungarian)*. Műszaki Könyvkiadó, Budapest, 1973.
- [25] J. H. Mathews, K. D. Fink. *Numerical Methods Using MATLAB*. Prentice Hall, Upper Saddle River, NJ, 1999.
- [26] M. Kuczmann. Using the NewtonRaphson Method in the Polarization Technique to Solve Nonlinear Static Magnetic Field Problems. *IEEE Transactions on Magnetics*, 46:875879, 2010.
- [27] M. Kuczmann. The polarization method combined with the Newton-Raphson technique in magnetostatic field problems. *Przegląd Elektrotechniczny*, 84:198-201, 2008.
- [28] J. Yuan, M. Clemens, H. De Gersem, T. Weiland. Solution of Transient Hysteretic Magnetic Field Problems with Hybrid Newton-Polarization Methods. *IEEE Transactions on Magnetics*, 41:17201723, 2005.
- [29] J. Saitz. Newton-Raphson Method and Fixed-Point Technique in Finite Element Computation of Magnetic Field Problems in Media with Hysteresis. *IEEE Transactions on Magnetics*, 35:13981401, 1999.

- [30] P. Sergeant, L. Dupré. Implementation of Hysteresis Material Characteristics in Finite Element Computations. *Proceedings of the COMSOL Users Conference*, Grenoble, 2007.
- [31] O. Bottauscio, M. Chiampi, C. Ragusa. Transient Analysis of Hysteretic Field Problems Using Fixed Point Technique. *IEEE Transactions on Magnetics*, 39:11791182, 2003.
- [32] F. I. Hantila. A Method of Solving Stationary Magnetic Field in Non-Linear Media. *Revue Roumaine Des Sciences Techniques, Électrotechnique et Énergétique*, 20:397407, 1975.
- [33] F. I. Hantila, G. Preda, M. Vasiliu. Polarisation Method For Static Fields. *IEEE Transactions on Magnetics*, 36:672-675, 2000.
- [34] F. I. Hantila. Electromagnetic Field in Non-Linear Media. *Balkan Journal of Geometry and Its Application*, 4:49-62, 1999.
- [35] F. I. Hantila, M. Maricar, C. Popescu, C. Ifrim, S. Ganatsios. Performances of a Waste Recycling Separator with Permanent Magnets. *Journal of Materials Processing Technology*, 181:246-248, 2007.
- [36] D. Marcsa, M. Kuczmann. Eddy Current Analysis With Non-Linearity. *Pollack Periodica*, 3:97-109, 2008.
- [37] D. Marcsa, M. Kuczmann. Nonlinear Two-Dimensional Motional Finite Element Modeling of a Rotational Eddy Current Field Problem. *Przegląd Elektrotechniczny*, 85:110-113, 2009.
- [38] D. Marcsa, M. Kuczmann. Analysis of Ferromagnetic Core Combining Preisach Hysteresis Modeling and Finite Element Techniques. *Journal of Advanced Research in Physics*, 1:14-18, 2010.
- [39] [www.mathworks.com/](http://www.mathworks.com/)
- [40] [www.comsol.com/](http://www.comsol.com/)
- [41] [www.femm.info/wiki/HomePage](http://www.femm.info/wiki/HomePage)
- [42] <http://www.cise.ufl.edu/research/sparse/umfpack/>
- [43] <http://mathworld.wolfram.com/>
- [44] A. Neumaier, R. S. Varga. Exact convergence and divergence domains for the symmetric successive overrelaxation iterative (SSOR) method applied to H-matrices. *Linear Algebra Application* 58:261-272, 1984.
- [45] C. Ashcraft, R. Grimes. SPOOLES: An object-oriented sparse matrix library. *In Proceedings of the 9th SIAM Conference on Parallel Processing for Scientific Computing*, 1999.
- [46] F. W. Sears. *Principles of Physics Series - Electricity and Magnetism*. Addison-Wesley, Cambridge Mass., 1964.

- [47] A. Arkkio. *Analysis of induction motors based on the numerical solution of the magnetic field and circuit equations*. Ph.D. Thesis, Helsinki University of Technology, Espoo, 1987.
- [48] A. A. Abdel-Razek, J. L. Coulomb, M. Felicahi, J. C. Sabonnadiere. The calculation of electromagnetic torque in saturated electrical machines within combined numerical and analytical solutions of the field equations. *IEEE Transactions on Magnetics*, MAG-17:3250-3252, 1981.
- [49] D. Marcsa, M. Kuczmann. Comparison of the  $A^* - A$  and  $T, \Phi - \Phi$  Formulations for the 2D Analysis of Solid-Rotor Induction Machines. *IEEE Transactions on Magnetics*, 45:3329-3333, 2009.
- [50] D. Marcsa. *Design and Simulation of Active Magnetic Bearing (in Hungarian)*. TMDK - Scientific and Art Student Conference, Széchenyi István University, 2010.
- [51] C. Schlensok, M. H. Gracia, K. Hameyer. Combined Numerical and Analytical Method for Geometry Optimization of a PM Motor. *IEEE Transactions on Magnetics*, 42:1211-1214, 2006.
- [52] G. Stumberger, D. Dolinar, U. Pahner, K. Hameyer. Optimization of Radial Active Magnetic Bearings Using the Finite Element Technique and the Differential Evolution Algorithm. *IEEE Transactions on Magnetics*, 36:1009-1013, 2000.
- [53] J. A. Nelder, R. Mead. A Simplex Method for Function Minimization. *Computer Journal*, 7:308-313, 1965.
- [54] J. H. Matthews, K. D. Fink. *Numerical Methods Using MATLAB*. Prentice Hall, Upper Saddle River, NJ, 1999.
- [55] E. Zahara, Y. Kao. Hybrid Nelder-Mead Simplex Search and Particle Swarm Optimization for Constrained Engineering Design Problems. *Expert Systems with Applications*, 36:3880-3886, 2009.
- [56] A. Ourai, M. M. Toufigh. Application of Nelder-Mead Simplex Method for Unconfined Seepage Problems. *Applied Mathematical Modelling*, 33:3589-3598, 2009.
- [57] M. Baulac, J. Defrance, P. Jean. Optimization of Multiple Edge Barriers with Genetic Algorithms coupled with a Nelder-Mead Local Search. *Journal of Sound and Vibration*, 300:71-87, 2007.
- [58] D. Marcsa, M. Kuczmann. Optimization and Finite Element Analysis of 3-Pole Magnetic Bearing with Nonlinear Material. *Przeglad Elektrotechniczny*, 12:91-94, 2010.
- [59] D. Marcsa, M. Kuczmann. Design and Numerical Simulation of a Y-Shaped Active Magnetic Bearing. *Przeglad Elektrotechniczny*, in press.
- [60] E. H. Maslen, C. R. Knospe. *Design of Radial Actuators*. In Short Course on Magnetic Bearings, Lecture 7, University of Virginia, 1997.
- [61] E. H. Maslen. *Magnetic Bearings*. Lecture Notes, University of Virginia, 2000.

- [62] K. Matsuda, Y. Kanemitsu, S. Kijimoto. Optimal Number fo Stator Poles for Compact Active Radial Magnetic Bearings. *IEEE Transactions on Magnetics*, 43:3420-3427, 2007.
- [63] Gy. Fodor, *Electromagnetism I. - Electrical Circuits (in Hungarian)*. Tankönyvkiadó, Budapest, 1985.
- [64] R. L. Haupt, D. H. Werner. *Genetic Algorithms in Electromagnetics*. John Wiley & Sons , Hoboken, New Jersey, 2007.
- [65] B. Lantos. *Fuzzy Systems and Genetic Algorithms*. Műegyetemi Kiadó, Budapest, 2002.
- [66] Y. Wen (Ed.). *Recent Advances in Intelligent Control Systems*. Springer, London, 2009.